Torque Controlled Drive for Permanent Magnet Direct Current Brushless Motors

by
Mark David Britten

Thesis submitted in partial fulfillment of
the requirements for the degree of:

Master of Science in Electrical Engineering
in the **Faculty of Engineering** at the

University of Cape Town.

Supervisor: **Prof. J. Tapson**
Co-Supervisor: **Dr. I.D. de Vries**

September 14, 2009

Declaration

This thesis has not been submitted anywhere before. This thesis is based on my own work. This thesis has been done to fulfill the requirements of the Master of Science in Electrical Engineering degree at the University of Cape Town.

Signed: _____

Mark David Britten

September 14, 2009

Acknowledgments

The financial assistance of the South African National Energy Research Institute towards this research is hereby acknowledged. Opinions expressed and conclusions arrived at, are those of the author and are not necessarily to be attributed to SANERI.

I would like to thank my supervisor, Professor Jonathan Tapson, and my co-supervisor, Doctor Ian de Vries, for their academic support and giving me encouragement and enthusiasm to write this document. Thanks to them for making many suggestions and corrections too.

Thank you to the University of Cape Town that has given me financial support and an office with all hours access.

I would like to thank Gwen, who provided a grammatical consult for most of the written text.

Abstract

This thesis describes the design and implementation of a simple variable speed drive (VSD) based on a brushless direct current (BLDC) machine and discrete logic circuits.

A practical VSD was built, capable of operating a BLDC machine in two quadrants, motoring and regenerative braking. The intended applications are electric scooters and electric bicycles, where the recovered energy from braking extends the range of the vehicle. A conceptual four quadrant VSD, suitable for three and four wheelers requiring reverse operation, was designed and tested in simulation.

Simplicity was emphasized in this design to help achieve a robust, easy to analyse system. The versatility of multi-function gate integrated circuits (ICs) made them ideal for implementing the commutation logic and keeping the system simple.

The BLDC machine has sensors with a resolution of $60°ed$ to determine rotor position. An electronic commutator or phase switcher module interprets the position signals and produces a switching pattern. This effectively transforms the BLDC machine into a direct current (DC) brushed machine. A synchronous step down converter controls the BLDC machine current with a tolerance band scheme. This module treats the BLDC machine as if it was a DC machine. The leakage inductance of the electric machine is used as the inductive filter element. The unipolar switching scheme used ensures that current flows out of the battery only for motoring operation and into the battery only during regeneration.

The current and torque are directly related in a DC brushed machine. The action of an electronic commutator or phase switcher creates that same relationship between torque and current in a BLDC machine. Torque control is achieved in the BLDC machine using a single channel current controller. The phase switcher current is monitored and used to control the duty ratio of the synchronous converter switches.

Successful operation of the practical VSD was achieved in two quadrants: forwards motoring and forwards regenerating. The maximum tested power outputs were $236W$ in motoring mode and $158W$ in regenerating mode. The output torque could be smoothly controlled from a positive to a negative value.

Simulation of the conceptual four quadrant design was successful in all the motoring, generating and active braking zones. The required manipulation of logic signals to achieve this type of operation was done automatically while the machine was running. The resulting output torque is smoothly controlled in all of the operating zones.

Commutation at certain speeds and torques are handled better by some topologies than others. Some current sensing strategies adversely affect instantaneous phase currents under certain conditions. The final design chose the method where phase currents experience no overshoot, minimizing component stress.

The battery, or energy storage system, used in verifying the operation of the VSD in the practical electric bicycle was found to be the most limiting component. In regenerating mode, the low charge acceptance rate of the battery reduced the maximum retarding torque and energy recovery rate.

Contents

List of Figures

List of Tables

Nomenclature

Acronyms

AC	–	Alternating current
ADC	–	Analog to digital converter
ASIC	–	Application specific integrated circuit
BL	–	Brushless
BLDC	–	Brushless direct current
DC	–	Direct current
DSP	–	Digital signal processor
EMF	–	Electro-motive force
EV	–	Electric vehicle
FOC	–	Field orientation control
FPGA	–	Field programmable gate array
IC	–	Integrated circuit
IGBT	–	Insulated gate bipolar transistor
LDO	–	Low drop out
MMF	–	Magneto motive force
MOSFET	–	Metal oxide semiconductor field effect transistor
μ**P**	–	Microprocessor
PCB	–	Printed circuit board
PM	–	Permanent magnet
PMDC	–	Permanent magnet direct current

PMSM – Permanent magnet synchronous machine

PWM – Pulse width modulation

SMPS – Switched mode power supply

SMD – Surface mounted device

SPICE – Simulation Program with Integrated Circuit Emphasis

SVPWM – Space vector pulse width modulation

VSD – Variable speed drive

Abbreviated Phrases

Op-Amp – Operational amplifier

d-axis – Direct magnetic axis

q-axis – Quadrature magnetic axis

Symbols

Symbol	Unit	Description
V_{batt}	V	The terminal voltage of the battery supplying the VSD high power circuitry.
V_{gnd}	V	The circuit node defined to be $0V$ in this text. It is the reference node for all parts of the VSD.
L_{phase}	H	The leakage inductance of a motor phase, measured from a phase connector to the star point in BLDC machines.
I_{phase}	A	The current flowing from a phase terminal to the neutral or star point of a BLDC machine.
R_{phase}	Ω	The resistance between a phase terminal and the neutral point of a star connected BLDC machine.
$V_{emf\,ph}$	V	The generated voltage between a phase terminal and the star point of a BLDC machine.
V_{phase}	V	The voltage between a phase terminal and the star point of a BLDC machine.
R_{arm}	Ω	The resistance between the terminals of a DC machine armature circuit.
L_{leak}	H	The inductance due to the flux that is not part of the electromagnetic conversion in a DC machine armature.
V_{arm}	V	The electro-motive force generated by rotation of a DC machine armature.
I_{arm}	A	The current flowing through a DC machine armature circuit.
V_T	V	The terminal voltage of a DC machine armature circuit.
k_{arm}	Vs/rad	The ratio between T_m and I_{arm} or V_T and ω_m in a DC machine.
R_{bldc}	Ω	The effective R_{arm} of a BLDC machine, equal to $2 \times R_{phase}$ for a 3 phase machine.
L_{bldc}	H	The effective L_{leak} of a BLDC machine, equal to $2 \times L_{phase}$ for a 3 phase machine.
I_{bldc}	A	The effective I_{arm} of a BLDC machine, usually equal to the I_{phase} in an active phase.
V_{bldc}	V	The equivalent of V_T, the DC machine terminal voltage, for a BLDC machine.
V_{emfBL}	V	The equivalent of V_{arm} in a BLDC machine, equal to the sum of $V_{emf\,ph}$ for the two active phases.
k_{bldc}	Vs/rad	The ratio between T_m and I_{bldc} or V_{bldc} and ω_m for a BLDC machine.
T_m	Nm	The mechanical torque at the shaft of an electric machine.
ω_m	rad/s	The rotational speed of the shaft in an electric machine.
R_{ON}	Ω	The resistance from drain to source of a fully turned on MOSFET.
θ_e	$^\circ ed$	Electrical degrees measure position in an electrical cycle.

Chapter 1

Introduction

1.1 Background to Research Problem

Electric bicycles in China have already demonstrated the ability to offer an inexpensive way to travel the short distances covered in urban use. The rising oil price has caused increased petrol prices and an increased cost of living. People need a way to reduce their increasing daily living expenses, transportation being a significant one. Electric vehicles (EVs) are going to become the mode of transport for many South Africans because of their low running cost when compared with internal combustion engine vehicles.

Concern about global warming is increasing and many governments are actively seeking ways to reduce fossil fuel emissions. EVs offer fewer generated emissions and better energy efficiency than internal combustion engined vehicles, making them desirable to implement from a political point of view.

Internal combustion engines are largely responsible for the levels of dangerous gases within big cities. EVs used as urban commuting vehicles are one way of providing the same level of transportation while eliminating the urban hazardous gas emissions, thus maintaining the standard of life without compromising the environment.

The development of hybrid vehicles, powered using petrol and electricity, has attempted to reduce emissions without sacrificing the power and range of the vehicle. Unfortunately the result is not much better than a modern internal combustion engined vehicle [46].

Hydrogen powered vehicles are considered zero emission vehicles because the burning of hydrogen with oxygen results in water, a harmless substance. However in South Africa, the infrastructure for a hydrogen consuming vehicle is not present, leaving electricity as the most accessible clean form of energy for transportation.

From a user's point of view a vehicle is expected to perform in certain way based on experience with internal combustion vehicles. A vehicle should be able to accelerate from rest to a reasonable cruising speed in a fairly short

time, and have a higher maximum speed. During normal driving, a user would expect a higher acceleration when they press harder on the accelerator pedal, and a mild deceleration when releasing the pedal. In this case the user is trying to control the output power of his vehicle, but since the speed of a vehicle doesn't change in an instant, the variable being manipulated is the force or torque produced by the engine.

Electric motor systems implementing torque control, as opposed to speed control, can achieve the same type of response to user input as the internal combustion engine. Furthermore, an important advantage of electric machines is in the area of slowing down. The internal combustion engined vehicle relies on friction wear pads, but the electric machine has the ability to produce reverse torque, and recover energy from the process. The amount of energy available for recovery depends on the mass and speed of the vehicle. In the past, light vehicles were not considered to have enough kinetic energy to make it worth the effort of recovering it, but the highly efficient motors available today have changed this situation.

Another characteristic of internal combustion vehicles is how far they go before having to refuel. Electric storage systems still have to improve before they achieve a comparable range, however the recovery of braking energy, called regenerative braking, can help with this problem. Whenever an EV is being forced to slow down, it is possible to convert the kinetic energy of the vehicle back into electrical energy, by using the electric machine to apply a braking force. This is called regenerative braking. It extends an EV's range by channeling the braking energy into the battery, where it can be used again later.

The aim of this project is to develop a torque controlled variable speed drive (VSD), that will be suitable for general low power, less than a $1kW$, permanent magnet direct current (PMDC) brushless (BL) motors used in light EVs. Currently, portable electrical energy storage systems produce a constant voltage. Brushless direct current (DC) motors make the best use of this type of power source by design and allow simple, efficient drive systems.

Many traction control systems use simple, open loop control, of voltage or petrol delivery, to regulate the mechanical speed. This leaves the user with the task of relating the control input to the desired acceleration, which can be a complex expression. Human users are very capable of this, but control of the mechanical output torque ultimately gives a better feel and operating experience.

1.2 Problem Definition

The small EV needs a low power, that is below $1kW$, PMDC BL motor drive, or VSD. The limited energy capacity of available battery technologies require the VSD to be efficient. A small EV will use a relatively small battery with a low voltage by comparison to the average industrial drive, therefore regeneration of electrical energy must be carried out at low voltages too.

The demands of a user's typical driving experience must be met; full torque should be available from a standstill up to cruising speed and output torque must be directly related to the throttle command.

Typically a vehicle owner will not be able to perform maintenance from home because of a lack of equipment, skill or both. A VSD that is simple and easy to repair with modest equipment and common skill gives the owner more responsibility and pride of ownership and can further reduce the running costs. A simple design leads to fewer parts and a more robust product, able to survive consumer treatment.

An electric machine producing a large output torque has corresponding large currents flowing through it. These electric currents produce heat in the machine that is typically transferred to the surrounding air. At low speeds the heat transfer to the air is slow because air flow is low, and the machine heats up quickly. The VSD must be robust; able to operate at high temperatures, high levels of electrical noise and in strong mechanical vibrations. To ensure survival in this environment the VSD design should use components that are reliable, even in these harsh conditions.

1.3 Current Trends

A DC motor needs some way of causing unidirectional rotation of its output shaft. In a brushed motor this is ensured by having a mechanical commutator switch between electrical conductors in the motor so that the electromagnetic force is always in the same direction. For a brushless direct current (BLDC) motor the commutator is electronically implemented instead.

Permanent magnet (PM) machines with no brushes that are made to operate with a multiphase sinusoidal supply are called permanent magnet synchronous machines (PMSMs). They can produce very smooth output torque and power.

The BLDC machine is made with the idea of being electronically commutated and used with a DC supply like a brushed motor. The output torque and power are disturbed by commutation events but the machine is simpler to operate than the PMSM type of machine.

Electronic Commutators

The electronic commutator in a BLDC machine needs rotor position information to achieve correct commutation. Either separate sensors for rotational position, or measurements made at the motor electrical connections are used.

For motors with separate position sensors, commutation signals can be generated using:

- Application specific integrated circuit (ASIC) based solutions – All the different types of circuitry needed to run the motor are contained in one chip that is specially designed. Some chips may have on board Hall sensor decoders, metal oxide semiconductor field effect transistor (MOSFET) drivers, comparators and operational amplifiers (Op-Amps).

- Microprocessor (μP) based solutions – The μP has limited computational power but can cope with generating commutation patterns. Nowadays many μPs contain Op-Amps and comparators which are useful in motor control applications.

- Digital signal processor (DSP) based solutions – These devices are capable of high speed mathematical calculation. Complex algorithms that can enhance efficiency of a motor system can be evaluated in real time. Calculations for direct torque control [25], field orientation control (FOC) [27], etc. need DSP processing power to be realised.

- Field programmable gate array (FPGA) based solutions – Complex logic functions can be built up on an FPGA by programming the interconnection of logic gates in the chip. On the higher end devices a whole microcontroller can be implemented by programming the interconnections of the contained logic gates. This device can imitate a huge variety of digital circuits giving it great flexibility.

Rotor Position Sensing

The term for a controller with position determination of the BL machine using only the electrical connections is *position sensorless*, or more simply *sensorless*. In sensorless controllers, sometimes the same kinds of devices can be used as those in the sensor based controllers. There are many ways to determine position using the electrical connections [1]; some are simple enough for a μP and others require DSP or FPGA calculation speed. One of the biggest challenges for the sensorless schemes is determination of the position of the machine at zero speed. The controllers in [50], [54] and [38] use guesswork to start the machine off and then change over to using a sensorless scheme above a critical speed. The absence of position information provided by sensorless techniques at standstill renders them unacceptable as position sensors for EV motor drives.

Control Methods

The BLDC machine can be supplied with power in two ways:

- Controlled terminal voltage or
- Controlled terminal current.

Feedback systems can use either of these, or switch between them, to produce controlled output torque, rotational speed, position, power, or some other characteristic.

The current flowing through a BLDC machine is closely related to the torque produced at the output shaft. By putting the machine into a controlled current scheme, protection of the motor and load is achieved inherently because the current is limited and therefore the torque is too.

For EVs, torque control is what an operator expects. Terminal pulse width modulation (PWM) voltage control is a rough approximation to torque control that is used in some low power controllers like the Crystalyte controller [9]. It doesn't perform well with brushless motors; especially at low speeds where large commutation torque ripple is experienced. A current controller could reduce the torque ripple at low speeds but will have similar performance at higher speed. In EVs the torque ripple is less evident at high speed because vehicles have large inertia and stored mechanical energy. However to control the braking of a vehicle, current or torque control is essential to keep consistency across the whole speed range.

The Tesla Roadster [55] is an example of an EV where torque is controlled up to a certain speed and after that power is limited. The electric motor used in the roadster operates from standstill to maximum speed without changing gears, which gives it a cost and maintenance advantage over an internal combustion engine. EVs make good use of the wide speed range of electric machines where maximum torque is available.

1.4 Proposed Solution

The VSD developed in this project will use discrete logic integrated circuits (ICs) to decode position sensor information. Position sensors will be used to create a low resolution absolute position signal.

Analog comparators and Op-Amps will form current sensing circuitry that will enable control of the BLDC machine line currents. Torque output will be controlled by comparing an input demand signal to the magnitude of the machine current. The torque and current can be positive or negative, which makes motoring and generating possible. The design will be carried out in two phases: first a controller able to operate in the quadrants labelled *Generating in Forward Direction* and *Motoring in Forward Direction*; then a controller able to operate in all four quadrants shown in Figure 1.1. The VSD will return kinetic energy from the drive to the energy storage system when operating in either of the *Generating* zones.

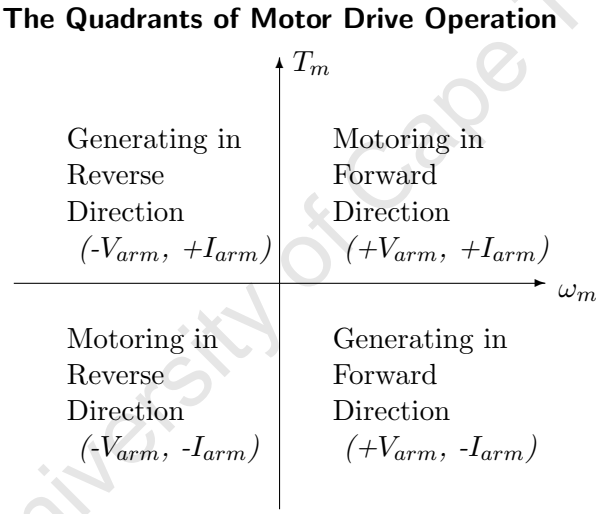

Figure 1.1: The four quadrants of motor drive operation are shown with reference to DC machine variables. T_m is the machine shaft torque, ω_m is the shaft rotation speed, I_{arm} is the machine armature current and V_{arm} is the generated voltage of the machine. Adapted from Mohan [37].

The decision to use position sensors makes it possible to provide maximum torque when the machine is stopped. The BLDC machine targeted in this project was already fitted with Hall effect position sensors. Placement of the other control circuitry near to the Hall effect position sensors would improve signal integrity.

To prevent the temperature of the controller from exceeding its operating limit, a sensor will cut off the power to the machine if a temperature threshold is exceeded. The electronics of the VSD can then be safely integrated into the mechanical arrangement of the machine.

1.5 Motivation for Proposed Solution

Discrete logic components are very robust when compared with other devices that can perform the same function, like μPs DSPs and FPGAs. Discrete logic components permanently perform their particular function unlike FLASH memory based devices that can have a range of functions programmed into them. Although FLASH is a mature technology, the failure of a single bit can change the entire meaning of a stored value or function code. Cappelletti [7] explains how flash memories operate and some of the mechanisms of failure. Programmable devices have many internal states and under extreme conditions can be coerced irreversibly into incorrect states, until a reset occurs. Discrete components have only valid operating states and easily recover from erroneous conditions. Therefore they can survive in harsher environments than devices that rely on programmable memories.

Discrete logic components easily achieve very high speed, low power operation while still being adequately observed by using low speed measurement equipment like a digital multimeter. This makes them a good choice for commercial production because they can be easily analysed. This design technique will produce the simplicity sought after in the problem definition.

The VSD is aimed at systems where the power used by the machine is low, that is below $1kW$. A typical DSP can consume a significant proportion of that power and reduce system efficiency, especially when low output powers are demanded.

The logic function required is very simple and can be implemented with very few parts. Therefore a discrete logic system uses less power than a μP system that does the same job, and responds faster. Discrete logic devices can be found with built in Schmitt triggers that improve the noise rejection and ease interfacing to analog electronics. Most μPs only make output changes or respond to input changes when a clock pulse arrives, but discrete logic is always responsive and therefore is better suited to the environment where events occur at any time.

Devices that use less power will produce less heat, and inject less electrical noise into the circuit because fewer switches are used to implement discrete gates. In some asynchronous logic designs [43] only the gates that need to respond to an input perform a switch, reducing both the average and instantaneous power consumption of the circuit. This is how the discrete logic system will behave.

The reason for an initial investigation into a two quadrant drive is that the simplest logic function can be used while still regenerating electrical energy from the electric machine. In an EV, the regenerative braking will help extend the range of the vehicle. As an added economic advantage, the mechanism for regenerating electrical energy can reduce friction pad wear and thus brake pad replacement frequency. With the ability to return energy to the energy storage device, the VSD could be used as an emergency low

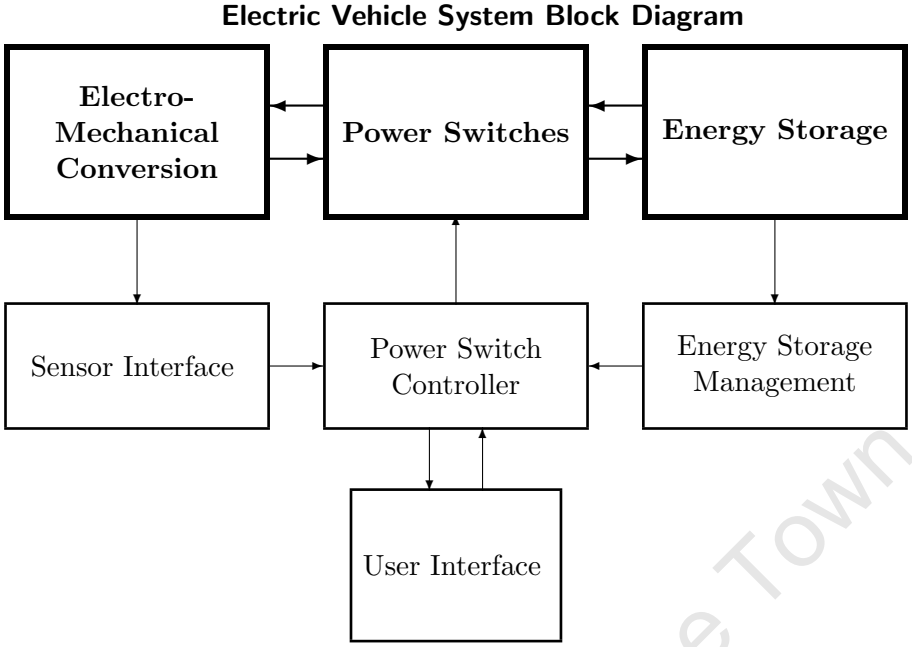

Figure 1.2: The block diagram above shows all the pieces of a stand alone motor drive system. An EV would implement all of the above blocks in its drive system. The individual parts are joined by thick lines where there are high power connections and thin lines where low power or controlling signals exist.

power generator.

In this project a BLDC motor is used as the electromechanical conversion element, shown in the system diagram of Figure 1.2. Brushless motors are popular because they have high power density and efficiency. This is mostly because rare earth magnets, which make very strong permanent magnets, provide the magnetic field in the motor. The magnets are put on the rotating part and therefore no electrical contact with the rotor is needed. This makes the BLDC motor low maintenance and highly reliable. The rotor can also be made very light and, without brushes, very high speeds can be achieved– up to $150\,000 rpm$ [54]. This is part of the reason that brushless motors are power dense; higher rotation speed allows more power output from the same size machine.

Brushless motors have windings only on a static frame, the stator. It is easier to remove heat from the stator because it has better thermal coupling to the environment than a rotating part. Higher currents can be handled when compared with motors where currents flow in the rotating parts. All motors without permanent magnets, even those without brushes such as induction motors, have currents flowing in their rotors that produce heat in the rotor. In BLDC machines there are no such currents, allowing the

PM machine to outperform other machine types in continuous high torque production. The one significant limitation of the present magnet technology is that the magnets lose their magnetism at a relatively low temperature, around 300 °C [28]. Therefore a shutdown scheme should be used to prevent this temperature from being reached.

For a typical three phase BLDC machine, the required external connections are:

- Three high power phase connections,
- Three low power Hall effect sensor connections,
- Two low power Hall sensor power connections.

With a controller integrated into the motor casing, the required cabling becomes:

- Two high power supply connections and
- One low power control signal connection.

If one of the connections of an external controller type fails then the motor drive will only function properly at certain rotor positions. With reduced cabling the motor will cease to function if any one of the connections fail. With only three cables to check, the lack of drive function is easy to remedy. However, in the external controller case the signals are not as easy to interpret and it may take some time to locate the faulty connection.

1.6 Specific Goals of the Project

The VSD of this project will drive a $400W$ BLDC electric motor supplied with a $36V$ sealed lead acid battery pack.

The desired features of the controller are as follows:

- The physical size of the controller should allow it to reside within the casing of the motor.
- Physically robust with a minimum of external connections.
- The controller must have a temperature shut down mechanism.
- The controller must interface to the Hall effect position sensors already mounted in the motor.
- The positive and negative current limit magnitudes should be at least $30A$.
- The controller should accept voltage supplies from $29V$ up to at least $60V$.
- A zero output torque or freewheel state must be easy for an operator to engage.

Fewer external connections means fewer possible failure points. Locating some control electronics inside the machine casing makes the VSD more robust and improves the signal quality from rotor position sensors.

This project is going to focus on the power switch controller and the power switches. The energy storage, energy management and the sensor interface need to be investigated to make decisions in the other system blocks of Figure 1.2.

1.7 Plan of Development

So far the background to the VSD and some reasons for the approach have been discussed. The thesis continues as outlined below.

The next chapter starts with a review of literature relevant to the components of an EV motor drive, shown in Figure 1.2.

The design of the hardware used in the two quadrant VSD is presented in Chapter 3. The four quadrant design concept is described in Chapter 4

The results chapter presents and explains the outcomes of the project. Both simulation and real data are analysed.

The conclusions deduced from the results and the recommendations for future work follow the results.

The source code for the simulation results is listed in Appendix A.

Chapter 2

Literature Review

Nowadays rare earth permanent magnets (PMs) are very popular because they have very high magnetic flux density and strongly keep their magnetisation under normal operating conditions [5]. The name rare earth refers to the proportions of the compounds and elements in the mixture, not the availability of the individual components, which are fairly common. Since these magnets have become affordable and easily available, many applications have arisen. The brushless direct current (BLDC) motor is a good example of this because even though the concept is not new, the possible uses have expanded because of these new stronger magnetic materials. At the same time, there has been development of high speed, efficient electronic switches. This enables practical implementation of an efficient BLDC motor drive. Metal oxide semiconductor field effect transistors (MOSFETs) and insulated gate bipolar transistors (IGBTs) are used as switches in PM motor applications because they have the speed and power handling ability that the new magnetic material gives brushless (BL) motors.

The high magnetic strength of the rare earth magnet reduces the amount of material needed for a specified amount of flux and therefore rotors can be made lighter with lower rotational inertia. Using more poles in the machine design reduces the amount of flux per pole. The magnetic circuit can then be made with less material and therefore less weight [21]. These factors make the rotor cheaper and gives the machine a higher torque to weight ratio and faster response in a speed or position control application.

With PMs providing the magnetic field in the machine, no brushes are needed to provide field currents. The absence of brushes simplifies construction and reduces maintenance tasks, lowering the cost of the machine. Without brushes, the possibility of electric sparks is eliminated, allowing safe operation in hazardous environments. Higher operational speeds, for example $150\,000 rpm$ [54], can also be achieved, giving the brushless motor high power density.

The efficiency of the BL machine is high because no power is lost in

order to provide a magnetic field. This is very important for low power applications where a field current can amount to a significant energy waste, especially when the machine is stopped or moving slowly.

The brushless machine has its windings installed in a frame, called the stator, used as a point of attachment. Heat, produced by the machine currents, can easily be removed from this frame. Thus the BL machine has the capacity to safely handle higher currents than a brushed machine, further increasing its power density and torque capability.

The BLDC motor is the electro-mechanical conversion part of the system block diagram shown in Figure 1.2.

2.1 Designs of Permanent Magnet Machine

There are two main varieties of permanent magnet (PM) brushless machines:

- Permanent magnet synchronous machines
- Brushless direct current machines

Permanent magnet synchronous machines (PMSMs) have phase to phase and phase to neutral voltages that vary approximately sinusoidally with the position of the rotor relative to the stator, as shown in Figure 2.4(a). This is achieved by using a distributed winding pattern and pole shaping in the motor to cause a sinusoidal flux distribution. The controller for this machine type keeps all phases in continuous conduction by applying sinusoidal signals to the phase windings.

Brushless direct current (BLDC) machines have concentrated windings and the pole shapes are designed to make the airgap uniform. The resulting flux distribution is trapezoidal. The pole shape is designed so that flux linkage to the phase windings is triangular, with the peaks and valleys of the waveform replaced with quadratic sections. The generated phase to phase and phase to neutral voltages are then trapezoidal, as shown in Figure 2.4(b), and Figure 3.20. In a three phase BLDC machine, a direct current (DC) voltage is applied to the two phases whose generated voltage is temporarily constant, so one phase is not normally conducting.

The torque production of an electric machine depends of the alignment of the magnetic field with electric currents. The direct magnetic axis (d-axis) and quadrature magnetic axis (q-axis) are defined to provide a reference for the measurement of the positions of the magnetic fields and currents from the perspective of the rotor. The d-axis is in line with the center of a magnetic pole, where the flux density is highest. The q-axis is in line with the lowest flux density angular position.

In electric machines, angular displacements are measured in electrical degrees (θ_e, unit $^\circ ed$). Electrical degrees are found by multiplying mechanical degrees with the number of pole pairs in a machine.

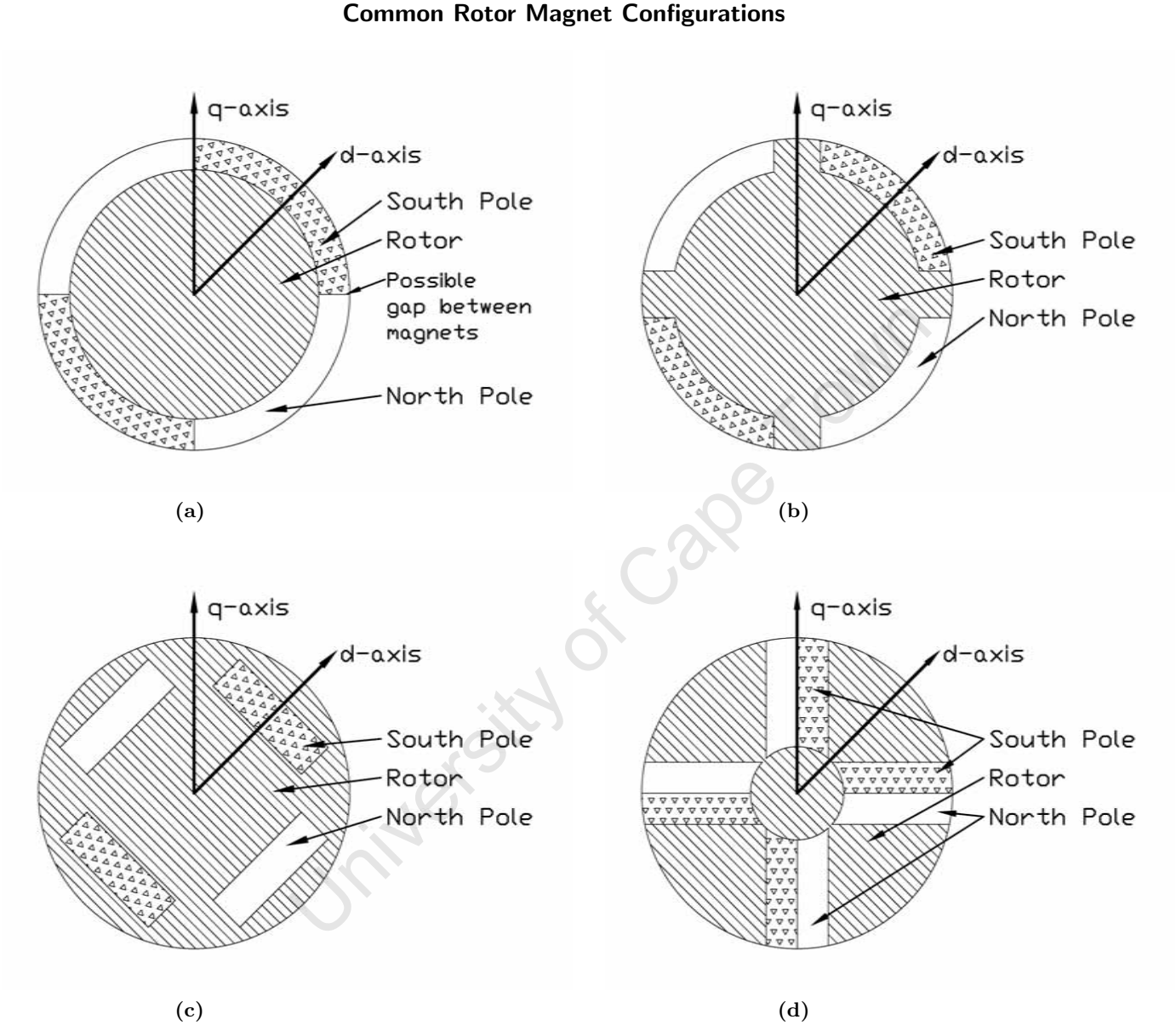

Figure 2.1: There are four common arrangements of permanent magnets in a brushless machine rotor. The magnetic flux in the air gap is in the direction of the d-axis. The diagram is adapted from Sen, P.C. [48]:

(a) Surface magnets.
(b) Inset or countersunk magnets.
(c) Interior magnets with radial magnetization.
(d) Interior magnets with circumferential magnetization.

In PM brushless (BL) machines there are several methods for mechanical arrangement of the magnets. Below is a summary of their descriptions in Sen, P.C. [48], pages 355 – 356:

- Surface magnets – Magnets are attached onto the surface of the rotor as shown in Figure 2.1(a). A gap between the magnets can reduce the torque ripple of the machine and improve the shape of the generated electro-motive force (EMF). The permeability of magnets is similar to air, giving this design a low inductance because of its large effective air gap.

- Inset or countersunk magnets – Magnets are visible from the surface of the rotor but have magnetic material between them on a circumferential path as shown in Figure 2.1(b). The d-axis has a larger effective air gap than the q-axis, so reluctance torque is possible. The reluctance torque enables thinner magnets to be used for the same torque production, giving this design a higher inductance than a similarly sized surface magnet machine.

- Interior magnets with radial magnetisation – Magnets are positioned beneath the magnetic material as shown in Figure 2.1(c), preventing the possibility of a magnet flying off and giving the design a higher inductance than surface and inset types. The rotor material between the magnets causes a significant difference between the magnetic reluctance between the d-axis and the q-axis, allowing a reluctance torque to be produced.

- Interior magnets with circumferential magnetization – Magnets are positioned as shown in Figure 2.1(d), which causes a flux focusing effect, useful for magnets with low flux density. Reluctance torque can be produced with this design as well, but the reluctance torque magneto motive force (MMF) must lead the electromagnetic torque MMF, unlike the inset and radially magnetised cases.

The above methods of magnet arrangement produce slightly different magnetic flux distributions in the air gap of the machine. The air gap flux density distribution and the stator winding pattern determine the shape of the natural EMF generated on the stator windings as the machine is rotated.

Of the designs of rotor, the surface magnet type has the simplest construction, making it a good candidate for high volume production. It also is easily rearranged into a machine where the magnets rotate around the stator as shown in Figure 2.2.

Outer Rotor Brushless Machine Structure

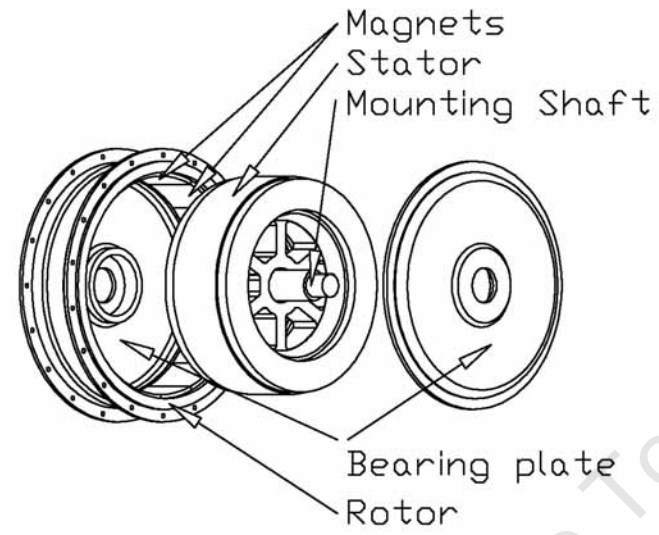

Figure 2.2: The rotor in this machine is made to fit around the stator and rotate around it. A wheel can easily be attached to form an "in the wheel" or "hub" motor from this outer rotor configuration, ideal for light electric vehicles.

Axial and Radial Flux Machine Designs

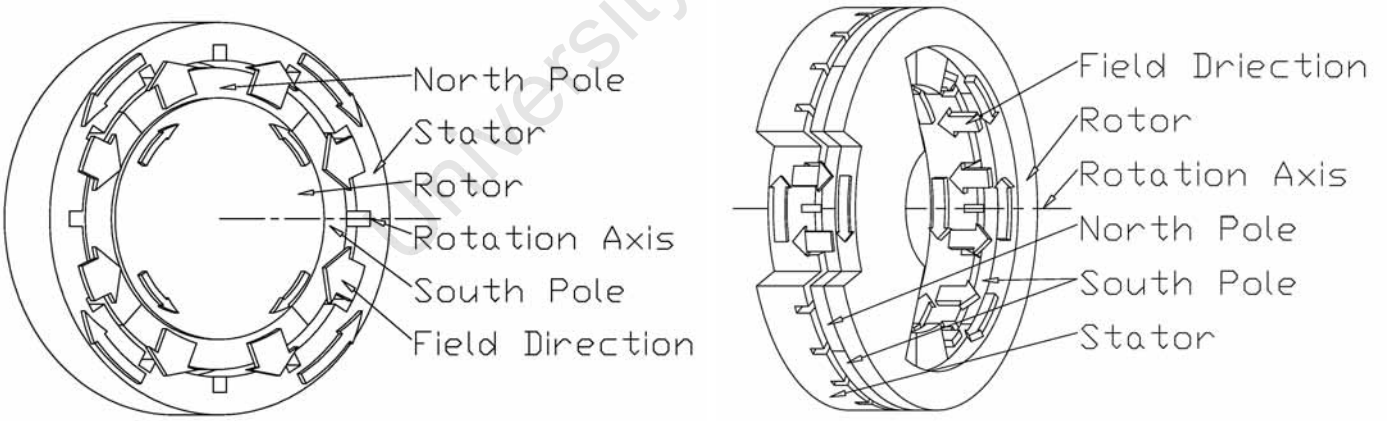

(a) Radial Flux **(b)** Axial Flux

Figure 2.3: The airgap flux of a PM motor can be along the axis of rotation, as in (a), or parallel to the radius of the rotor, as in (b). The axial flux arrangement has the potential for changing the air gap size while the motor is running.

There is potentially a big advantage to the arrangement of Figure 2.2: The outer spinning part can be directly connected to the wheel of an electric vehicle (EV), eliminating gearboxes, driveshafts and the associated efficiency losses caused by such parts. A motor with a driving wheel built around the rotor is called a hub motor, wheel motor, out runner or outer rotor motor. There are two possibilities for this idea, illustrated in Figure 2.3:

- Axial flux machine – The flux from the permanent magnets is directed parallel to the axis of rotation of the machine, illustrated in Figure 2.3(b). This configuration allows for a simple air gap manipulation mechanism while running, as Patterson and Spée [44] suggested. The rotor slides along the axis of rotation to achieve any air gap size. This design allows attachment to a wheel without limiting the heat transfer path from the stator. More magnet airgap area can be achieved per unit volume in this configuration.

- Radial flux machine – The magnetic flux is generated parallel to the radius of the rotor, as shown in Figure 2.3(a). This is a more conventional configuration that can be turned inside out to make the motor into a wheel hub. The axle in this design is free from the force of the magnetic attraction between the rotor and stator, but radial flux makes less efficient use of space than the axial flux type of machine.

In order for a motor with the magnets spinning on the outside to be strong enough to mobilise a vehicle, it must be made with enough torque to perform a standing start. This means that it will typically be bigger and heavier than a motor that is made to rotate faster to produce the same power. However, the added size gives the bigger "wheel" motor an advantage; the extra weight increases heat capacity and therefore high torque demands can be tolerated for longer. Patterson and Spée [44] note that the heavier "wheel" motor does not necessarily degrade the overall performance of a vehicle because the efficiency advantage of eliminating the gears makes up for the efficiency loss of the extra weight.

As stated earlier in this section, the PMSM is designed to generate sinusoidal EMFs. The purpose of a machine is to convert electric power to mechanical power and vice versa. With sinusoidal EMFs, the currents required to produce a constant power conversion rate are also sinusoidal.

However, for the three phase BLDC machine with two phases conducting at a time, a constant power is achieved with square wave phase currents, illustrated in Figure 2.5(a). One way to achieve this is to connect the motor phases to a DC supply only when current is needed in that phase. This task was previously done with a mechanical commutator, but now it is done with semiconductor switches. In practice, the current waveforms will never be exactly square because the stator winding has leakage inductance. This makes it impossible to instantaneously change a phase current. Taking this

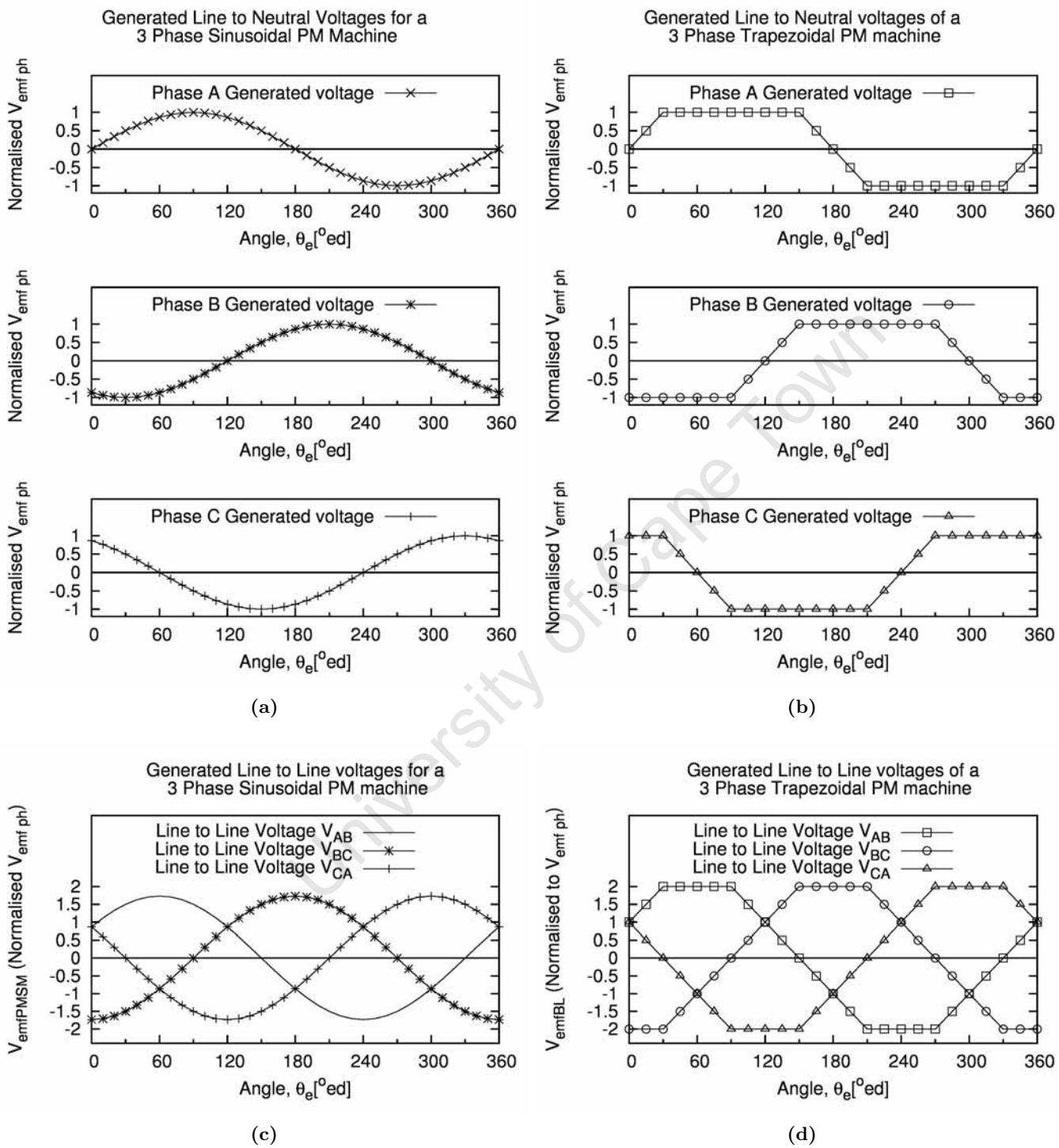

Figure 2.4: Generated voltages for a three phase PM machine. (a) and (c) show ideal voltages for a PMSM type of motor where continuous variation of the applied voltage is necessary. Graphs (b) and (d) show the BLDC ideal voltages, where a DC supply can easily accommodate flat portions of the waveform.

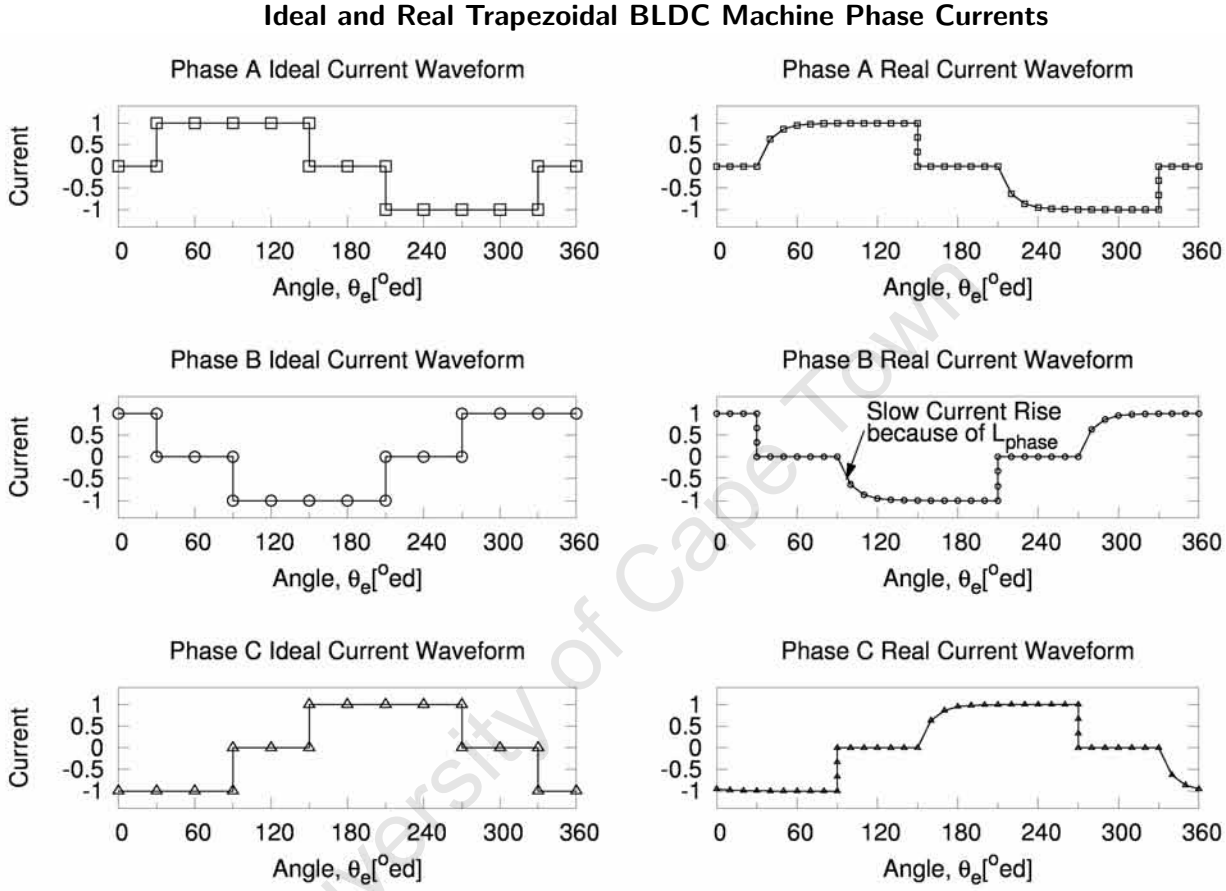

(a) Ideal phase currents **(b)** Realistic phase currents

Figure 2.5: The ideal phase to neutral currents shown in (a) above would result in a smooth output torque in a BLDC machine. The achievable currents shown in (b) produce a glitch in output torque at each commutation. The slower rise of the real current waveform from zero is due to machine inductance. The quick decay of phase current, I_{phase}, is caused by the applied phase voltage and the generated voltage adding constructively to the voltage across the phase leakage inductance, L_{phase}. Section 5.2.2 explains this mechanism in more detail.

effect into account, the actual phase currents would be as Figure 2.5(b) shows. The more realistic currents cause a fluctuation in the output power and torque that cannot be avoided with machine design techniques. The electronic controller must deal with this source of torque ripple.

The interaction of the magnets, stator winding and core, as well as the flux distribution in the machine and the high power signals from the controller, produce forces that cause ripple or pulsation of the output torque of the machine. The components of the pulsating torque that are affected by machine design, as described by Aydin *et al.* [4], are:

- Cogging Torque – Torque produced by the magnetic reluctance changing as stator teeth pass over magnetic poles.
- Torque ripple – Torque produced by the MMF distribution of the stator interacting with the MMF caused by the magnets.

To reduce cogging torque, in some designs the stator winding slots are skewed – that is made at a diagonal to the north-south magnet boundary. This aims to make a smooth transition from one stator tooth to the next. A different approach by Ishikawa and Slemon [22] successfully reduced cogging torque using careful magnet placement and varying the magnet pole arc length. The manufacturing cost of making skewed slots is higher than having straight slots, so it is advantageous from a cost perspective to avoid skewing.

It is impossible to get a perfectly sinusoidal or trapezoidal distribution of flux from a stator or a rotor design. The aim of machine design is to get as close as possible to the ideal situation, so that the machine produces smooth output torque and power. The unwanted torque components waste power while the machine is running. Despite designers best efforts, the torque ripple is still present. In BLDC machines, the practical result of attempting to drive square wave currents into the motor introduces torque ripple at commutation. PMSMs do not suffer from this problem since their currents are continuous. Direct torque controllers, such as the one developed by Kang and Sul [25], counteract the torque ripple using careful control of the phase currents at commutation.

2.2 AC and DC Machine Models

DC brushed motors can be represented by the simple electrical circuit model in Figure 2.6 because the mechanical commutator always keeps the rotor field magnetically perpendicular to the stator field. The fields are said to be in quadrature because they are virtually independent of one another; changing the stator field does not affect the rotor field and vice versa. In alternating current (AC) machines, the physical position of the field is always changing as the rotor changes position. To keep these magnetic fields in quadrature, the electric signals applied to the machine must be continuously adjusted.

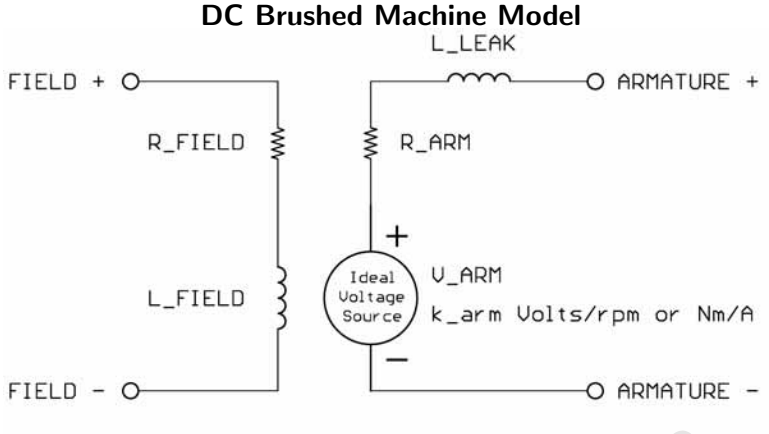

Figure 2.6: The electric circuit equivalent of a DC brushed machine with the field and armature loops decoupled by the mechanical commutator.

The DC machine model is still relevant to an AC machine; all that is needed is a way to transform the alternating currents and voltages to equivalent DC machine quantities.

A stator current component is represented by a vector of the same magnitude in the direction of the magnetic field it produces. The machine is analysed using current vectors to represent permanent magnets as well as real currents.

The AC machine has multiple current and voltage signals, that constantly change, even in steady state operation. On the other hand, the DC machine in steady state has constant values for currents and voltages in the field and armature circuits.

Complex numbers are used to handle phase displacement, in time and space, of current and voltage signals. Two transforms are used to convert stator currents and voltages into DC type quantities:

Clarke transform – computes real and imaginary components of the vector obtained by vectorially adding complex representations of all the individual phase vectors. The result is usually referenced to a complex plane fixed to the stator.

Parke transform – computes real and imaginary components of a vector in a coordinate system that is a rotation of the original coordinate system. This is used to create a vector representing stator referenced voltages and currents that is now lined up with the d-axis.

To transform AC machine currents and voltages to equivalent DC *armature* and *field* currents and voltages, first the **Clarke transform** is applied to convert the phase currents or voltages into two components on a coordinate system referenced to the stator. The **Parke transform** is used to rotate

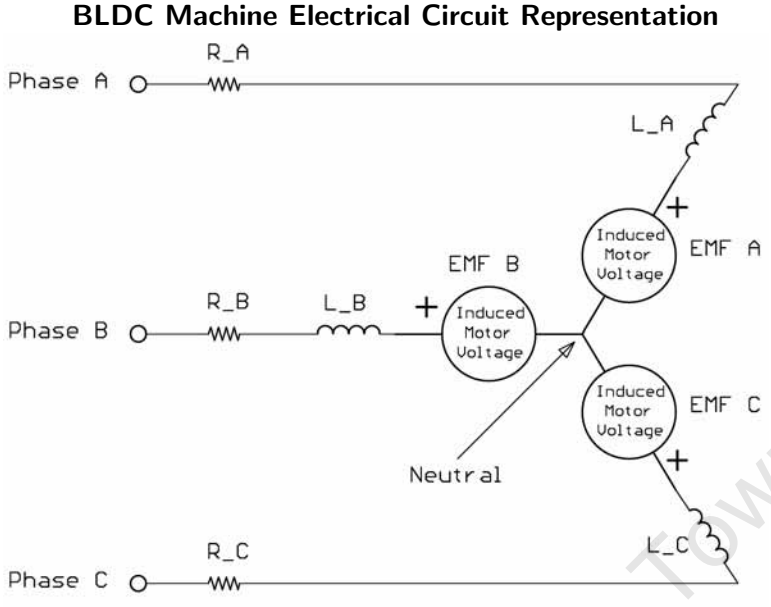

Figure 2.7: BLDC motor electrical circuit representation showing the interconnection of the phase resistance and inductance. The induced motor phase voltages are trapezoidal as in Figure 2.4, with polarities indicated by the + signs.

the stator orthogonal coordinate system to the rotor orthogonal coordinate system. These transforms allow the AC machine to resemble a DC machine and be analysed in a similar way. The d-axis is positioned in the direction of the maximum field strength of the PMs as shown in Figure 2.1. The q-axis is in the direction of zero magnetic field strength.

The calculation power of a digital signal processor (DSP) is used to perform the **Parke transform** and **Clarke transform** in real time so that AC machines can be controlled as if they were DC machines. The inverses of the transforms are used to calculate the correct AC machine phase currents and generate the signals to be applied to the phases [27].

In AC machines, field and torque producing currents can both be present in the stator winding. The complex vector representing a current in a winding has direction parallel to the force it produces on a North magnetic pole at the center of the winding. PM machines already have a magnetic field, so a field current component is not necessary in the stator. If the d-axis current component is controlled to zero, the stator current will be directly related to the output torque; just as the armature current is related to the output torque in a DC machine.

BLDC machines have been designed to simplify the calculations required to achieve DC machine performance.

During each flat section of the line to line phase voltages, Figure 2.4(b),

the two phases that are involved can be interpreted as equivalent DC brushed machine armature connections.

The electromechanical power output of the machine at these times is the product of the current in those phases and their summed EMFs.

A different pair of the BLDC phases has to be used over each sixth of an electrical revolution, or $60°ed$ interval, while the unused phase must be left open circuit, to achieve similar behaviour to a DC brushed machine. The process of changing the pairs of phases in use is called commutation. The three phase BLDC machine is always star connected, as shown in Figure 2.7; so that conduction in the unused phase does not normally occur.

The BLDC machine needs information about when to change from one pair of phases to another. Since these changes only have to be made every $60°ed$, the information can be provided with a sensor that has low resolution.

The electric circuit model in Figure 2.7 represents the BLDC motor adequately for most controller design purposes. In Figure 2.6, the DC machine model has armature resistance R_{arm}; the equivalent in the BLDC machine is R_{bldc}, which equals $R_A + R_B$, or any other two phase combination. The BLDC machine can have less armature resistance because a bigger winding can be accommodated on the static part of a machine. The phase resistances R_A, R_B and R_C are equal, and the symbol R_{phase} is used to denote any one of them.

The L_{leak} of a DC machine does not interfere with the commutation process; but in the BLDC machine the inductances L_A, L_B and L_C hinder every commutation event. L_{phase} is used to refer to the inductance of an arbitrary phase. Thus the controller for a BLDC machine has to compensate for current build up, or the drive will suffer from the commutation-induced torque fluctuation mentioned in the previous section.

2.3 Sensor Interface

In this variable speed drive (VSD), three types of sensor will be used. They are: rotor position sensors, current sensors and temperature sensors. This section reviews the methods used in recent research and guides the choice of sensor to meet the requirements of the proposed solution in Section 1.4 and the goals in Section 1.6.

2.3.1 Rotor Position Sensing

In order to efficiently operate a permanent magnet direct current (PMDC) BL motor, the position of the rotor must be known to the driving electronics. There are two approaches to determining rotor position:

- Use explicit sensors to obtain rotor position information, or
- Use a *sensorless* scheme; the three electrical phase connections to the machine are used to derive the rotor position.

A lot of research has been done into ways that use only the electrical connections to a motor to determine rotor position. Acarnley and Watson [1] divided the approaches to *sensorless* PMDC motor control into the following categories:

Back EMF monitoring: The diagonal parts of the trapezoidal back-EMFs, in Figure 2.4(b), can be used to determine rotor position. Shao, J. *et al.* [50] used a zero crossing detector on the unused phase when both active phases were grounded. This gave them information on when the next phase was reaching the flat portion of its back-EMF. Another scheme uses the neutral point of the machine to extract the third harmonic of the trapezoidal back-EMF. Moreira [38] and Shen *et al.* [51] used this type of information to obtain position estimates more quickly, over a wider range of conditions than in the case of sensing the fundamental component of the back-EMF.

Flux Estimation: Position can be estimated by integrating the back EMF of the machine using the phase voltage minus the $I_{phase} \cdot R_{phase}$ volt drop. In some implementations machine parameters must be known to the controller to get a good position estimate. The machine is often modelled on a DSP that corrects its estimates in an iterative feeback loop. Alternatively, the mechanical dynamics of the machine could be used in estimating the position and speed of the machine, but the resulting system is less suited to varying loads. Ertugrul and Acarnley [16] created a two loop correction scheme to estimate the position of their machine's rotor.

Magnetic Reluctance Detection: The current rise and decay rates are inversely proportional to inductance. In a PM machine the inductance of a phase winding depends on the reluctance of the magnetic path, which changes as the rotor magnets move past it. Nakashima *et al.* [39] used this effect to estimate the position of a stopped PMDC motor with a maximum error of 18°*ed*, although most of the time the error was around 3.75°*ed*. Jang *et al.* [23] used the injection of a high frequency voltage signal to cause currents to flow that revealed the complex impedance difference between the magnet and inter-magnet axes of the machine. In Jang's implementation the estimation was possible for a speed range including zero speed. Hartas *et al.* [19] used the natural operating frequency of a tolerance band current controller to determine inductance changes that indicated rotor position. In their case the motor had a modified stator structure where a number of phases were always unused and could be employed to obtain motor position without the disturbing torque production.

The sensorless techniques for motor control require fast real time calculations to be done, and have difficulty operating a PMDC motor from zero speed under full load. While it has been done, the computational cost and complexity of software is much greater than for a sensor based approach. Sensorless schemes are often implemented on field programmable gate arrays (FPGAs), microprocessors (μPs) and DSPs, where coding errors and FLASH memory failure can reduce reliability. Takahashi *et al.* [54] pointed out that at very high speeds a position sensor is not practical and used a sensorless approach. In this project speeds below 3 000rpm are expected and so an explicit sensor is practical and full torque can easily be achieved from a standing start. With a well situated position sensor, the required computation to determine a commutation becomes very simple and quick.

Explicit position sensors for BL motors are used to get the absolute position of the motor shaft. The required resolution of the sensor depends on the type of control to be implemented.

Low Resolution Sensors: Hall sensors, optical sensors and reed switches can be used in the BLDC type of machine where only a phase change needs to be signalled. For an n-phase system, $2n$ commutations occur per 360°ed. Therefore at least $log_2(2n)$, rounded up to the nearest integer, binary digits or *bits* of sensor output are needed for an n-phase system. For a three phase machine, six commutations are needed and $log_2(2{\cdot}3) = 2.58 \Rightarrow N_{bits} = 3$. Digital Hall sensors are a popular choice for representing the N_{bits}. The sensors are often positioned using one of the following schemes:

360°ed/n sensors – The sense elements are phase displaced 360°ed/n

from each other around an electrical rotation. Figure 2.8(a) shows the output from this type of sensor in a three phase machine.

180°ed/n sensors – The sense elements are instead phase displaced by $180°ed/n$. Figure 2.8(b) shows the typical outputs given a three phase machine. If Sensor B is logically inverted and swapped for Sensor C, the resulting output is the same as the $360°ed/n$ type of arrangement. For an n phase system, n sensors would be needed if one of the above two schemes is used. The sensor outputs can be encoded to N_{bits} bits to transmit the information if the number of signal wires must be minimised.

High Resolution Sensors: High resolution optical shaft encoders, analog Hall sensors, resistive sensors, capacitive sensors and inductive sensors can be used to accurately determine angular position. The popular choices are optical or magnetic shaft encoders and servo potentiometers (a resistive potentiometer that can be rotated an indefinite number of times). The controller can compensate for some machine design quirks, like non-ideal phase voltages, by using the additional position information. Operation in flux weakening mode [51] is another possibility with high resolution sensors. The commutation times can also be finely tuned to allow current to build up to the desired value in the next phase so that commutation torque fluctuation is minimised.

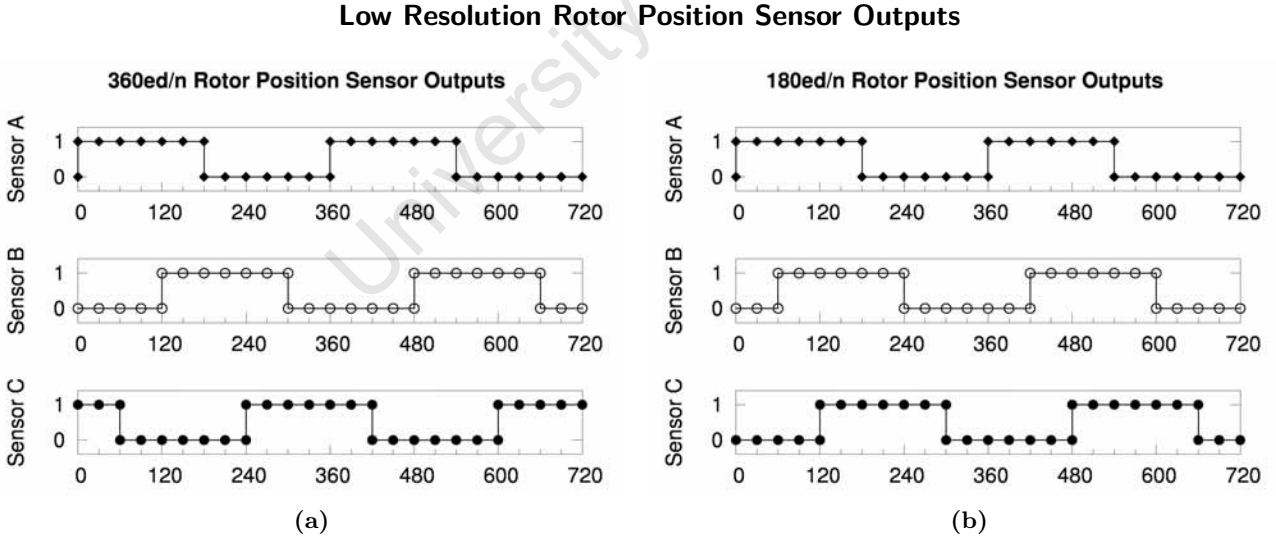

Figure 2.8: Over two electrical cycles, graph (a) shows how the outputs of a $360°ed/n$ sensor varies for a sensor designed for a three phase machine; each sensor output is phase shifted by $120°ed$ from the previous one. Graph (b) shows $180°ed/n$ sensor outputs, each phase being shifted by $60°ed$ from the previous, also suitable for the same purpose.

The $360°ed/n$ and $180°ed/n$ sensor outputs are both very simple and similar to each other. A controller can easily be made that deals with both types of input. Alternatively, a simple logic circuit, in a separate module, could convert the $360°ed/n$ outputs to $180°ed/n$ outputs and vice versa.

To convert the output of a $360°ed/n$ sensor to a $180°ed/n$ sensor:

- Use Sensor A with no adjustment.
- Notice that Sensor B of the $360°ed/n$ type matches the output of Sensor C of the $180°ed/n$ type.
- Invert the Sensor C of the $360°ed/n$ type to match it to Sensor B of the $180°ed/n$ type.

The reverse process can be followed to convert from the $180°ed/n$ sensor outputs to the $360°ed/n$ sensor outputs.

2.3.2 Current Sensing

In the low power VSD proposed, sensing the motor current is necessary but must be realisable with simple hardware to be effective. The concept of measuring the phase current using the actual wires that connect to the phases requires isolation of the current sense element or a sensor with a wide common-mode range of acceptable input voltages.

In electronics, analog voltage signals, representing the magnitude of some physical variable, are almost always processed by amplifiers, comparators and analog to digital converters (ADCs). When a current must be measured, the aim of a sensor is to convert that current magnitude into a voltage signal.

There are two main effects used to determine the current in a circuit:

- The voltage loss as a current flows in a circuit path – according to Ohm's law,
$$V = I \cdot R$$
a voltage, V, is present across a fixed resistance, R, when a current, I, flows through it.
- The magnetic field caused by current – a current causes a magnetic field with strength proportional to its magnitude. The magnetic field direction is perpendicular to the current direction. Magnetic fields cause other physical effects that can be measured by other voltage transducers. The Hall effect sensor exploits direction change of electrons in the presence of a magnetic field to generate a proportional voltage. The Faraday rotation effect causes the polarization of light to change, which can then be measured using optical transducers to produce a proportional voltage. The magnetic field around a current

can induce a current in another parallel conducting path. Transformers use this effect to create a secondary current that is a ratio of the original current.

In power electronics, there exist many inventive ways to use the resistances that arise from using real components in real circuits. An inductor has winding resistance, used by Dallago *et al.* [11], [12] in their lossless current sensing schemes. A metal oxide semiconductor field effect transistor (MOSFET) has on resistance, R_{ON}, and a printed circuit board (PCB) has trace resistance. All of these can be used to obtain a voltage proportional to the current flowing in the path. Another method of measuring current uses the change in polarity of light passing through a magnetic field, the Faraday rotation effect, to determine the magnitude of the current [29], [30].

Zhang *et al.* [60] demonstrated a method of using MOSFET on resistance as a current detector. The variation of the MOSFET on resistance with temperature causes low accuracy current measurements with this system. To increase the accuracy, the main MOSFET was deactivated for one cycle out of ten or a hundred and instead a current sense resistor in series with another MOSFET was switched in. The current during this cycle could be accurately determined from the sense resistor. The controller would then update the working value for the main MOSFET on resistance, allowing the same accuracy of current measurement as the sense resistor. The loss of using a separate sense resistor is effectively avoided, but the accuracy of the current measurement is kept.

Dake and Özalevli [10] created an amplifier for a method where a power MOSFET is copied on a smaller scale, but with the same gate, drain and source voltages as the power MOSFET. The current in the smaller MOSFET is proportional to the current in the power MOSFET, and a low power resistor can be used in the path of the smaller MOSFET as a current sense device.

The Hall sensor and current transformer methods achieve isolation from the current they are measuring. However, the analog Hall sensor has complex implementation, and the current transformer can saturate and lose accuracy while measuring DC currents. There are ready made modules for measuring current using Hall sensors that simplify connections [58].

In a three phase machine, more than one circuit branch has to be monitored to get a complete representation of the currents flowing. Dixon and Leal [13] merged all the current signals from several phases of a BLDC motor into one equivalent DC machine type signal. With DSPs and FPGAs, the problem of monitoring many currents is easier to solve since ADC modules typically have an easy way to select one from a number of inputs. On some devices many currents can be measured simultaneously and easily manipulated in digital form afterwards.

When it is difficult to insert a measurement device where it is needed, the current can sometimes be obtained from measurements elsewhere in the circuit. Green and Williams [18] used only one current sensor in a three phase inverter and reconstructed the phase current waveforms accurately. The disadvantage with this approach is having to use a certain switching pattern to ensure that at a specific time, the current is flowing only through the branch in question.

2.3.3 Temperature Sensing

PM machines are limited in operational temperature range by the magnetic material used. The Curie Temperature of the magnet material, NdFeB, is approximately $300°C$ [28], but to maintain a usable flux density in the motor the temperature should be kept to below $\pm 150°C$. Bai *et al.* [5] developed a NdFeB mixture with the rate of loss of flux density of 0.53% per $°C$ in the $20°C$ to $150°C$ range, which means that a significant loss of flux is possible within a typical motor temperature range. Kang and Sul [25] noted a drop of 19% in the magnetic flux for a $100°C$ temperature rise in the material, illustrating the temperature sensitivity of the NdFeB type of magnet.

Fans and surrounding air are often used to remove unwanted heat energy. When that is not effective enough, other systems involving water and heat pumps or actively reducing the production of heat, are needed. Horowitz and Hill, in the Art of Electronics, pages 988 – 996 [20], describe many methods of measuring temperature in an electrical circuit. Some parameters of sensors for the PM and semiconductor operating range are summarised in Table 2.1.

Table 2.1: Characteristics of some popular Temperature Sensors

Sensor Type	**Range** [$°C$]	**Accuracy** [$°C$]	**Sensitivity**
IC temperature sensors	-55 to 150	± 0.1 to ± 1	a few $mV/°C$
Platinum thermometers	-200 to 1000	± 0.02 to ± 0.2	$0.4\%/°C$
Thermistors	-50 to 300	± 0.1 to ± 0.5	$4.0\%/°C$
Quartz thermometer	-50 to 150	± 0.04	$5ppm/°C$
Thermocouple (J-Type)	-270 to 2500	± 0.5 to ± 2	$\pm 40\mu V/°C$

IC temperature sensors: Semiconductor junction electrical behaviour is temperature dependant. Such effects are used to determine the absolute temperature of the device. e.g. in the LM35 temperature sensor [41].

Platinum resistance thermometers: Platinum has a very stable relationship between its resistivity and its temperature. JUMO produce a

surface mounted device (SMD) version of this type of sensor, ideal for integration into a design [24]. Platinum is an expensive material but has good linearity and accuracy over a wide temperature range.

Thermistor: A thermistor is a semiconductor device whose resistance is very sensitive to temperature. It suffers from a low temperature range and a non-linear relationship between temperature and its resistance. However, it is very easy to use and makes a good threshold detector because of its high sensitivity. The stock listing of RS Components illustrates the range of available thermistors and some useful formulas to calculate the temperature [47].

Quartz thermometer: A quartz crystal oscillator can be made with significant temperature dependence by cutting the raw crystal in a certain way. Hewlett Packard have made a very accurate temperature sensor based on this approach: the 2804A. Statek claim to make crystals with a $46.4 ppm/^{\circ}C$ frequency sensitivity and recommend a second order model to relate the temperature with the operating frequency [52].

Thermocouples: A thermocouple is a pair of wires made of different metals or metal alloys, that are formed into a junction at one end. The open end is connected to a high impedance measurement circuit where a small voltage is observed, representing the temperature difference between the ends. Linear Technology and Analog Devices have products in their range specifically for use with thermocouples [3], [33], making implementation relatively straight forward.

In power electronic systems, one way to prevent overload damage is to shut down when the temperature reaches a certain threshold. Therefore the thermistor makes a good candidate for a simple solution because it has high sensitivity.

2.4 Power Electronic Converters

2.4.1 Variable Speed Drives

In Section 1.6 a block diagram was presented showing the modules of an EV system. In Figure 2.9 the portion of that figure that makes up the component called a *variable speed drive* has been extracted. In previous sections of the literature review the **Electromechanical Conversion** and **Sensor Interface** technologies making up the two left hand blocks were presented. The power switches are left for discussion in the Hardware chapter of this thesis, leaving the **Power Switch Controller** to be discussed here.

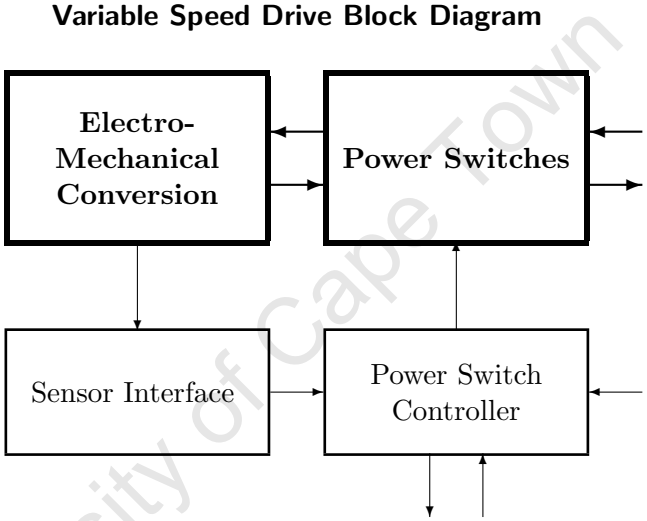

Figure 2.9: The above block diagram shows the parts of a VSD as an extract from Figure 1.2.

As Figure 2.9 shows, the term VSD refers to a system of several modules. This section will focus on presenting existing research on the control block of a VSD.

In VSDs made for brushless motors there are two basic types of controller: The BLDC type of controller produces realistic square wave currents, shown in Figure 2.5, and applies constant phase voltages to match the flat portions of the phase EMFs, shown in Figure 2.4(b) and (d). The VSD uses low resolution position information and treats the machine like a DC machine with an electronic commutator. One of the motor phases is left uncontrolled between commutation events.

The PMSM type of controllers supply the machine with sinusoidally varying voltages, shown in Figure 2.4(a) and (c), and sinusoidal currents. High resolution position information is needed to maintain the orientation of the applied voltages and currents with the rotor. All the phases of the motor are continuously supplied with a controlled voltage or current.

Table 2.2: Comparison of PMSM and BLDC VSD Modes

	PMSM	**BLDC**
Position sensor requirement	High resolution only.	Low resolution, can make use of High Resolution for commutation phase advance.
Type of motor	Either a BLDC or PMSM can be used.	Better with a BLDC. A PMSM could be used but with reduced rating because of the harmonics present in square waves.
Modulation strategy	SVPWM or normal sinusoidal PWM with all legs of inverter bridge in constant conduction.	Single channel PWM, superimposed on a logic circuit to commutate the phases.
Torque ripple	No sharp commutations occur, therefore output torque has less ripple.	Commutation torque ripple is significant and can cause audible noise and vibration.
Complexity	Typically sine wave references and PWM signals are needed. Many calculation intensive algorithms, like FOC and SVPWM, exist that achieve better machine performance.	Typically one PWM channel is used to control the active phases. Methods to reduce commutation torque ripple, and other undesirable machine characteristics, have comparable complexity to the PMSM algorithms for better performance.
Efficiency	Switching losses are higher in sinusoidal controllers because PWM occurs on all inverter switches. Current harmonic content in the output waveform is low; resulting in low machine losses.	Fewer PWM channels are used, resulting in lower switching losses. The phase currents contain stronger harmonics because of their square shape. This causes more machine losses than a sinusoidal scheme.

Table 2.2 shows a comparison of the two types of drive. From a cost perspective, the BLDC type of controller has an advantage because low resolution sensors are cheaper than the high resolution sensors used in PMSMs. Furthermore, the typical method of controlling the machine voltages and currents – the modulation strategy – is easier to implement for a BLDC controller. One drawback to BLDC systems is the torque ripple that occurs during commutation events. However, both types of drive can achieve excellent transient performance by using the abilities of DSPs and FPGAs. The efficiency of a modern controller is typically higher than 90% because they are designed with switched mode techniques. The BLDC controller obtains lower switching losses by switching only one inverter leg at a time. This advantage may, however, be less rewarding than having the reduced machine loss of a PMSM.

The field orientation control (FOC) approach allows the d-axis and q-axis currents to be independently controlled. Sen [49] points out that for synchronous machines this has an advantage; the field strength can be quickly regulated by using the q-axis stator current component instead of waiting for the field excitation circuit to respond. In surface permanent magnet machines this is less useful because the magnets essentially increase the airgap length. This forces high currents to be used in regulating the field strength and therefore lower efficiency.

2.4.2 Current Control Methods

The current in an active phase of a BLDC machine is proportional to the torque produced by it. One type of VSD aims to control the output torque and therefore the current of the machine in the drive. In order to maintain high efficiency, a switching converter design is used in VSDs; this requires an output filter to produce steady currents or voltages.

Figure 2.7 shows the inductance of a BLDC machine in series with the generated EMF of each phase. The VSD can exploit this inductance by using it as the output filter of a converter that produces a controlled current. Thus the current in a phase branch can be efficiently controlled and the addition of an extra output filter element avoided.

Tight control of the exact current magnitude is achieved using one of three strategies, Mohan [37], pages 337 to 340, describes them as:

- Tolerance band control.
- Constant-"off"-time, peak detection control.
- Constant-frequency peak detecting, with turn on at clock time.

The current in an inductive element rises at a rate proportional to the

voltage present across it, according to the following equation:

$$V_L = L \cdot \frac{dI_L}{dt} \tag{2.1}$$

where V_L is the voltage across the inductor, L is the inductance of the inductor, I_L is the current flowing in the inductor and t is time.

Constant duty ratio pulse width modulation (PWM) is not considered a current control method because the voltage applied to the load is the variable being controlled. In this scheme large currents can arise from the natural response of the output filter, necessitating a current monitoring and control system. In practice, current control strategies use the same hardware as a constant duty ratio scheme.

The "Tolerance band current control" method, also called hysteretic control, is illustrated in Figure 2.10. When the current I_L exceeds level I_{high}, the voltage V_{lower} is applied to the output filter to drive I_L towards I_{low}. When I_L is less than I_{low}, the applied voltage is switched to V_{higher} that drives I_L towards I_{high}. The process then repeats. This method of control uses the current to be controlled, I_L, to make all decisions about what the applied voltage should be.

The "Constant-'off-time' current control" method, illustrated in Figure 2.11, applies V_{higher} until I_L reaches the threshold I_{high}, the current peak. Then V_{lower} is applied for a specific amount of time, t_{off}, called the off time; when that time has elapsed V_{higher} is once again applied, restarting the cycle. This method requires a monostable timing circuit to create t_{off}.

The "Constant-frequency with turn on at clock time" method, illustrated in Figure 2.12, applies V_{higher} at the beginning of every cycle of duration T. When I_L reaches I_{high}, V_{lower} is applied. The constant T makes this scheme operate at a constant frequency, f, given by:

$$f = \frac{1}{T} \tag{2.2}$$

If the current I_L is decreasing when V_{higher} or increasing when V_{lower} is applied, then the controller has lost control of the current. This situation can sometimes be remedied by changing the applied voltages using the switch states.

At each point where the applied voltage is changed from V_{higher} to V_{lower} or vice versa; parasitic circuit inductance, capacitance and resistance can cause transient currents in the measurement path which disturb the ideal operation described above.

In a BLDC machine drive that operates in more than one quadrant, the current controller may lose control of the current. If this condition could be detected, then the system could change the switching patterns for V_{lower} and V_{higher} to restore control.

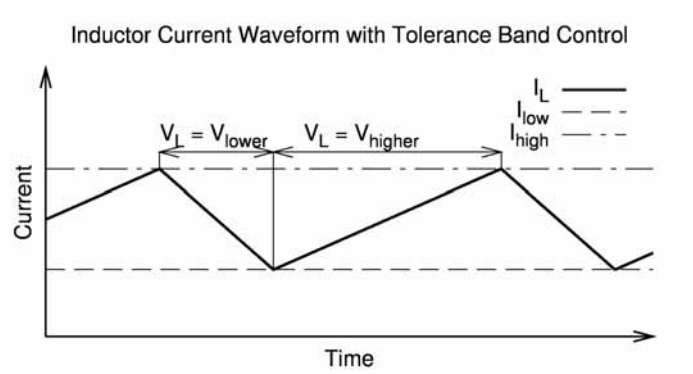

Figure 2.10: Tolerance band current control. The current plot I_L is kept between I_{low} and I_{high} by changing V_L to V_{lower} or V_{higher}.

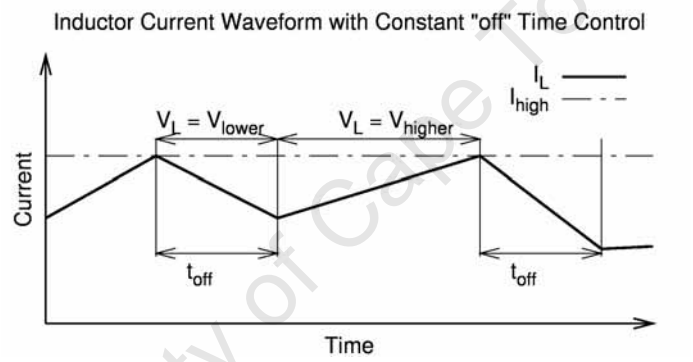

Figure 2.11: Constant "off-time" current control. I_L is increased by applying V_{higher} until the threshold I_{high} is reached. Then V_{lower} is applied for a fixed time, t_{off}. When t_{off} has elapsed V_{higher} is applied again.

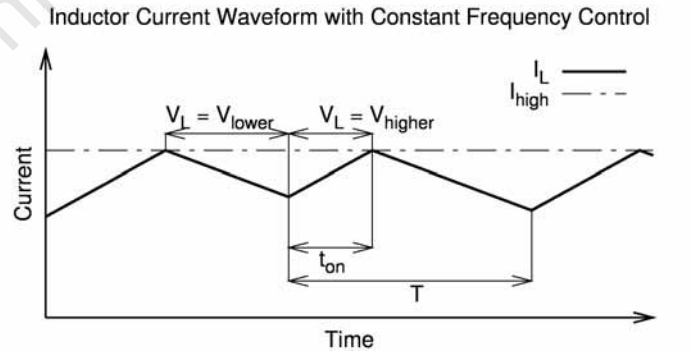

Figure 2.12: Constant-frequency with turn on at clock time current control. The application of V_{higher} from the beginning of a period causes current I_L to rise until reaching I_{high} when V_{lower} is applied until the beginning of the next period.

Table 2.3: Comparison of Different Current Control Methods

Method	Advantages	Disadvantages
Hysteresis Band	Easy to achieve 100% duty cycle and 0% duty cycle. Fastest possible response. Always using actual current for decisions. Can detect loss of control at any time. Current ripple is constant.	Wide variation in frequency range. However, stabilization can be implemented as discussed by Szepesi [53].
Constant off-time Peak Detecting	Less sensitive to switching events. Constant frequency operation possible with t_{off} adjustment.	Difficult to achieve 0% duty cycle because of the switch on after t_{off}. Average current is not directly related to the I_{peak} control variable. Unable to detect loss of current control during t_{off}. Wide frequency range of operation.
Constant Frequency Peak Detecting	Easier to design filter elements for constant frequency case. Less sensitive to switching transients.	Unable to detect loss of current control during t_{off}. Duty cycle is not always constant for constant output leading to sub-harmonic oscillation.

Table 2.3 compares the three current control schemes with the requirements of BLDC motor control in mind. In the above current control schemes, the situation may arise where the current is changing at a very low rate, which can lead to a large uncertainty about the precise moment that a switching event will occur. Often the switching pattern then contains a frequency component that is in the audible range and is therefore undesirable. To alleviate this problem, the current slope compensation technique effectively increases the rate of change of current, restoring the precision of switching events. Average current mode control [15] applies the principle behind slope compensation to obtain better performance over a wide current range.

2.4.3 Switching Topologies

There are two strategies for controlling the average voltage across a load in a switching converter that can apply bi-directional currents and voltages to the load. They are called bipolar switching and unipolar switching. The operation can be explained with reference to a standard H-Bridge circuit, Figure 2.13, but is also extendable to a bridge circuit with more legs.

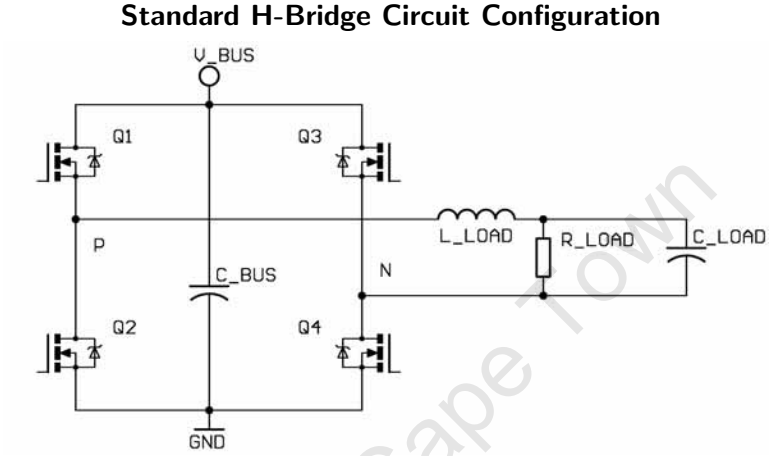

Figure 2.13: Standard H-Bridge Circuit Configuration. The inductor, L_{LOAD}, and the capacitor, C_{LOAD}, form a low pass filter that causes the load, represented by R_{LOAD}, to have a more steady voltage across it than the P and N nodes.

Bipolar Switching – The load is connected in one of two states:

- Q_1 and Q_4 are switched on, with Q_2 and Q_3 off; connecting P to V_{bus}, and N to V_{gnd}.
- Q_1 and Q_4 are turned off, Q_2 and Q_3 are turned on; connecting P to V_{gnd} and N to V_{bus}.

In this method both load and supply experience large ripple currents. The load sees a voltage of either $+V_{bus}$ or $-V_{bus}$. Thus the load current is always changing at a high rate. The current supplied from V_{bus} will be $+I_{LOAD}$ in one state and $-I_{LOAD}$ in the other. Thus the supply current has to accommodate a change of $2 \times I_{LOAD}$, twice each cycle.

Unipolar Switching – The load is connected in one of four states:

- P connected to V_{bus} and N connected to V_{gnd}
- P connected to V_{gnd} and N connected to V_{bus}
- P and N connected to V_{bus}
- P and N connected to V_{gnd}

> This strategy always passes through one case where the terminals of the load are connected together; so that for a positive load current the supply only experiences a unidirectional current draw. The supply current ripple is effectively halved. The load ripple current is also reduced because the full supply voltage is only applied to the load for one part of the cycle, the rest of the time the current is allowed to decay with $V_{LOAD} = 0$.

PMSM inverters use pairs of switches, such as Q_1 and Q_2, to control the average voltage at a point shared by the switches, such as P. The traditional way of creating a switch pattern for applying the desired average voltage to the machine was based on an analog comparison of a sine wave with a triangular modulating function. Now there is a digital method with many advantages over this analog technique.

Space vector pulse width modulation (SVPWM), first conceptualised in 1988 by Van der Broeck *et al.* [57], is the digitisation of analog sinusoidal modulation techniques. The calculation of switch duty cycles results in a sinusoidal PWM scheme that uses the DC voltage of the supply to the inverter to create undistorted line to line voltages with the greatest possible magnitude. This is similar to a regular sinusoidal technique with a triangular zero sequence modulating function [62], but one more advantage arises; the switching patterns used by SVPWM ensure that only one switch changes state at a time, and over one switching period attempts to minimise the current and flux distortion created by the voltage modulation process [57].

Bus clamping techniques for SVPWM, [56] and [40], apply the concept behind unipolar switching to a three phase bridge system. The number of devices switching in a period can be reduced using these methods, but the distortion of the current output increases. The combination of several bus clamping styles can accomplish a system where the switching losses are reduced even further by making sure the switches that are handling higher power are "bus clamped" [56].

The basic switching DC-DC converter topologies, buck and boost, can easily be realised using the full bridge shown in Figure 2.13. To implement buck or step down conversion, the switch Q_4 is permanently on and switch Q_1 is operated at a duty cycle D. The voltage at the output is then $V_{bus} \times D$. If the bottom switch, Q_2, is switched on when a current flows through it then the converter is called a synchronously rectifying buck converter. If the bottom switch is always on when the top switch is off, then the load current can be maintained at a positive or negative value.

A boost converter uses the energy stored in an inductor to create an output voltage that is higher than the input voltage. If the load components of Figure 2.13 are seen as the circuit supply, then the operation of Q_2 with Q_4 on will boost the voltage across C_{load} to V_{bus}. The same synchronous idea can be applied to the boost converter with Q_1 being operated as a

synchronous rectifier.

This means that if the load is a motor and operation of the switches is synchronous; then it is possible to achieve positive and negative motor currents, with no extra hardware. The circuit shown in Figure 2.13 can transfer energy from the load to the motor and vice versa, which means motoring and generating are possible.

Carrichi *et al.* [8] used a separate boost converter in an EV drive to increase the inverter bus voltage when the motor speed increased. The aim of this was to keep the current ripple smaller and achieve regeneration of the braking energy at higher speeds.

2.5 Energy Storage

Electric vehicles require a source of electrical energy to power their motors and control systems. Since the EV is a stand alone device it is impractical to use the electricity grid to supply all its demands. Portable energy storage like batteries, fuel cells and ultra capacitors have the potential to meet the requirements of an EV as a zero emission vehicle. Energy storage devices can be compared on the following criteria:

Energy Density is the amount of energy that the device can hold per unit mass or volume. The per unit mass figure is more meaningful in the EV case because mass affects range and efficiency more than volume.

Power Density is the amount of instantaneous power that a device can produce consistently. For batteries, incoming and outgoing power is different depending on the present level of charge and the technology used.

Endurance or life time, is how many times the device can store and reproduce its energy capacity. For batteries this figure usually improves if less energy than the maximum is extracted and replaced in each cycle.

Cost is measured per unit of power or energy to allow comparison between the energy storage devices.

Table 2.4 shows a comparison between some representative energy storage technologies. Petrol is listed in the table to illustrate the challenge that electric systems have in competing with fossil fuel systems.

The high energy density supercapacitors are a new development that may be a significant motivator to electric vehicles. With very high power densities, a supercapacitor system could be comparable to a fossil fuel or fuel cell system in terms of power in and out of the energy storage system.

Table 2.4: Energy and Power Density, Endurance and Cost of Energy storage

Type	**Energy** $Wh\,kg^{-1}$	**Power** $W\,kg^{-1}$	**Endurance** in Cycles	**Cost**[1] R Wh^{-1}
Lead Acid battery [45]	18 - 40	25 - 80	200 - 600	R 2.00
Nimh battery [17]	40 - 85	200 - 600	2 000	R 9.00
Li-polymer battery	60 - 130	300 - 2 800	600	R 13.00
Super Capacitors [34][61]	2-30	150 - 5 100	200 000	R 1 000.00
H_2 fuel cell[2]	33 600	$8.4MW\,\ell^{-1}s^{-1}$	N/A	R 2 380·10^{-6}
Petrol[2]	12000	$34MW\,\ell^{-1}s^{-1}$	N/A	R 677·10^{-6}

[1]These figures are obtained by converting the US$ prices into Rand prices.
[2]The conversion of fuel into useful work is around 20% to 25% in a vehicle; for a comparison to other energy supplies this should be taken into account.

2.6 Energy Storage Management

Battery technologies each have specific charge and discharge characteristics. A system that observes the limitations of the battery technology used will achieve better lifetime and efficiency. For batteries in an EV situation, a mechanism for controlling the power output and power input during motoring and regenerative braking must be aware of the limits of the battery.

The supercapacitor technology behaves like a capacitor where charge and discharge rates can be very high and can be repeated often without damaging the device. Virtually no conditioning of the input and output of energy flow is necessary for this type of energy storage.

Yen and Patterson [59] proposed a energy management scheme that combines the supercapacitor with a battery technology to achieve an overall energy supply system with high power ability and high energy density. To quantify this kind of energy supply system driving cycle analyses are consulted to determine the typical energy and power demands. Lin [32], proposed a fuel cell powered electric scooter. An urban driving cycle was used to determine the size of peak power demand battery packs that would allow a reduction in the fuel cell size and therefore the cost as well.

On many industrial drives a heating element is used to dissipate excess energy when the drive speed is forcefully reduced. This heater, called a dump load, could be employed in an EV situation as a last resort for circumstances that arise on exceptional occasions. This might offer a level of safety for energy storage methods that are intolerant to overcharging.

Chapter 3

Hardware Design

An electric machine converts electrical energy to mechanical energy. On the one side is an electrical system that provides the terminal current and voltage; on the other side a mechanical system coupled to the torque and speed of the machine.

Figure 3.1 is drawn with reference to a direct current (DC) machine. In an electric machine, the effect of resistance creates operation points where energy is absorbed from both the mechanical and the electrical external systems. This is labelled *active braking*.

The generating zones are where V_T is of opposite polarity to I_{arm} and ω_m is of opposite polarity to T_m. Here power flows from the mechanical system to the electrical system. In an EV application, operation in the generating zone would be called regenerative braking, since the effect of such operation is to slow down the mechanical system and regenerate electrical energy that was expended to accelerate the mechanical system.

The areas where V_T, ω_m, T_m and I_{arm} are all in the same polarity are motoring areas. In the BLDC machine the symbols V_{bldc} and I_{bldc} have the same meaning as the DC brushed machine variables, V_T and I_{arm}.

The VSD in this project must be capable of operation in the zones where V_{bldc} and ω_m are both > 0. This excludes the active braking region where V_{bldc} is negative. In order to achieve a negative V_{bldc}, the effective armature terminals of the brushless direct current (BLDC) machine are swapped.

The design has to accommodate the following practical points on the machine and other components available for this project:

- The input voltage of between $35V$ and $40V$ is from a battery.
- The motor is a trapezoidal back EMF BLDC type.
- The motor is equipped with three open collector digital Hall effect rotor position sensors, in a $360°ed/n$ configuration.
- The control input or throttle signal is derived from an angular position sensor that produces a $1V$ to $4V$ signal.

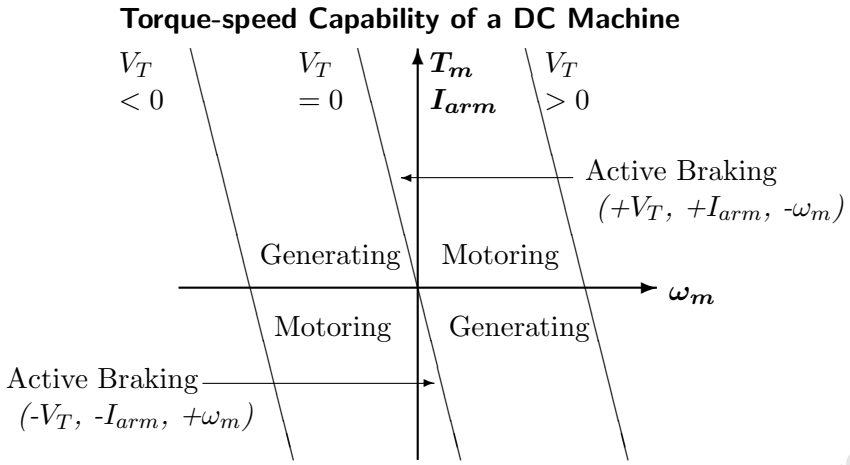

Figure 3.1: The torque-speed capability of a DC machine, shown above, is limited by physical factors. Maximum speed is limited by mechanical stresses, electrical insulation and resistance. Maximum torque is limited by magnetic strength, thermal design, and mechanical size. The resistance of the winding material causes the terminal voltage of a DC machine to deviate from the generated EMF at non zero output torque. "Active Braking" zones arise where both electrical and mechanical energy are dissipated within the machine.

3.1 Overview of Two Quadrant Design

The design of the variable speed drive (VSD) is shown in block form in Figure 3.2, and in electric circuit schematic form in Figures 3.3 and 3.4; thin arrows represent low power signals and thick arrows represent high power signals. The current controller block gets feedback from the current sensor, which is positioned to detect the effective machine current, I_{bldc}. The phase switcher directs the current supplied by the previous stage into the correct machine phases based on the information provided by the rotor position sensors. In the event of an overload, the temperature sensor triggers a shutdown state in the phase switcher.

The metal oxide semiconductor field effect transistor (MOSFET) driver power supply is shared by the two modules. The MOSFET driver requires an input voltage greater than $7.5V$, and the logic and analog components are separately supplied with $5V$.

The logic of the current controller and the phase switcher are isolated from each other, as it is with the mechanical commutator and controller for a brushed DC machine. This is shown in Figure 3.2 by the one thick arrow joining the current controller and the phase switcher, indicating only a high power connection exists between the two parts.

This arrangement of components is good at dealing with the way current flows during a commutation event. The simulated results in Section 5.2.2 discusses the advantages of this approach.

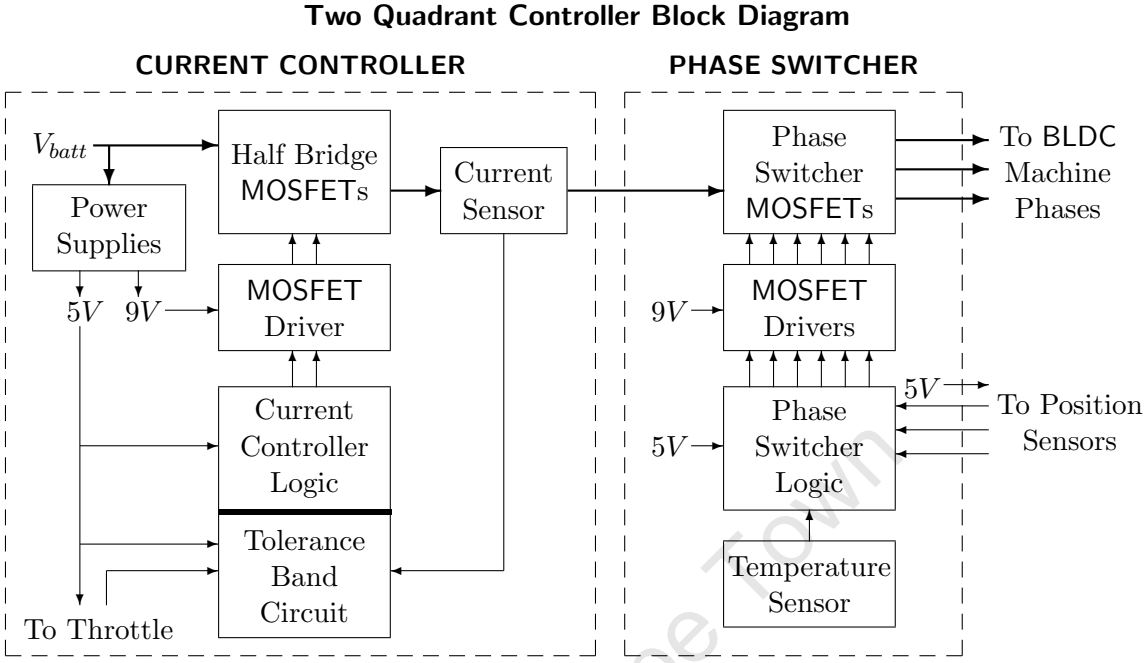

Figure 3.2: The two quadrant controller is arranged as two modules, the current controller and the phase switcher. The current sensor is only used by the current controller and the rotor position sensors are only used by the phase switcher. The temperature sensor is connected to the phase switcher where it can implement a shut down of the VSD.

3.2 Power Supplies

The MOSFET drivers used in this project are the LM5101 devices from National Semiconductor. In order to operate properly, a minimum of $7.4V$ [42] must be maintained at the V_{DD} terminal of the device. This requirement makes it incompatible with analog and logic devices that operate from a $5V$ supply. Therefore a separate voltage source is needed for the MOSFET drivers and the analog and logic devices.

The power supply for analog parts should be as stable as possible so that analog signals keep their form. The disturbance produced by a switched mode power supply (SMPS) is undesirable in this situation. The source of energy to the whole VSD is a battery with a terminal voltage of $35V$ to $40V$, as mentioned at the beginning of the chapter. Both linear and switched mode supplies are good at producing an output voltage lower than the input voltage. Unfortunately the linear supply is inefficient and the switching supply introduces high frequency noise into the circuit.

In the VSD proposed, the control circuitry is designed with low power in mind, therefore the linear supply is an option worth considering. Even though the proportion of power wasted is high in a linear supply, the total

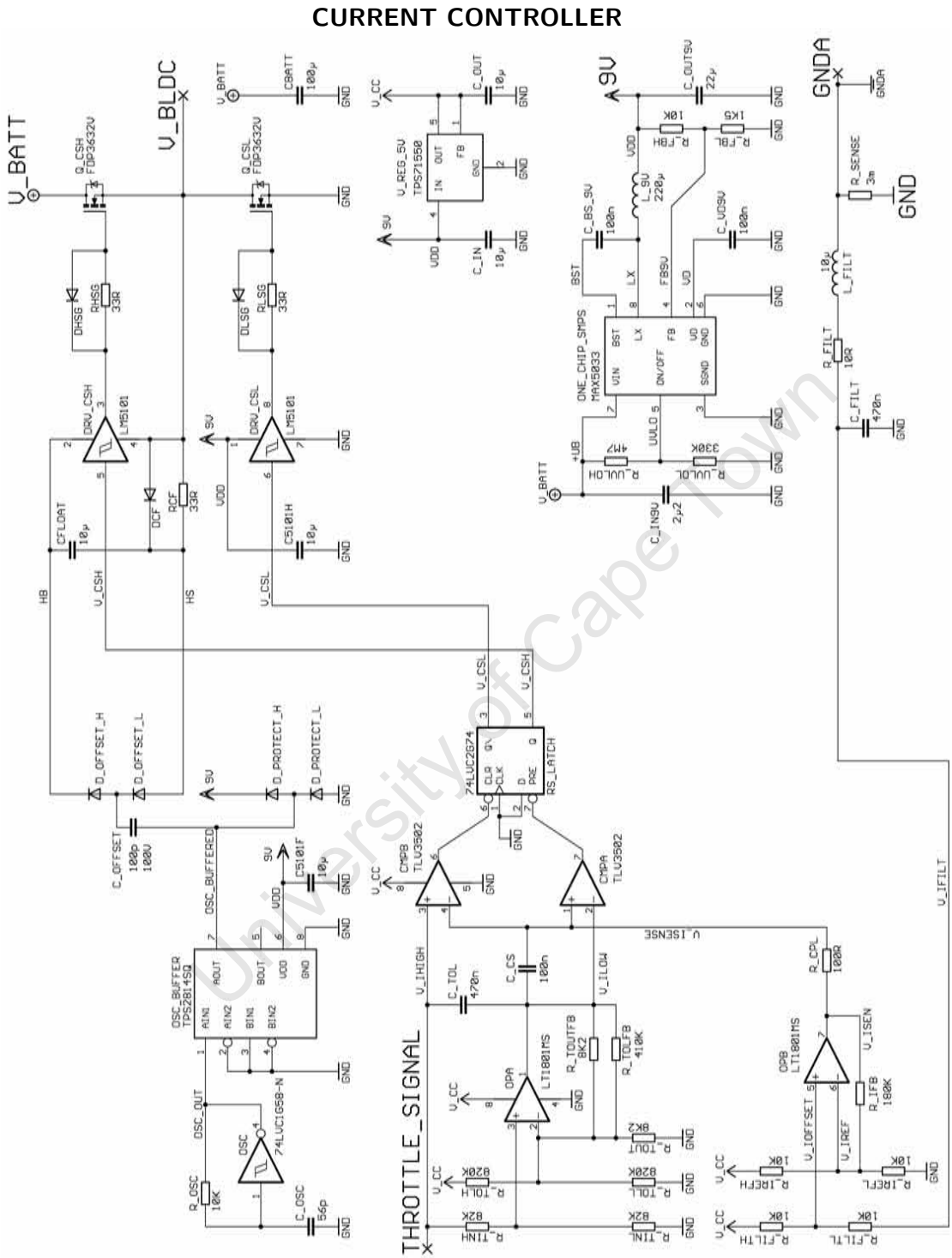

Figure 3.3: The complete current controller circuit diagram is shown above. The larger labels indicate the connections that the module makes with the outside world. All the circuits in this diagram are individually explained in the Hardware chapter.

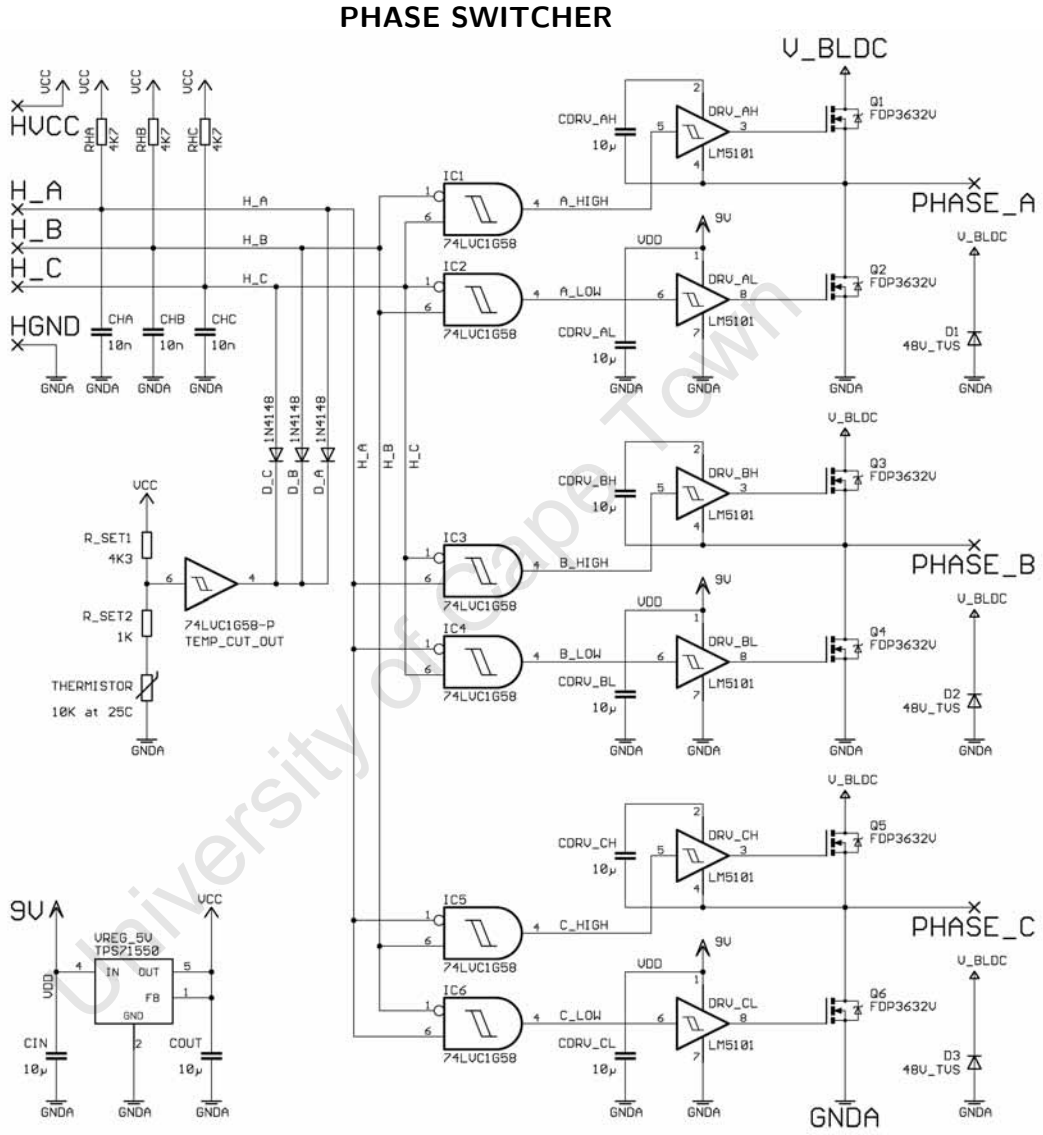

Figure 3.4: The complete phase switcher circuit diagram is shown above. The larger labels indicate the external connections. All the circuits in this diagram are also individually explained in the Hardware chapter.

Table 3.1: Comparison of Different Power Supply Arrangements

Advantages	Disadvantages
SMPS only	
Most efficient. Low heat produced by power supplies. Accepts high input voltages.	Switching noise can reduce signal to noise ratio in analog sections. Large circuit area required. Regulation and stability at light loads gets worse. Slower response to transients.
SMPS with Linear	
SMPS makes efficient step down for MOSFET supply. Linear supplies powered from MOSFET supply waste less energy. Still accepts high input voltages. Quick response to low voltage transients. Less low voltage noise than SMPSs.	Switching noise is still introduced into the low voltage circuits.
Linear only	
Linear supplies simple to set up. Response to disturbance is quick. Accurate output voltage at all loads. Low noise in output and low idle current.	Large proportion of energy wasted as heat to achieve the correct output level with high input voltages. Heat build up can limit operational range.

power used is small and the system is simple and robust.

Switching converters have larger quiescent currents than comparable linear regulators. However, technological improvements are reducing control circuit power consumption, and resonant converters exist that use additional energy storage components to virtually eliminate the transients that cause undesirable disturbance.

Table 3.1 compares the situations where different types of supply are used to meet the power needs of the VSD control circuits. The MOSFET drivers are less sensitive to supply noise, indicating a switching supply to be adequate . The analog circuitry is not as tolerant and would perform better with a linear supply. The mixed solution with a SMPS stepping down the battery voltage, and a linear regulator providing the $5V$ source, gets the best of both worlds. A high voltage input is still possible, and the linear supplies waste less energy because the input voltage is much lower than the battery voltage.

The charge pump supply is used to ensure that 100% duty cycle is possible on the high side switch of the current controller described in section 3.4.

Based on the datasheets of the parts, the power supply requirement was

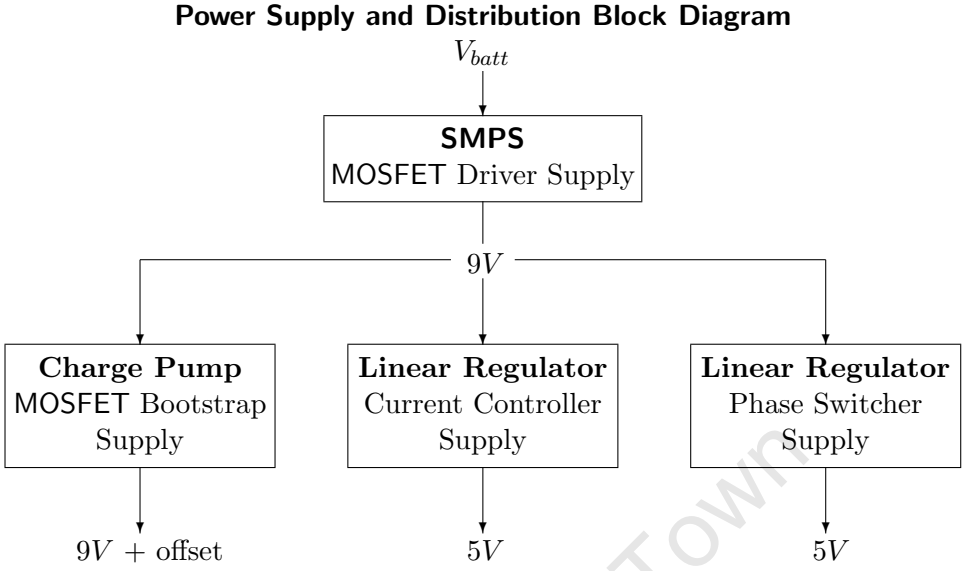

Figure 3.5: Power supply and distribution in the VSD is based on a hybrid SMPS and linear regulator approach. The battery voltage is stepped down to the MOSFET driver level by a switching converter and then further reduced by linear regulators to provide power to analog and logic devices.

calculated at $59mA$ from the MOSFET supply, of which $51mA$ is used by $5V$ regulators.

3.2.1 MOSFET Driver Supply

The MOSFET driver is creates a high power gate drive signal from a low voltage digital input signal. The driver integrated circuit (IC) has a mechanism to prevent operation if the voltage supply to the output buffer is below the level that ensures complete switch on of the MOSFET. The quality of this supply voltage is less critical than the quality of a supply for analog components, as long as the minimum voltage requirement is met. A switching regulator is therefore satisfactory for these devices. Furthermore, linear regulators for the analog and logic circuits will have improved efficiency when using the MOSFET driver supply as their source.

Nowadays, semiconductor manufacturers are increasingly concerned about creating energy efficient solutions and offer many innovative devices for power conversion. The single chip SMPS from Maxim-Dallas Semiconductors was selected for creating a $9V$ supply for the MOSFET drivers because it can operate with high input voltages, has low quiescent current and is easy to set up.

The MAX5033 has an ON/OFF pin used to activate the device. This pin has a Schmitt trigger built in; the chip is activated by a positive voltage greater than $\approx 1.69V$ [36], and only deactivated once the voltage at the

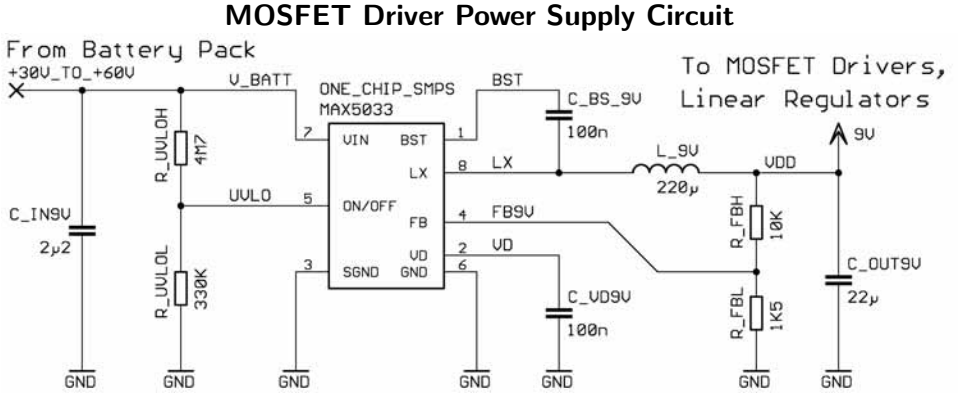

Figure 3.6: The MAX5033 is configured here as a $9V$ supply for the MOSFET drivers. The single chip solution simplifies implementation and achieves high efficiency operation. This IC manages its own bootstrap supply for the power switch and works off input voltages of up to $76V$ [36].

pin falls $100mV$ below the switch on voltage. In Figure 3.6, the resistors R_{UVLOL} and R_{UVLOH} are chosen to cause switch on at $\approx 25V$. The voltage at which operation ceases is then $\approx 23.5V$. In order to protect the battery from excessive discharge the values of R_{UVLOL} and R_{UVLOH} can be chosen to cause turn on or off at any voltage. The unequal turn on and turn off thresholds ensure that switch on or off is less sensitive to input voltage fluctuation caused by the act of switch on or off.

The resistor divider R_{FBL} and R_{FBH} sets the voltage on FB_{9V} to $1.22V$ [36] when the output is at the desired voltage. The ratio $^{R_{FBL}}/_{R_{FBH}}$ is given by:

$$\frac{R_{FbL}}{R_{FbH}} = \frac{V_{Fb_{9V}}}{V_{DD} - V_{Fb_{9V}}} = \frac{1.22V}{9V - 1.22V} = \frac{1.22}{7.78} \approx \frac{1.5}{10} \tag{3.1}$$

Figure 3.6 shows R_{FBL} and R_{FBH} set at $1.5k\Omega$ and $10k\Omega$ respectively, to give an output voltage of $9.35V$. The feedback resistors also provide an electrical load to the regulator that helps to improve stability by increasing the damping factor of the L-C output filter.

The inductor L_{9V} was chosen using the typical operating circuit as a guide. The C_{In9V} and C_{Out9V} capacitors are smaller than those in the typical operating circuit on the datasheet because other capacitors in the system combine with them and surpass that value.

The LM5101 MOSFET driver uses an external bootstrap capacitor and internal diode, shown in Figure 3.7, to provide power to the upper switch of a half bridge configuration. The bootstrap capacitor is charged whenever the lower switch is turned on. However, in the current controller design it is necessary to hold the upper switch of a MOSFET half bridge in the on state for extended periods of time. The bootstrap capacitor discharges over

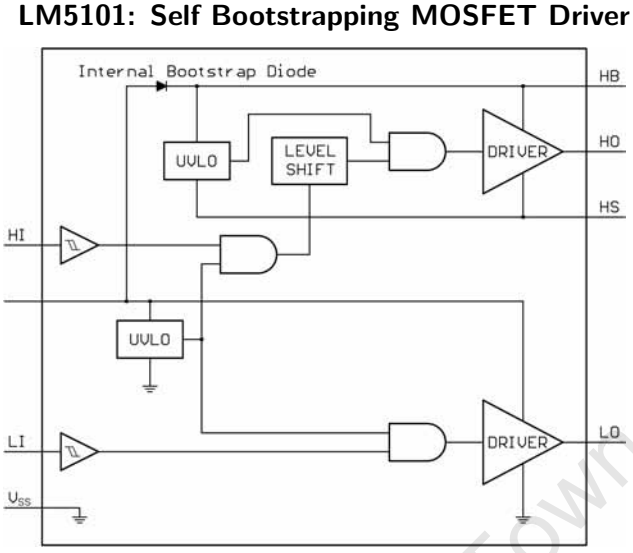

Figure 3.7: Taken from the LM5101 datasheet [42]. The LM5101 MOSFET driver IC uses an internal diode to recharge the capacitor between HB and HS whenever the switch connected to LO is on.

time because of the quiescent current of the MOSFET driver, limiting the maximum time that the upper switch can be continuously on.

An extra bootstrap power supply is necessary to allow the upper switch to remain on indefinitely. The supply has to be able to create the minimum operating voltage, which is $7.1V$ according to the datasheet [42], at the power pins of the upper MOSFET driver. The negative power pin for the upper driver can have a voltage, compared to the circuit ground, of anywhere between $-0.7V$ and V_{batt}. Similarly, the positive power pin on the upper driver, during normal operation, varies by the same amount but with an offset of at least $7.1V$. During operation of the switches in a half bridge, the voltage offset of the upper MOSFET driver changes rapidly from one extreme to the other. Whatever type of supply is used to provide it, power must be able to tolerate this type of transient while not inhibiting the speed of the transient significantly. The efficiency of a switching supply is dependant on the speed of the transition from one switch being on, to its complement being on.

There are several options for the bootstrap supply needed in the VSD.

Low Voltage Transformer A transformer provides isolation from the large voltage differences between the input and output circuitry.

Boost Converter A boost converter creates voltages greater than its input that could be used to supply the power pin of the upper driver.

Half Bridge Control A system could be made that interrupts the on time

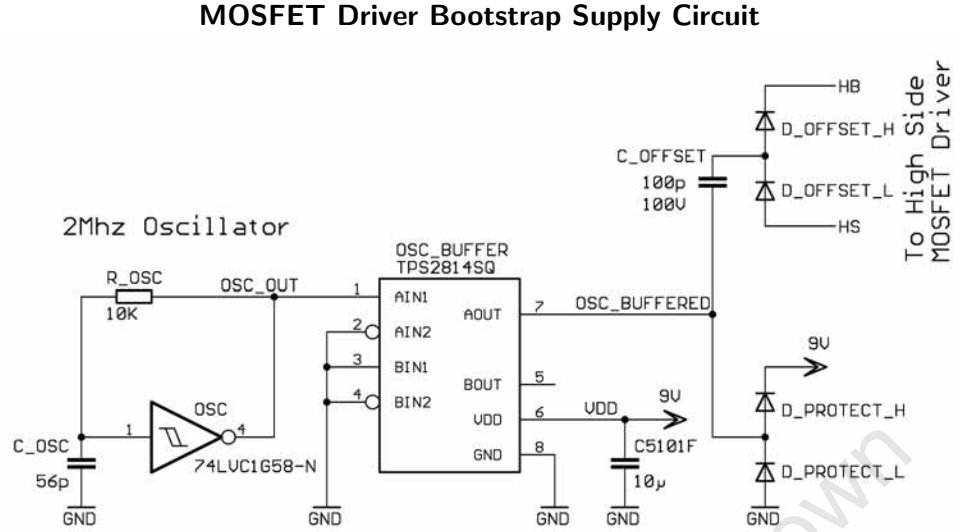

Figure 3.8: The bootstrap power supply combines three operations. First OSC generates a frequency. Secondly OSC_{buffer} translates this into a higher power square wave signal. Finally, the capacitor, C_{offset}, shifts the square wave by the voltage difference V_{HS} to V_{gnd}, where it is rectified to produce the level shifted supply V_{HB-HS}.

of the upper switch briefly, so that the bootstrap capacitor can quickly be recharged.

Auxiliary Half Bridge An auxiliary half bridge can be used to pump charge up to the upper driver while it is on.

Charge Pump A capacitor can be used as a charge pump to supply the upper driver.

The capacitor charge pump idea, described in Horowitz and Hill pp. 377 [20], was the most appropriate solution in this case because the amount of power needed by the upper driver is small; $0.2mA$ is drawn by the MOSFET driver at $7.1V$, totaling $1.42mW$. Another reason to use the charge pump idea is the high effective resistance of the link between the input and output.

The charge pump is an unregulated voltage translator, it shifts a fixed voltage from one potential to another but has an effective series resistance. The impedance of a capacitor at a given frequency, f, is given by the equation:

$$X_C = \frac{1}{fC} \tag{3.2}$$

Since the MOSFET driver power supply produces $\approx 9V$, the OSC_{buffer} in Figure 3.8 can be expected to output a square wave of that amplitude. The

diodes $D_{offset\,L}$ and $D_{offset\,H}$ each drop about $0.5V$, thus the allowable effective resistance of the capacitor C_{offset} is:

$$X_C = R_{internal} = \frac{9V - 7.1V - 2 \times 0.5V}{0.2mA} = 4500\Omega$$

From Equation 3.2, the compromise between the capacitor size and the frequency of oscillation for a fixed impedance is evident. An acceptable compromise was found with a frequency of $2MHz$ and a capacitance of $100pF$, leading to an impedance of around $5k\Omega$. Although the maximum desired impedance for the capacitor is lower than $5k\Omega$, that calculation was done for the cases where the bootstrap supply had to overcome the MOSFET driver minimum switch-on threshold. The bootstrap supply can afford a further $0.4V$ droop in output voltage before the driver actually turns off. In addition to that, the typical operating power consumption of the driver is much lower than in the case stated above, which is an extreme example.

The Schmitt trigger thresholds in the inverter gate, and the resistor R_{OSC} and the capacitor C_{OSC} all affect the frequency produced by the oscillator. From the datasheet, the thresholds of the inverter are about 20% of the supply voltage apart, near the middle of the supply voltage range. The frequency produced by the arrangement in Figure 3.8 is approximately given by:

$$f = \frac{1}{0.8 \cdot R_{OSC} \cdot C_{OSC}} = \frac{1}{0.8 \cdot 56pF \cdot 10k\Omega} \approx 2.2MHz$$

The diodes $D_{protect\,H}$ and $D_{protect\,L}$ are in place to prevent damage to the OSC_{buffer} output.

3.2.2 Logic and Analog Supplies

The analog components are sensitive to power supply variations, especially if they are quick transients, like the type found in a switching regulator. Linear regulators are thus chosen for the purpose of powering the more sensitive analog circuitry. Low power linear regulators have corresponding low input voltage limits and low current limits. The MOSFET driver power supply conveniently provides a suitably low voltage for powering these regulators. There are linear regulators that will work off high voltage supplies [35] but they waste more power than connecting a linear regulator to an intermediate voltage like that produced by the MOSFET supply. Figure 3.9 illustrates the small number of components required to set up a linear regulator; the input capacitor, the output capacitor and the regulator itself.

The efficiency advantage to first using a switching converter and then a linear regulator is large. Consider the power loss for a linear regulator with negligible bias current compared to the load. The efficiency is given by

$$\text{Efficiency} = \frac{P_{out}}{P_{in}} = \frac{5V \times I_{load}}{V_{batt} \times I_{load}} = \frac{5}{35} = 14\% \tag{3.3}$$

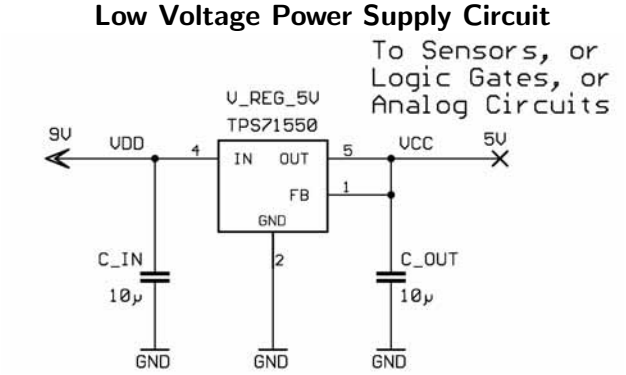

Figure 3.9: $5V$ Supply using a Linear LDO Regulator. The only components needed for operation are the input and output capacitors.

And now the power loss in total when a switching converter of 80% efficiency first provides a $9V$ source:

$$\text{Efficiency} = \frac{5V \times I_{load}}{(9V \times \frac{1}{0.8}) \cdot I_{load}} = 44\%$$

Approximately three times less input power is now required for all the logic and analog circuitry. The LDO type of linear regulators offer very low quiescent currents, of the order of a few μA, ideal for saving power.

The link between the current controller and the phase switcher is made by the sense resistor, preventing the accurate transfer of the $5V$ supply to between the two parts. Luckily the voltages present across the sense resistor are small, of the order of $\pm 150mV$, such that the $9V$ supply can be directly linked to it without compromising operation of the MOSFET drivers or the linear regulator. The phase switcher and current controller therefore each have their own linear regulator to supply their respective $5V$ components.

3.3 Sensor Interface

The sensor interface relays the measurements made by transducers to the controller in a way that the controller can easily interpret it.

The controller is powered with a $5V$ regulator, and so the sensor interface must level shift and scale the transducers' outputs to an appropriate level.

The transducers used in the sensor modules are:

- Rotor position sensor : Digital open collector Hall sensors
- Current sensor : Sense resistor
- Temperature sensor : Thermistor

3.3.1 Rotor Position Sensor

The Hall sensors were built into the electric machine, as illustrated in Figure 3.10. They are positioned to produce the $360°ed/n$ type of outputs shown in Figure 2.8(a), described in Section 2.3.1.

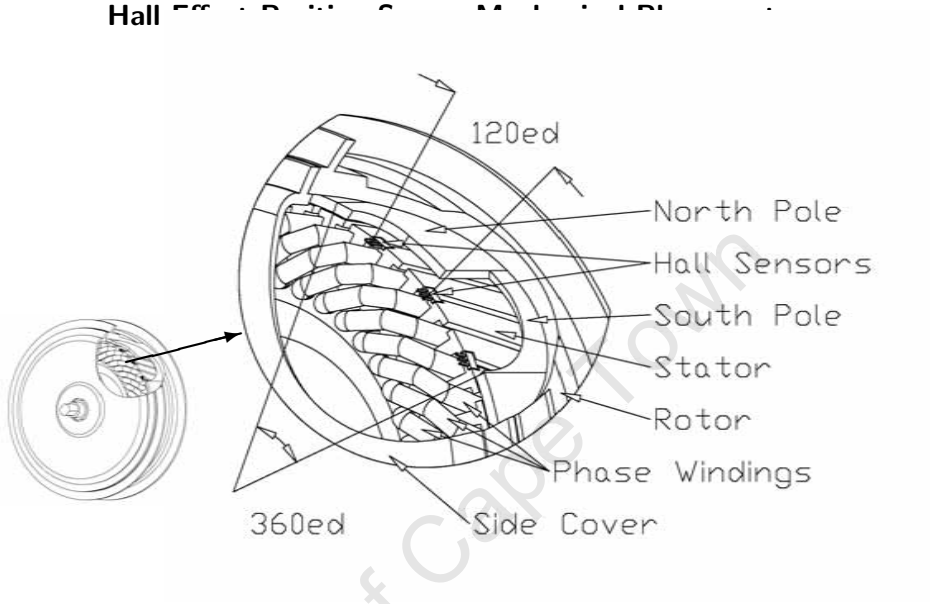

Figure 3.10: The Hall effect Postion sensors are placed $120°ed$ apart in the machine used in this project. One pair of north and south magnets covers $360°ed$, which in this machine, that has 8 poles, covers 45° mechanically. The skew in the stator slots is also visible in the diagram.

The CS 3075 Hall effect sensors used in the machine have open collector outputs. The logic gates that make up the phase switcher in Section 3.5 have Schmitt triggers on their inputs. The connection between them uses a pull up resistor to enable the sensor to output a logic high, and a small capacitor in parallel to help prevent the logic gate from responding to glitches caused by electric and magnetic coupling to nearby machine windings.

The size of the pull up resistor and glitch suppression capacitor were determined by trial and error during experimentation. The resistor size affected the power consumption of the position sensor system and the signal to noise ratio; a lower resistance increased power consumption and signal to noise ratio simultaneously. The capacitor made little difference to the fall time of the signal but increased the rise time because of the open collector output. The glitches were reduced in magnitude by the presence of the capacitor, allowing a smaller resistor to be used for the same signal to noise ratio. The resistor value was traded off with the capacitor size to balance the signal delay and the power consumption while maintaining good signal strength.

The pull up resistor was $4.7k\Omega$ and the capacitor was $10nF$. The resulting time delay from when the Hall sensor changes state to when the logic gate detects the change is $36\mu s$. This causes a phase shift of $0.5°ed$ at the maximum speed of the BLDC machine when run with a $36V$ battery pack. The error is proportionately smaller at lower speeds.

The open collector outputs cause the rise time of the Hall sensor signal to be dominated by the pull up resistor and capacitor, but the fall time of the signal depends on the current limit of the output transistor in the Hall sensor device instead. The output current limit in the CS-3075 is $20mA$; resulting in a fall time of about $1.5\mu s$, making the phase shift on the falling edge of a Hall sensor change about $0.02°ed$.

3.3.2 Temperature Sensor

The temperature sensor is required to generate a signal when a certain temperature has been reached. The literature review promoted the thermistor as the most suitable type of sensor for this application.

The aim of the temperature sensor is to protect components from destructive heat levels. The intended location for the circuitry was within the casing of the electric machine. With the circuits attached to the material of the stator, the heat levels in the circuitry and the machine became similar. Therefore the temperature sensor design was integrated into the phase switcher circuit.

Each phase switcher MOSFET has one logic gate with input signals from two position sensor signals. The logic function of this gate, in Figure 3.22, is an **AND** gate with one input inverted. It has a logic low output if both of the inputs are high or if both the inputs are low. Either of these cases turns off the associated MOSFET.

Since the Hall sensor devices have open collector outputs, it is possible to ensure a logic low output by externally forcing the output to ground; without conflicting with the Hall sensor. The temperature cut out circuit, shown in Figure 3.11, uses diodes D_A, D_B and D_C to simulate open collector outputs so that when the temperature threshold is reached, all the Hall sensor outputs are driven to logic low. The combining of open collector outputs in this way behaves like an **AND** gate. This wired **AND** arrangement has the effect of switching off all the MOSFETs in the phase switcher and prevents the electric machine from receiving any power from the battery.

The temperature sensor is built around the same multi-function gate as the phase switcher logic. The SN74LVC1G58 from Texas instruments has input Schmitt triggers that give the temperature sensor different cut out and re-enable thresholds. The resistance of the thermistor decreases when it heats up, which causes the voltage at pin 6 (the input of the Schmitt trigger inverter in Figure 3.11) to decrease. When the input threshold is crossed, the gate output transitions to logic low. The re-enable process is

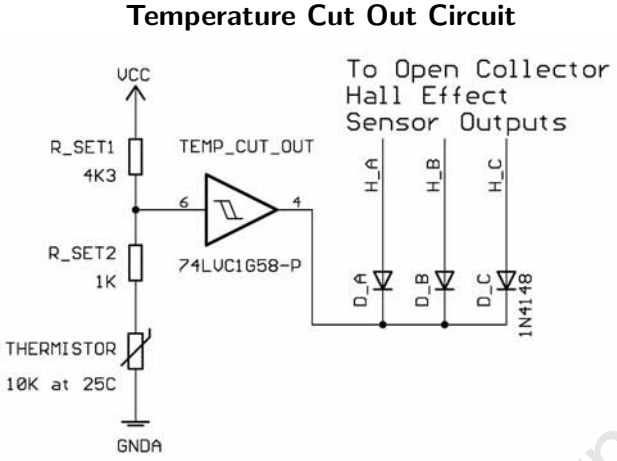

Figure 3.11: Temperature cut out circuit. The temperature cut out and re-enable points are decided by R_{set1}, R_{set2} and the thermistor used. The output is made to behave like multiple open collector outputs by D_A, D_B and D_C before being interfaced with the Hall sensor outputs.

the reverse of the cut out process.

The values of R_{set1} and R_{set2} are calculated for the case of a thermistor that has $10k\Omega$ resistance at $25°C$. To set the temperature trip points, the input thresholds of the gate and the thermistor resistance at certain temperatures, must be known.

The logic gates had the lowest *maximum recommended operating temperature*, $85°C$, of the components in the phase switcher. The temperature cut out point was set at $80°C$ to protect the gates. The re-enable point was set at $50°C$ to ensure that the system had properly cooled off before attempting operation again.

The input thresholds for the logic gate were obtained by interpolating information in the data sheet; typical values were estimated to be $0.54 \cdot V_{CC}$ for the rising threshold and $0.37 \cdot V_{CC}$ for the falling threshold.

The relationship of temperature to resistance in the thermistor was calculated using the Steinhart-Hart equation, reproduced in the Agilent Technologies application note [2]:

$$\frac{1}{T} = A + B \cdot ln(R) + C \cdot (ln(R))^3 \tag{3.4}$$

where A, B and C are constant coefficients, T is the temperature on the Kelvin scale and R is the resistance of the thermistor in ohms. At $80°C$, the resistance of the $10k\Omega$ thermistor was $\approx 1500\Omega$; at $50°C$ the resistance was $\approx 4100\Omega$.

The voltage at the input pin of the gate, pin 6 in Figure 3.11, can be

calculated using the resistor divider equation:

$$\frac{R_{set2} + R_{thermistor}}{R_{set1} + R_{set2} + R_{thermistor}} = \frac{V_6}{V_{CC}} \tag{3.5}$$

The calculated values of R_{set1} and R_{set2} are 4345Ω and 1026Ω respectively. The nearest standard resistor values are $4.3k\Omega$ and $1k\Omega$.

In the extreme situation, where input threshold levels and 5% resistors are at their most deviant, the temperature cut out point varies from $101°C$ to $67°C$, while the re-enable temperature varies from $38°C$ to $62°C$.

The current flowing in the resistor divider causes heating in the thermistor that can change the temperature measurement. This power dissipation is acceptable if the error is less than $1°C$. The thermistor would have a significant error in free air, but the leads make good thermal contact with the phase switcher, resulting in negligible error.

3.3.3 Current Sensor

The current control methods depend strongly on an accurate current sensing method to achieve torque control. The sense resistor and MOSFET on resistance methods are most attractive to achieve current control with a minimum of extra circuitry. However, as Zhang *et al.* [60] pointed out, the variation of on resistance of a MOSFET is large and requires compensation to achieve an accurate result.

Motorola application note AN894 [31] claims that a current sense resistor is only practical if the measured current is going to be less than approximately $20A$; because heat dissipation in the sense resistor becomes unmanageable at higher currents. The use of a lower valued resistor may solve the problem of power dissipation at high current, but there is a disadvantage. The leakage inductance present in a resistor allows high speed current changes, typical in switching converters, to produce voltages across the sense resistor that are much greater than the steady state values. The moment a switch changes state, a low energy but high speed current transient is often generated, which can easily be observed across the sense resistor. The size of the transient voltage across the sense resistor is a function of the speed of current change and the leakage inductance of the sense resistor arrangement. The leakage inductance of the sense element only depends on its size and shape, therefore the transients from short current spikes often have constant magnitude, independent of resistance, and the signal to noise ratio is degraded when lower resistances are used.

The battery used is capable of supplying approximately $1kW$, therefore the VSD must be able to handle $1kW$ also. Since

$$P = I \cdot V = \frac{V^2}{R} = I^2 \cdot R \tag{3.6}$$

and the battery voltage is between 35 and $40V$, the required current capability of the VSD is:

$$I = \frac{P}{V} = \frac{1000W}{40V \text{ to } 35V} = 25A \text{ to } 29A$$

Based on the expected driving cycle for an electric vehicle (EV), the current sense element would only handle this amount of current briefly and intermittently. The continuous power rating of the BLDC machine is $400W$, giving an average sense resistor current of $10A$ to $12A$. Thus a sense resistor would provide an acceptable current sensing mechanism.

The current controller module is designed to receive a single voltage signal that represents the current. Specifically the point at which the current in the electric machine is zero must to correlate to $^{V_{CC}}/_{2}$, and a $1A$ change in machine current should cause a $50mV$ change in the voltage signal from the sensor. Whenever a power switch changes state in the controller, a transient is generated and often superimposes itself on the current signal; it is part of the current sense module to reduce these disturbances to an acceptable level.

The BLDC machine is first connected to the phase switcher module, which uses $Q1$ through $Q6$ to transform the machine phase connections into DC machine armature connections. The current sense module is placed after this transformation has taken place to simplify measurement and interpretation of the current signal.

Figure 3.12 shows the three stages of signal conditioning in the current sense module. Firstly, a sense resistor is used to convert the current flowing through it into a voltage. Next, a passive filter is used to reduce the switching transient magnitude. Finally, the signal is amplified and offset so that $0A$ is represented by $^{V_{CC}}/_{2}$, that is $2.5V$.

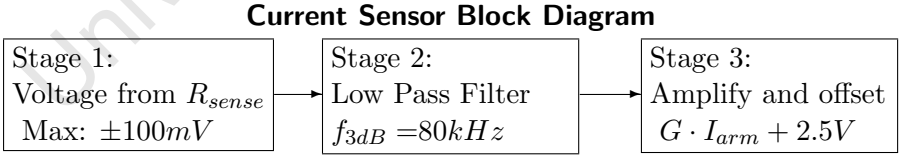

Figure 3.12: The stages of current measurement in the brushless DC VSD

A $3m\Omega$ resistor was used to sense the current flowing through the motor. The maximum power dissipation of

$$P_{max} = I_{bldc}^2 \cdot R_{sense} = 30A^2 \times 3m\Omega = 2.7W$$

occurs at the maximum motor current, $\pm 30A$. The MOSFETs used as the power switches were FDP3632s that have a nominal R_{ON} of $9m\Omega$, causing them to dissipate three times the power that the sense resistor does at the

same current level. In future work, the MOSFET R_{ON} could be used to sense current, eliminating the power dissipation of the current sense resistor. The sense resistor had a maximum power dissipation of $5W$. The voltage present across the resistor per amp flowing through it is $3mV/A$, obtained using Ohm's law. The amplifier then has the task of implementing a gain of:

$$\frac{50mV/A}{3mV/A} = 16\tfrac{2}{3} \tag{3.7}$$

The position of the current sense element has one significant disadvantage; the MOSFET has capacitance present between the drain and source terminals. Figure 3.15 shows the node V_{bldc} connected to the top of the phase switcher inverter bridge. The voltage at V_{bldc} changes from V_{gnd} to V_{batt} rapidly in order to achieve high efficiency. The result is that the drain-source capacitances of $Q1$ through $Q6$ are discharged through R_{sense}, causing a high power current spike each time V_{bldc} transitions from V_{gnd} to V_{batt} and vice versa. This is the main reason that a filter is required on the current sense element.

Fortunately, the speed of the current spikes produce frequencies much higher than the useful components of the current signal. The low pass filter is suited to reducing high frequency components while preserving the low frequency content. The initial attempt used a first order filter comprising a resistor and a capacitor. In order to attenuate the current spikes satisfactorily, the cut off frequency had to be set so low that it interfered with the low frequency parts of the signal. Therefore a second order low pass filter was used; giving an acceptable response. Figure 3.13 shows the second order low pass filter used to prevent the recursive nature of the switching transients.

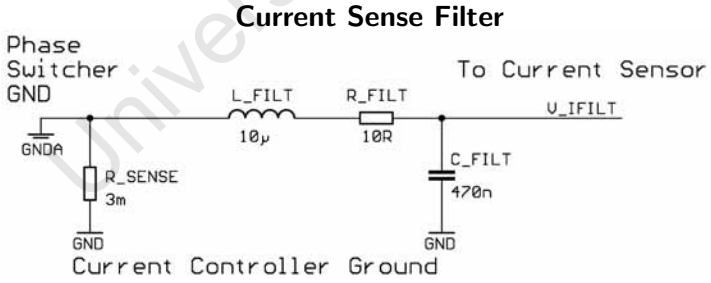

Figure 3.13: The resistor sensing the current flowing in the phase switcher bridge was exposed to high frequency transients from switching events. This second order filter has a sharper response than a first order filter, and was necessary to attenuate the switching transients satisfactorily.

The frequency response of the resistor-inductor-capacitor circuit in Figure 3.13, is found by evaluating the transfer function,

$$\frac{V_{filt}}{V_{sense}} = \frac{1}{s^2 \cdot L_{filt} \cdot C_{filt} + s \cdot C_{filt} \cdot R_{filt} + 1} \tag{3.8}$$

for values of s equal to $j\omega$. ω is the angular frequency of the input signal in radians per second, and s is the complex variable resulting from the Laplace transform.

The resonant frequency is the frequency at which the impedance of the inductor, equal to $j\omega L$, cancels the impedance of the capacitor, equal to $^1/_{j\omega C}$. The input to the filter in this case would experience an impedance equal to the resistance of R_{filt}. If the value of R_{filt} is low, then the output of the filter can be many times bigger than the input because the energy stored in the reactive components builds up and oscillates between them. This frequency also marks the point where the ratio $^{V_{filt}}/_{V_{sense}}$ begins to decrease like a function that approaches $^1/_{\omega^2}$; instead of $^1/_{(1+k^2)}$ for $k < 1$. $V_{sense} \approx 2V_{filt}$ at the point of resonance; provided R_{filt} dissipates enough energy to prevent a build up of the amplitude at resonance.

The response of the filter depends on two factors, the resonant frequency and the value of R_{filt} for a given L_{filt} and C_{filt}. The resonant frequency was chosen to be around $75kHz$, to allow good pass through of the motor current frequencies; which are in the vicinity of $10kHz$, as seen in the results. The resonant frequency is calculated by putting $j\omega L$ equal to $^1/_{j\omega C}$ and solving for ω. Thus

$$\omega_{resonant} = \frac{1}{\sqrt{L \cdot C}} \tag{3.9}$$

The inductor was chosen to be $10\mu H$ and the capacitor $470nF$ to give a resonant frequency of $73.5kHz$.

The value of R_{filt} is determined by applying the quadratic equation solution formula to Equation 3.8, and then ensuring that the complex component of the roots is ≤ 0. This condition translates to a situation where the response of the filter contains no sinusoidal terms in the time domain.

Equation 3.10 shows that s has complex roots if the value of the square root is negative, hence R_{filt} was chosen to cause that term to be ≥ 0.

$$s = \frac{-R_{filt} \cdot C_{filt} \pm \sqrt{R_{filt}^2 \cdot C_{filt}^2 - 4 \cdot L_{filt} \cdot C_{filt}}}{2 \cdot L_{filt} \cdot C_{filt}} \tag{3.10}$$

Therefore,

$$R_{filt} \geq +\sqrt{\frac{4 \cdot L_{filt}}{C_{filt}}}$$

giving R_{filt} a minimum value of 9.22Ω; so R_{filt} was chosen to be 10Ω.

Positioning the filter directly after R_{sense} allowed the amplifier stage to operate within the bandwidth limits of the operational amplifier (Op-Amp). As Horowitz and Hill pp. 1064 [20] pointed out, using an active filter based on an Op-Amp for filtering at high frequencies places unrealistic demands on the bandwidth of the Op-Amp, or requires an expensive Op-Amp that uses much more power. Further advantages of passive filters are the low cost, zero power overhead and simple structure.

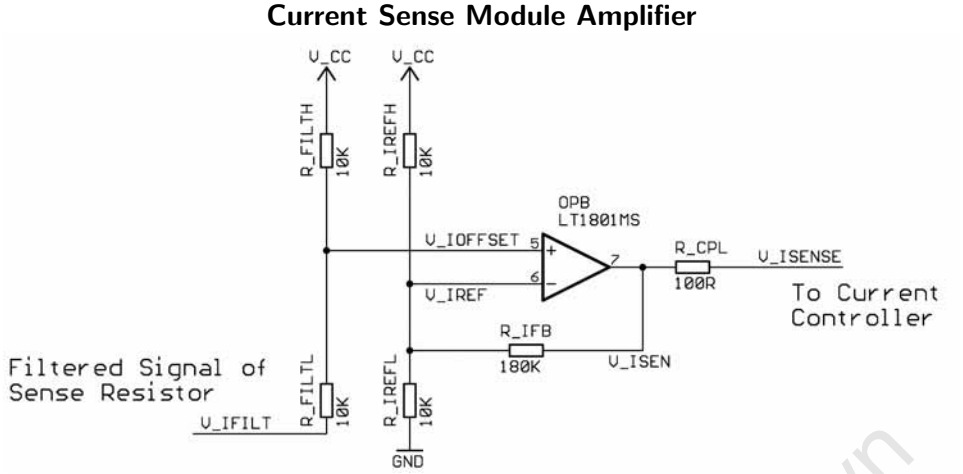

Figure 3.14: The Current Sense Module Amplifier. The signal from the current sense resistor is scaled and combined with an offset in this amplifier stage. The offset is set by R_{IrefL} and R_{IrefH} so that there is equal output swing for positive and negative currents in R_{sense}. The gain is set by R_{IFB} so that $\pm 30A$ can be measured by the amplifier.

The last step to producing the current signal for the current controller is amplification and offset addition. The throttle input used in this project varies from $1V$ to $4V$, with higher voltages corresponding to higher or more positive demand torque. Therefore, the amplifier here should produce a more positive output for higher machine currents; a non inverting amplifier configuration must be used. The gain of the amplifier should be $16^2/_3$, as per Equation 3.7.

Figure 3.14 shows how the above requirements are achieved using a single Op-Amp.

By setting R_{filtH} equal to R_{filtL}, the signal present at $V_{Ioffset}$ is

$$V_{Ioffset} = \frac{V_{Rsense}}{2} + \frac{V_{CC}}{2} \tag{3.11}$$

The resistors R_{IrefH} and R_{IrefL} are made equal to create a Thevenin equivalent voltage source with an open terminal voltage of $^{V_{CC}}/_2$ and internal resistance $^{R_{IrefH}}/_2$ or $^{R_{IrefL}}/_2$, since $R_{IrefH} = R_{IrefL}$.

The resistors R_{filtH}, R_{filtL}, R_{IrefH} and R_{IrefL} are chosen to be $10k\Omega$. After the resistor dividers create the $^{V_{CC}}/_2$ offset, the gain of the amplifier, G, is set with R_{IFB} using the following equation:

$$G = \frac{\Delta V_{Isen}}{\Delta V_{Ifilt}} = \frac{R_{IFB} + \frac{1}{2} \cdot R_{IrefH}}{R_{IrefH}}$$

R_{IFB} is used to obtain the required G of $16\,^2/_3$, calculated in Equation 3.7.

Hence:

$$R_{IFB} = G \cdot R_{IrefH} - \frac{1}{2} \cdot R_{IrefH} = 16\,{}^2\!/_3 \times 10k\Omega - 5k\Omega \approx 162k\Omega$$

The nearest resistor values to this are $150k\Omega$ and $180k\Omega$. The $180k\Omega$ resistor was used because it allowed the tolerance band voltage thresholds to have a greater difference, which was better for cleanly discriminating a crossing of a threshold. The slew rate of the signal V_{Isen} is increased by having higher gain, which further promotes cleaner threshold crossings. The resistor choices lead to a final gain of the amplifier of 18.5.

The bandwidth required to achieve the gain of the amplifier is $G \cdot f_{max}$, which is $18.5 \cdot 10kHz \cdot n = (185 \cdot n)kHz$ where n is the highest number of the harmonic of the current signal that should be allowed to pass through the amplifier to keep the signal integrity. Since the current signal is approximately triangular, the highest harmonic of interest was the 7^{th}, corresponding to a bandwidth of $\approx 1.4MHz$. The low pass filter connected before the Op-Amp, was designed with a cut off frequency of $\approx 70kHz$, for the same reason.

3.4 Two Quadrant Current Controller

Torque in a DC machine is directly proportional to the armature current; control of the armature current is the same as controlling the output torque. The phase switcher module ensures that the BLDC machine presents connections to the current controller that resemble those of a permanent magnet (PM) DC brushed machine. The aim of torque control can then be achieved using a single channel controller with one of the control schemes from Section 2.4.2.

The current controller interprets the current sensor signal and the throttle signal to control the MOSFETs Q_{CSH} and Q_{CSL}. They are used to apply a voltage to the BLDC machine, through the phase switcher, so that the current in the machine approaches the current demanded by the throttle signal. Figure 3.15 shows the position of Q_{CSH} and Q_{CSL} relative to the phase switcher and the supply, V_{batt}. The voltage V_{bldc}, across the phase switcher, is determined by V_{batt} and the state of Q_{CSH} and Q_{CSL}.

The flow diagram in Figure 3.16 shows the logical operation of the current controller, which performs tolerance band current control, described on page 33. V_{Ihigh} is the throttle output signal and V_{Ilow} is made to be fixed amount lower using an Op-Amp. These two voltages set the tolerance band for V_{Isense}, the current sensor output.

In order for the two states **Decrease Current** and **Increase Current** to persist, a one bit digital memory device is required. Asynchronous systems are as easy to design as synchronous systems at this level of complexity, but they have some advantages in this case. An asynchronous circuit

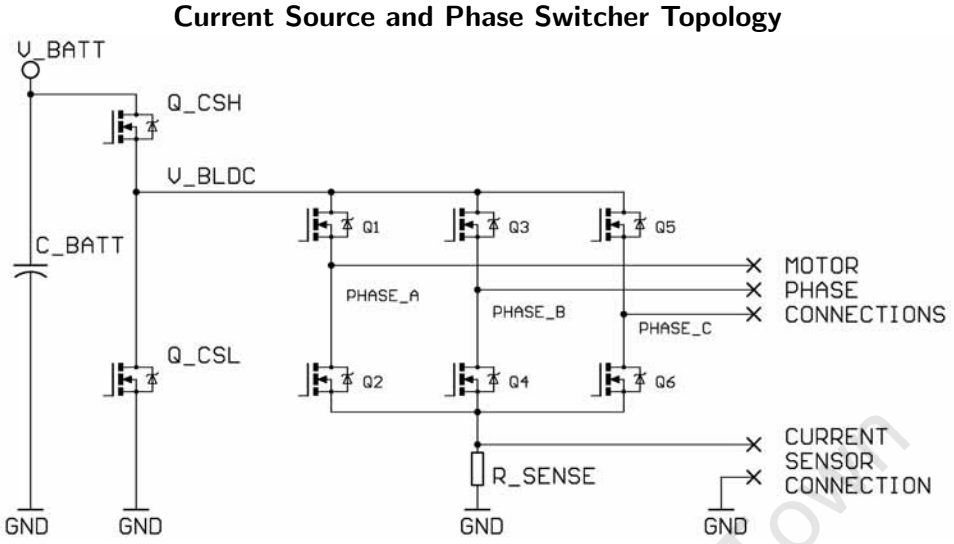

Figure 3.15: The current source half bridge is connected to the phase switcher power stage as shown, with the sense resistor positioned so that the load or motor current always flows through it. The half bridge applies V_{batt} or V_{gnd} to the phase switcher to increase or decrease I_{bldc}. V_{bldc} is effectively the average value of the half bridge output.

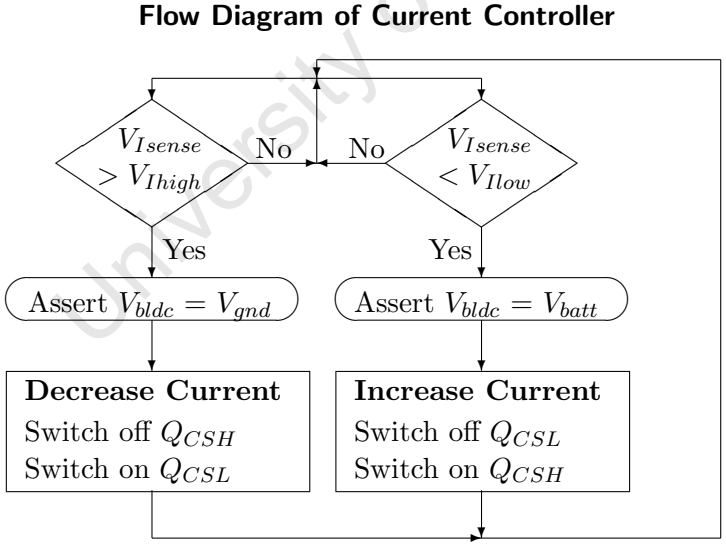

Figure 3.16: The Current Controller Flow Chart. The current controller is level sensitive and asynchronous. The conditions are constantly evaluated in parallel, indicated by the split flow path to the top decision blocks. $V_{Ihigh} > V_{Ilow}$, making it impossible for both "Yes" paths to be followed simultaneously.[1]

responds instantly to events, recovers from errors as soon as the error condition ceases, and requires no global synchronizing signal.

The circuit in Figure 3.17 shows how the flow diagram is implemented in hardware. There are two main parts to the circuit; in the bottom left area is an Op-Amp that is configured to create the voltages V_{Ihigh} and V_{Ilow} that form the tolerance band for V_{Isense}. On the right is a pair of comparators that trigger RS_{latch}, which provides the signals for switching Q_{CSH} and Q_{CSL} on and off. The timing diagram shows the sequence of events: firstly $CMPB$ fires when it detects the current signal above the tolerance band, secondly the latch registers the $CMPB$ transition by setting V_{CSH} low and finally $CMPB$ returns to the idle state. A similar series of events occur when V_{Isense} goes below V_{Ilow}. The propagation delays are exaggerated in Figure 3.17 for clarity.

Op-Amp OPA has a voltage at its output, V_{Ilow}, which is a fixed amount below V_{Ihigh}. The signal from the current sensor is scaled to $\approx 50mV$ per amp; a tolerance band of $\approx 1A$, requires an offset of $50mV$.

In a pulse width modulation (PWM) converter, the output is usually derived from a voltage source that is switched on and off very quickly and then filtered to produce a steady voltage or current at the output. In the case of the current controller the machine inductance can be used as the filter element. The current controller exploits this to reduce the number of components in the VSD; a passive filter for the V_{bldc} signal would be bulky and expensive since it would have to handle the full power of the VSD.

During machine parameter measurement, Section 5.1, it was observed that the effective inductance of a series pair of phase windings, $2L_{phase}$, reduced as the frequency of the test signal was increased past $1kHz$. Simultaneously, measurements showed increased electrical resistance of the machine at higher frequencies. In choosing a tolerance band for the current signal, the switching frequency of the current controller is also decided.

The rate of change of current in an inductor is determined by its inductance, L, and the voltage across the inductance, V_L. The time between each current controller switching event is short enough such that Equation 2.1 can be approximated by:

$$V_L = L \cdot \frac{\Delta I_L}{\Delta t} \Rightarrow \Delta t = L \cdot \frac{\Delta I_L}{V_L}$$

Here, ΔI_L is the magnitude of the tolerance band of the current controller and L is the inductance of two series connected phases of the BLDC machine. The voltage V_L is found by subtracting $2 \cdot V_{emf\,ph}$ and $2 \cdot I_{phase} \cdot R_{phase}$ from V_{bldc}.

[1] The chart is drawn using algorithmic state machine symbols, but because it represents a hardware system and not a sequential program, the flow lines are allowed to split before entering the decision boxes. This is a better representation of the real world situation.

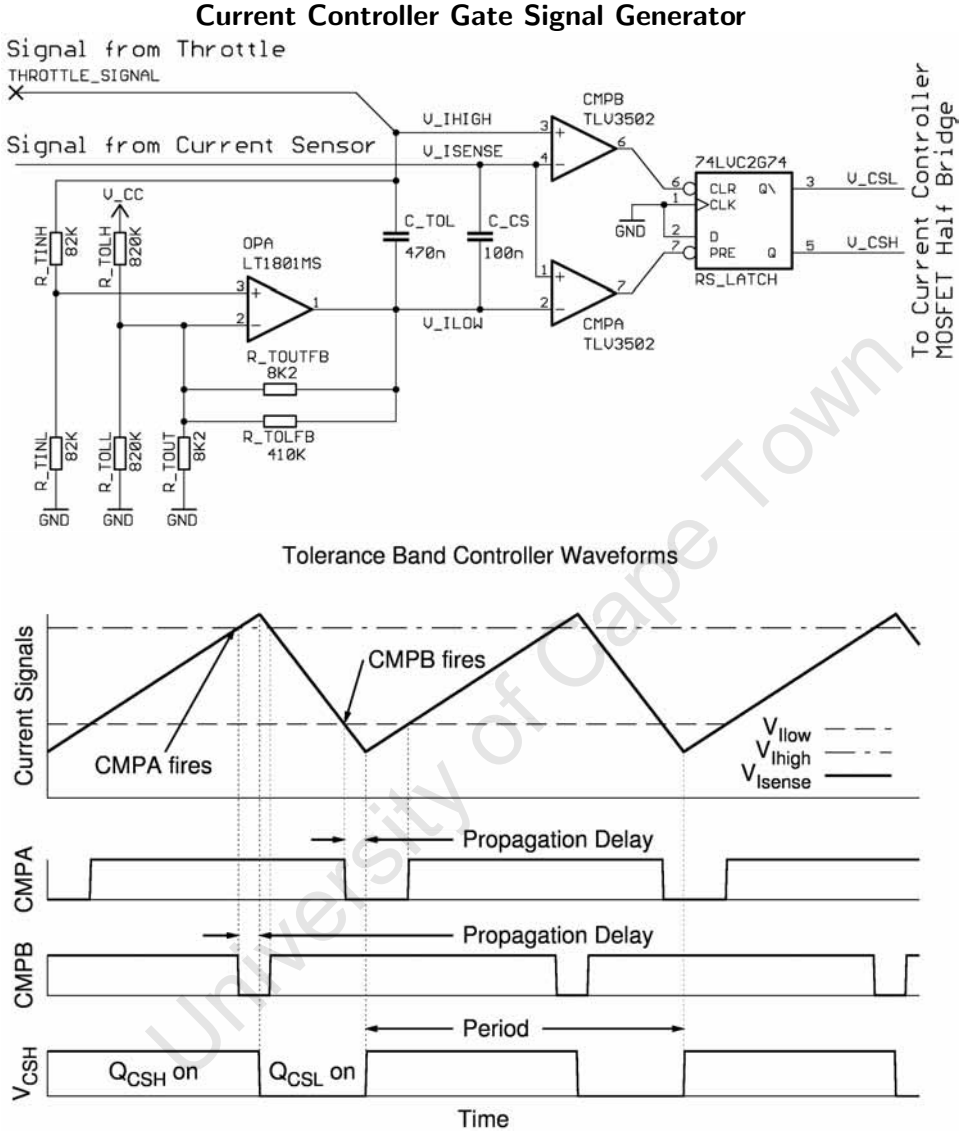

Figure 3.17: The current controller schematic and operating waveforms are shown above. The throttle signal is directly connected to V_{Ihigh} and OPA is used to generate V_{Ilow}. $CMPA$ and $CMPB$ asynchronously determine the state of RS_{LATCH}. The gate drive signals, V_{CSH} and V_{CSL}, for the MOSFETs in Figure 3.15 are generated by the complementary outputs Q and $\overline{Q}$, shown in the figure as $Q\backslash$. The timing diagram shows the order of events from a comparator detecting the current signal leaving the tolerance band to the assertion of a new switch state.

Then, the time taken for a phase current to rise or fall by ΔI_L is

$$T_{change} = 2L_{phase} \cdot \frac{\Delta I_L}{V_{batt} - 2V_{emf\,ph} - 2I_{phase}R_{phase}}$$

where V_{bldc} is at V_{batt} or V_{gnd}; and ΔI_L is positive or negative depending on the direction of the change. The total period T can be shown to be

$$T = T_{rise} + T_{fall} = 2L_{phase}\Delta I_L \left(\frac{1}{V_{in} - V_{out}} + \frac{1}{V_{out}}\right) \tag{3.12}$$

where the duty ratio of the V_{bldc} signal is $^{V_{out}}/_{V_{in}}$ and $V_{batt} = V_{in}$.

The maximum frequency of operation occurs when the period T is smallest. From Equation 3.12, this occurs when:

$$\left(\frac{1}{V_{in} - V_{out}} + \frac{1}{V_{out}}\right) \rightarrow \text{minimum}$$

which, from occurs at $^{V_{out}}/_{V_{in}} = {}^1/_2$, corresponding to a 50% duty cycle.

The resistive losses from the copper windings and the mechanical friction are power losses determined by machine design. Eddy currents in the magnetic core material are also increased by higher rotational speed, but this cannot be helped with any controller action. Therefore the switching frequency of the controller is the only adjustable factor in determining total operating machine power loss. The higher switching frequencies, or lower switching periods, cause larger losses. Equation 3.12 can be used to relate the current ripple and minimum switching period, T_{min}. A duty of 50% means V_{out} is $^1/_2$ V_{in}. Therefore, since $V_{in} = V_{batt}$,

$$T_{min} = 2L_{phase}\Delta I_L \cdot \frac{4}{V_{batt}} \tag{3.13}$$

The current ripple was chosen to be $1A$ as a trade off between the increasing machine core losses and a tolerable amount of ripple torque. The maximum switching frequency with this tolerance band is around $5kHz$.

Figure 3.17 shows OPA, which can be understood as a modified differential amplifier. If R_{tolH} is connected to V_{gnd} then the circuit is a differential amplifier with V_{Ihigh} being the reference voltage and both inputs at V_{gnd}. However R_{tolH} is actually connected to V_{CC} where it combines with R_{tolL} and R_{Tout} to make a Thevenin equivalent voltage of:

$$V_{Thevenin} = V_{CC} \cdot \frac{R_{Tout} \parallel R_{tolL}}{R_{tolH} + R_{Tout} \parallel R_{tolL}} = 5V \times \frac{\frac{100 \cdot 1}{100+1}}{100 + \frac{100 \cdot 1}{100+1}} = 49mV$$

where $8.2k\Omega$ has been factored out of the resistance values. The impedance of this Thevenin source matches the feedback impedance, $R_{tolFB} \parallel R_{ToutFB}$, making the differential inputs $V_{Thevenin}$ apart and therefore the output of the Op-Amp, V_{Ilow}, is $V_{Thevenin}$ lower than V_{Ihigh}.

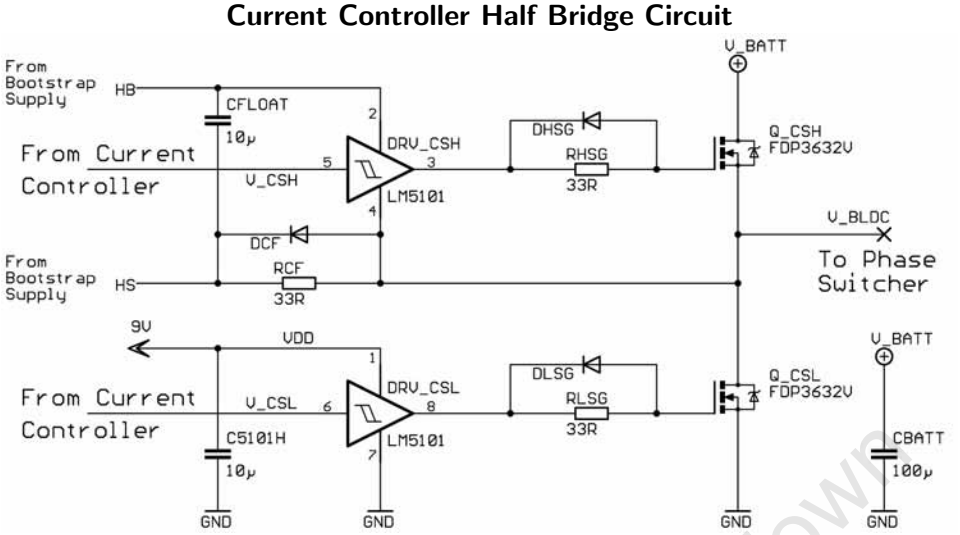

Figure 3.18: The current controller half bridge is connected to the common drain connections of the phase switcher through V_{bldc}. The power to the driver for Q_{CSH} comes from the bootstrap supply described in Section 3.2.1. The current controller gate signal generator supplies the V_{CSH} and V_{CSL} signals to the LM5101 MOSFET driver.

The comparators are configured to produce a low output when V_{Isense} leaves the tolerance band. These signals then propagate through the RS-latch to generate MOSFET gate signals V_{CSH} and V_{CSL}.

Figure 3.18 shows the way the bootstrap supply connects to DRV_{CSH} and how the signals V_{CSH} and V_{CSL} are connected through the LM5101 MOSFET driver to control the switches Q_{CSH} and Q_{CSL} respectively. The diode and resistor arrangement on the gate of each MOSFET cause the turn on of the switch to be slower than the turn off, introducing deadtime into the switching pattern. The FDP3632 is an enhancement mode MOSFET, which only begins to conduct when the gate voltage exceeds a certain threshold. The diode and resistor arrangement use this fact to ensure than one switch is off before the other one turns on, to avoid large current flow from V_{batt} to V_{gnd} during switching. Another resistor diode pair is used to reduce the stress on the bootstrap diode that normally recharges C_{float} while still allowing full power discharge of C_{float}.

The FDP3632 MOSFET has a breakdown voltage of $100V$, a current rating of $90A$, and $9m\Omega$ of resistance when in the on state. This gives it approximately a safety factor of two when handling the current and voltage requirements of the VSD. The LM5101 driver matches the breakdown voltage of the FDP3632 and provides up to $3A$ to drive the MOSFET gate, turning on and off the MOSFETs in well under $1\mu s$.

3.5 Phase Switcher

The phase switcher module of the VSD is required to accept the inputs from the Hall effect position sensors and use that information to effectively transform the BLDC machine into its DC machine equivalent. Figure 3.19 is a block diagram showing the basic steps that make a BLDC machine work similarly to a DC machine.

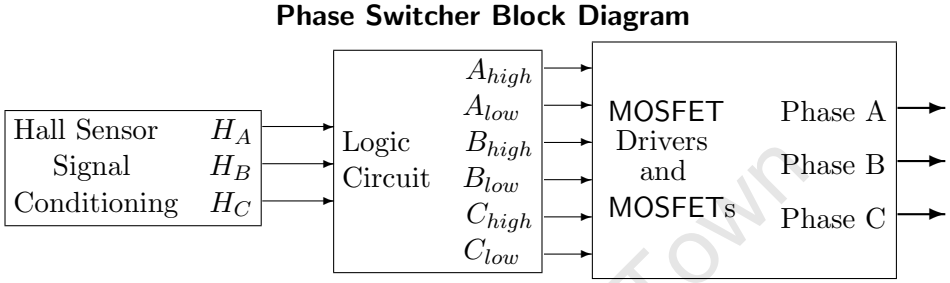

Figure 3.19: The phase switcher design involves three steps. First the Hall effect sensors signals are conditioned for digital input. Next, the phase switcher logic circuit uses this information to calculate the gate drive signals. Finally MOSFET drivers and associated MOSFETs apply the desired voltage to the BLDC machine terminals.

Figure 3.20 is a pictorial summary of the operation of a BLDC machine. At the top of the figure, the magnets, stator slots, Hall sensor positions and *Phase A* partial windings are shown. To improve clarity the conductors of the other two phases are not shown. Next down is the graph of the flux linkage of *Phase A* coils resulting from the presence of the magnets. The smooth transition from steadily increasing flux to steadily decreasing flux linkage is a result of the slot skewing in the machine design.

The next three graphs are the Hall sensor output signals, which indicate the absolute magnetic field direction at their indicated locations. All three Hall sensor outputs are shown since the sensor in the middle of each phase turn is given the same letter as that phase but is inconsequential in determining the state of the switches for that phase. Thus for *Phase A*, sensors H_B and H_C must be used to determine the A_{high} and A_{low} gate drive signals.

The graph of the generated voltage across *Phase A* is presented next but is only valid for the case when the machine is rotating and in a particular direction. With no movement the graph would be a flat line, and by turning in the other direction the graph would be inverted. The shape of the EMF is the derivative of the flux linkage waveform; the machine design can dictate a wide variety of shapes for this graph.

Finally the bottom two graphs show the ideal gate drive signals for *Phase A* coincident with the flat portions of the EMF of *Phase A*.

Table 3.2 is the truth table for $360°ed/n$ Hall sensors in three phase

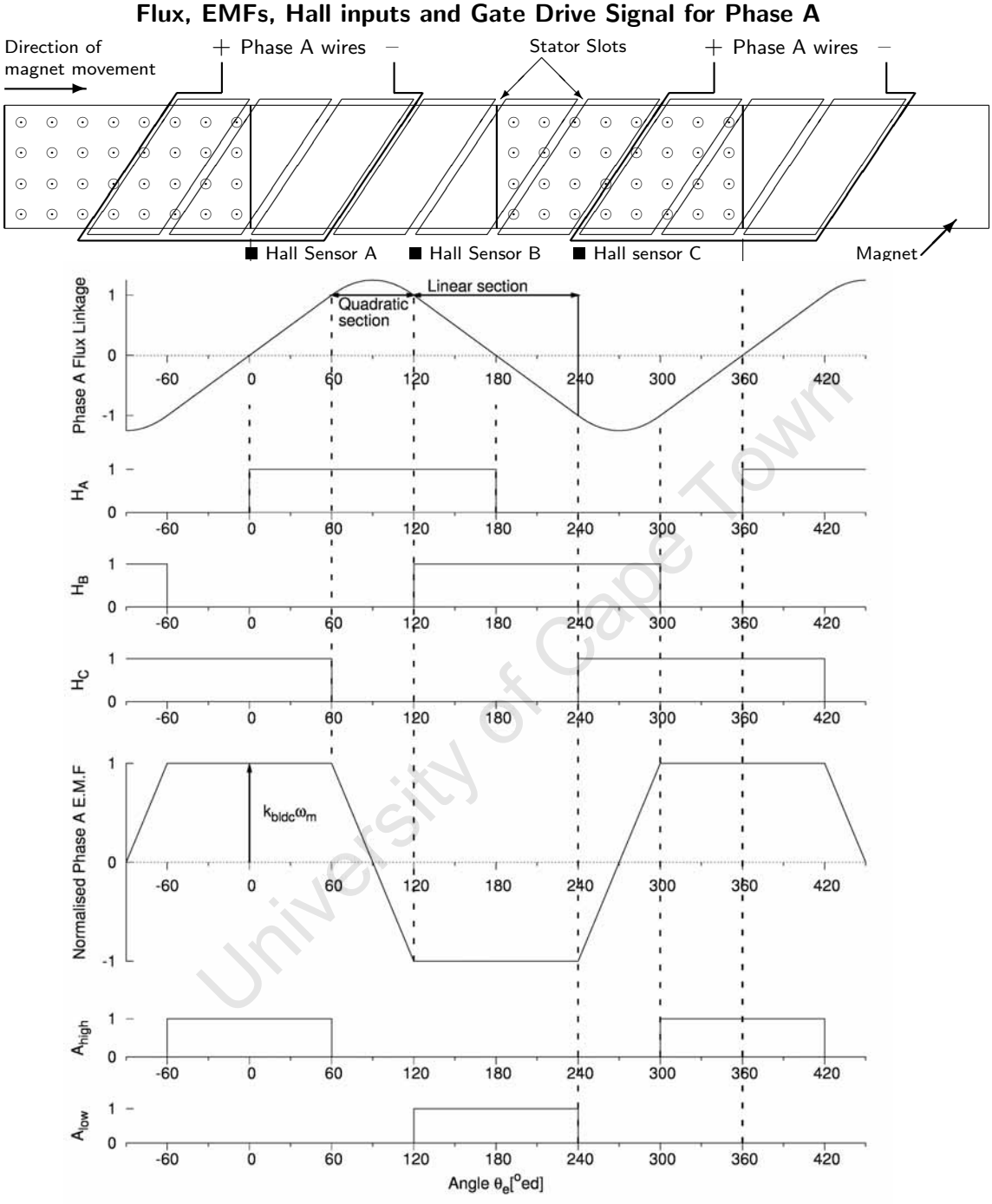

Figure 3.20: This set of graphs show the correlation between the position of the rotor, the magnitude of the flux linking a phase winding, the Hall sensor signals, the generated phase voltage and the gate drive signals for that phase. The diagram is accurate for increasing angular position of the rotor as indicated. ⊙ represents magnetic field out of the page.

BLDC motors and the switch states that must be enforced to operate from a DC supply.

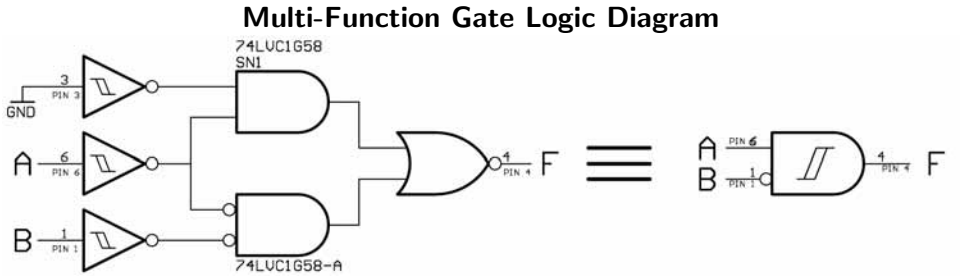

Figure 3.21: The 74LVC1G58 multi-function gate from Texas instruments implements the function on the left. By connecting input pin 3 to the IC ground pin, it implements the function required for the phase switcher gate signals. It can easily be configured as a buffer or an inverter by connecting one of the other pins to V_{CC} or V_{gnd}.

The rows in Table 3.2, where the relevant function is high, are combined to design the logic function for the *Phase A* gate signals. For A_{low}, the two rows where it is logic high result in the following boolean equation:

$$\begin{aligned} A_{low} &= \overline{H_A} \bullet H_B \bullet \overline{H_C} + H_A \bullet H_B \bullet \overline{H_C} \\ &= (\overline{H_A} + H_A) \bullet H_B \bullet \overline{H_C} \\ &= H_B \bullet \overline{H_C} \end{aligned} \tag{3.14}$$

The symbol $\bullet$ represents a logical **AND** operation and $+$ represents the logical **OR** operation. In the same way, the equation for A_{high} is obtained:

$$A_{high} = \overline{H_B} \bullet H_C$$

Both A_{low} and A_{high} use the same function, but with the inputs swapped around. The remaining gate drive signals also use the same function; each gate has a unique permutation of two logic inputs. In the two quadrant VSD $V_{bldc} \geq 0$, hence logical reversal of V_{bldc} is unnecessary. Now only the **AND** function with one inverted input is needed for the whole phase switcher.

The Hall sensor signals change one at a time, such that only one MOSFET in one leg changes state at a particular position. The advantage of this is that the MOSFETs in the phase switcher never switch on simultaneously or even change simultaneously in the same phase leg. Hence there is no need for blanking time, where both switches in one leg are driven low for a short time.

Discrete logic gates have a standard production IC that can perform the required function, called a multi-function gate. There are a number of different single gate ICs called multi-function gates, with three inputs and

Table 3.2: Gate Drive Signal Truth Table

Inputs			Gate Driver Logic Input Signals					
			Phase A		Phase B		Phase C	
H_A	H_B	H_C	A_{High}	A_{Low}	B_{High}	B_{Low}	C_{High}	C_{Low}
0	0	1	1	0	0	1	0	0
0	1	1	0	0	0	1	1	0
0	1	0	0	1	0	0	1	0
1	1	0	0	1	1	0	0	0
1	0	0	0	0	1	0	0	1
1	0	1	1	0	0	0	0	1
Unused Combinations of H_A, H_B, H_C								
0	0	0	0	0	0	0	0	0
1	1	1	0	0	0	0	0	0

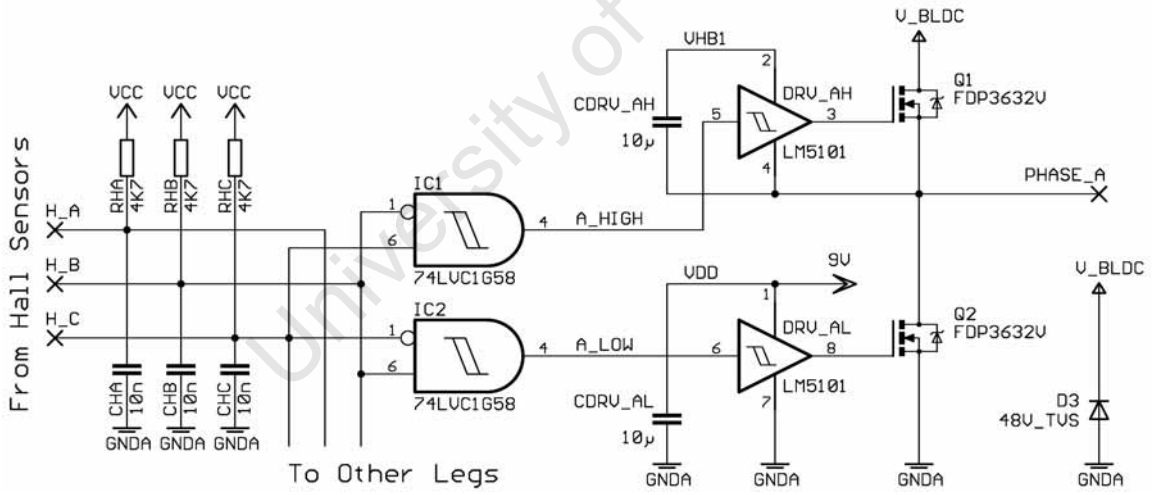

Figure 3.22: The phase switcher consists of three of the above circuit, except the Hall sensor conditioning parts have only one instance. Each leg has a different permutation of the Hall sensor signals as input to the logic gates that control the MOSFET drivers. The A_{high} and A_{low} signals are never high at exactly the same times because of the function of $IC1$ and $IC2$, making shoot through impossible in this circuit.

one output. One input is used to determine the function by holding it high or low or joining it to another input, leaving two inputs and one output to implement almost any logic function. The 74LVC1G58, shown in Figure 3.21 from Texas instruments has the ability to implement the $F = A \bullet \overline{B}$ function, and, because it has great versatility, was used in other parts of the design. This significantly reduced the number of different parts in the design.[1]

One leg of the phase switcher is shown in Figure 3.22. The phase switcher does not need a bootstrap power supply for the upper MOSFET and driver because as the BLDC machine rotates, $C_{DRV\,AH}$ gets periodically recharged by the activation of Q_2 and the LM5101 internal bootstrap diode. Even when the machine is at rest, $C_{DRV\,AH}$ will usually still get charged when the current controller forces V_{bldc} low.

The MOSFETs and MOSFET drivers used in the phase switcher are the same as those used in the current controller, since they both handle the same currents and voltages.

An initial prototype of the phase switcher design, described in [6], was supplied with a variable voltage to control the machine torque and speed. Capacitors were put across each phase leg to keep V_{bldc} steady at the phase connections.

In order to allow the current controller to utilise the inductance of the electric machine, the phase switcher had to avoid capacitances across the V_{bldc} and V_{GNDA} nodes. This led to voltage surges at each current controller switching event, because the link between the current controller and the phase switcher had some leakage inductance which combined with the output capacitance of the phase switcher MOSFETs to create a resonant circuit. With the link resistance being low, the resulting transient voltage easily exceeded the tolerance of the components. Therefore transient voltage suppressors were installed.

The temperature sensor takes advantage of the all zero unused Hall sensor combination to cause all of the switches in the inverter bridge to go off, shutting down the VSD. It is the only possibility in this case because the all ones case will cause the Hall sensor and the temperature sensor to attempt asserting opposing logic levels with low impedance, potentially causing damage and unpredictable operation.

3.5.1 Printed Circuit Board Design Considerations

The phase switcher was built on a separate printed circuit board (PCB) to the current controller in order to make the VSD modular in design. The layout of the high power components was done by hand to achieve short

[1] The multi-function gate can also implement some types of latch if an input is connected to the output signal. The RS_{LATCH} could have been replaced with one such gate, but multi-function gates were not used there because complementary outputs were needed.

paths for the high power signals and protection of the logic device signals with a ground plane. A two layer process was used to fabricate the design.

3.6 Throttle

The throttle in this project refers to the part that provides the input to the current controller. The important characteristic of the throttle for this application is the idle or resting state of the throttle. For the current controller to give the effect of freewheeling the throttle must give an output of $^{V_{CC}}/_{2}$ with no user input. This ensures that the average torque produced by the machine is zero since the demanded current is zero at that input. Then the operation of the throttle in the positive sense causes a positive machine torque. Negative or braking torque is then achieved by operating the throttle in the other direction. So the user has smooth control from accelerating to decelerating.

There is no need for a deadband in the middle of the throttle range, even if there exists a small offset in the throttle itself. Ideally the middle of the throttle range will correspond to V_{Ihigh} and V_{Ilow} being either side of the voltage that represents an I_{bldc} of zero. This would result in the system settling with V_{bldc} equal to zero. If this offset is small enough such that V_{Ilow} is below the zero I_{bldc} point and V_{Ihigh} is still above it, there is no difference from the ideal case.

If the throttle offset causes V_{Ihigh} to be below the zero current threshold, then V_{bldc} is automatically set to the lowest possible value. This is zero because this VSD only operates in two quadrants, making a negative V_{bldc} impossible. A user would experience additional mechanical resistance when attempting movement with the throttle in the idle position, because EMF generated by the movement would cause currents that produce retarding torque.

If the throttle produces a slightly higher output, then I_{bldc} would be made slightly positive with no user input. This could be beneficial because it partly compensates for the weight of the system, making it more responsive to increasing throttle input.

The deviation from zero, of the throttle idle output, is directly proportional to the I_{bldc} error. For small deviations, a human user will not notice the difference when operating the VSD. The case where the offset causes the system to idle with a positive I_{bldc} is going to use more energy. Therefore the preferred situation is an unnoticeable offset or an offset that moves V_{Ihigh} slightly below the zero I_{bldc} threshold.

Another possibility would be to install a push button or switch that enables the controller when activated. This would function similarly to a mechanical clutch.

Chapter 4

Conceptual Four Quadrant Design

The two quadrant design of the previous chapter is suitable for applications that only require one direction of movement. A four quadrant controller is able to operate in either mechanical direction while producing a positive or negative torque. Two important advantages of this are insensitivity to installation direction and full torque availability in both directions at standstill. The range of applications for a four quadrant drive at this power level includes light three and four wheeled vehicles.

The two quadrant controller automatically switches between applying $+V_{batt}$ or V_{gnd} to the brushless direct current (BLDC) machine. The four quadrant controller extends this by automatically selecting V_{bldc} to be either $+V_{batt}$ and V_{gnd} or $-V_{batt}$ and V_{gnd}. This enables operation in all of the labeled zones of Figure 3.1. The throttle input could now be varied to all positions, achieving all possible output torques, at some arbitrary speed.

The meaning of *Forwards* and *Reverse* is a matter of opinion in four quadrant drives. Since the variable speed drive (VSD) can produce rotation and torque in any permutation of directions, one can arbitrarily assign the direction *Forwards* to one direction of rotation, even if the controller is using apparently *Reverse* logic to achieve it. The meaning of being in the *Forwards* direction is that a more positive throttle signal voltage causes a more positive sense resistor voltage. *Reverse* operation inverts this relationship.

4.1 Overview of Four Quadrant Design

Figure 4.1 is a block diagram of the conceptual four quadrant system. It is similar in structure to Figure 3.2 with modifications that provide *Reverse* operation as well. Figure 4.2 is a schematic showing the four threshold tolerance band logic, the optional inverter summing amplifier arrangement,

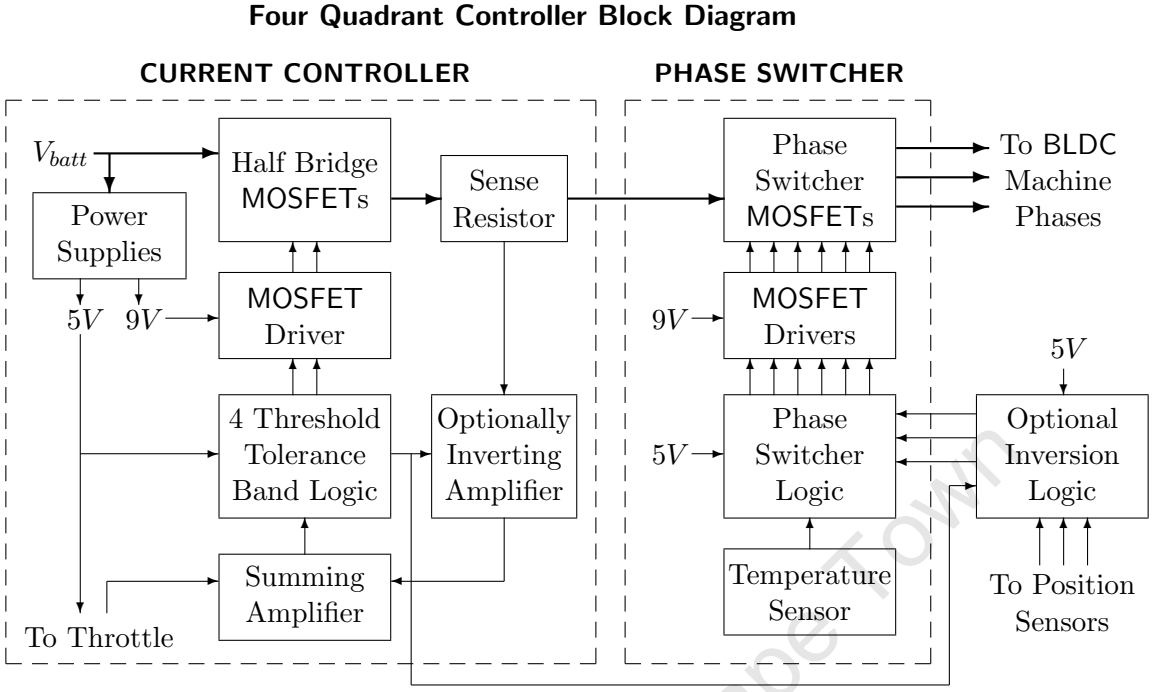

Figure 4.1: The four quadrant design differs from the two quadrant design mainly in the use of optional inversion of Hall sensor and current signals. An additional logic signal now has to be routed to control the optional inverter for the Hall sensor signals.

and the digital optional inverter. These are the modified parts and the additional parts when compared with the two quadrant design.

The switch from being able to apply $+V_{batt}$ and V_{gnd} to being able to apply $-V_{batt}$ and V_{gnd} to the machine requires inversion of the Hall sensor elements. This swaps the state of all the $_{high}$ switches with the corresponding $_{low}$ switches in the phase switcher, having the same effect as swapping the terminals in a direct current (DC) machine.

For the rotor position sensors, an **XOR** gate makes a suitable digital optional inverter. However, when the position sensor signals are inverted, the current in the sense resistor becomes exactly the negative of its previous value. This changes the meaning of all the current thresholds and produces a discontinuous current signal. An optional inverter on the analog current measurement is therefore used to keep the current signal continuous and representative of I_{bldc}. The tolerance band comparators can then be used in the same way for *Forwards* and *Reverse* operation.

The control of the extra optionally inverting modules requires a low power signal from the current controller to the digital optional inverter, which has to be near the phase switcher. The high power phase connections nearby may disrupt this signal if no electrical shielding is used.

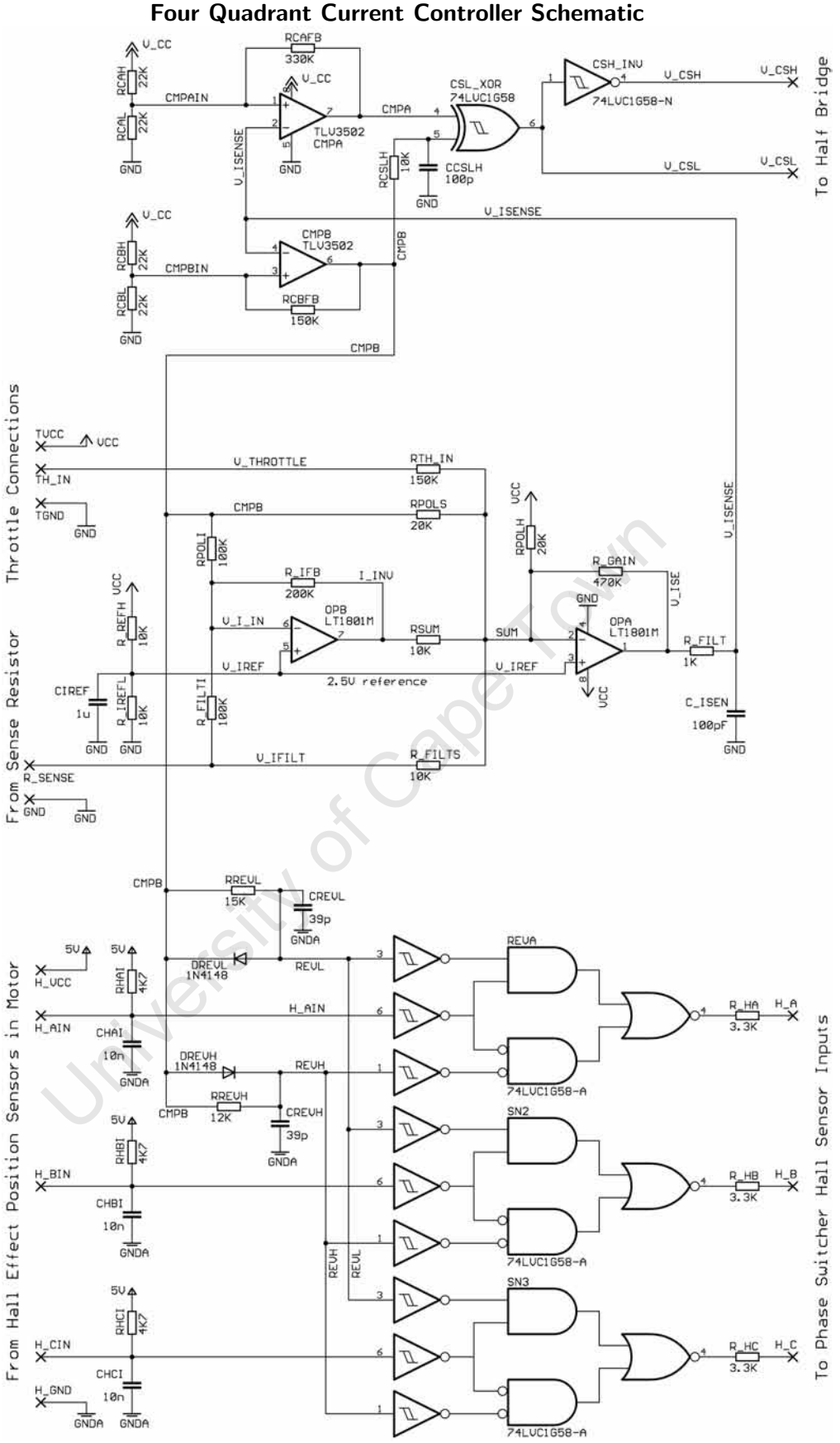

Figure 4.2: The essential parts of the conceptual four quadrant current controller are shown above. The power supplies, half bridge and sense resistor filter are omitted here because they are the same as in Figure 3.3, the two quadrant design. At the top is where two bits of information are stored in $CMPA$ and $CMPB$. In the middle is the optional inverter for the current signal and at the bottom is the digital optional inverter with blanking time.

The phase switcher can be used, almost unmodified, in this extension to the two quadrant design. In order for the digital optional inverter circuit, described fully in Section 4.3, to function with the temperature cut out circuit, the resistors RHA, RHB and RHC must be removed, leaving an open circuit in their place. The power supplies, temperature cut out, metal oxide semiconductor field effect transistors (MOSFETs) drivers, MOSFETs and current filter are kept the same as for the two quadrant design and require no further discussion.

The four quadrant design keeps current freewheeling through the phase switcher when V_{CSH} is low. This is consistent with the unipolar switching topology in [37]. The alternative, bipolar switching, can be achieved by making $A = \overline{B}$ and then using B as a pulse width modulation (PWM) input. However, the current ripple and discontinuity of signals are aggravated.

4.2 Four Quadrant Current Controller

In the two quadrant design, one digital bit described the state of the current controller, applying V_{batt} or V_{gnd}. The four quadrant current controller needs to distinguish between at least three states, $+V_{batt}$, V_{gnd} and $-V_{batt}$, requiring two digital bits.

Figure 4.3 shows how the four quadrant design uses all four states possible with two bits of digital memory. The 'B' bit determined if *Forwards* or *Reverse* mode was in effect and 'A' toggled the value of V_{CSH}. The flow from one state to the next is designed with only one state bit changing at a time, so that glitches in the outputs are avoided.

The definition of *Forwards* requires the current sensor to deliver the signal V_{Isense}, from a buffered and amplified version of the signal across R_{sense}. This decision promotes positive logic design which the author believes is more easily understood. In *Reverse* mode the R_{sense} signal must be inverted before amplification to stay aligned with I_{bldc}.

Of the three methods of current control in Section 2.4.2, the tolerance band method is the only one that uses the same approach to decide on an output of $V_L = V_{higher}$ as it does for $V_L = V_{lower}$. This gives it the advantage of having a smooth and symmetrical response to *Forwards* and *Reverse* modes without reconfiguration.

The decision boxes in Figure 4.3 are implemented with a system of four thresholds. They are ordered as their names suggest: V_{Ilower} is lower than V_{Ilow} and $V_{Ihigher}$ is higher than V_{Ihigh}. These thresholds are in the same scale as the output of the current sensor, V_{Isense}. Steady operation in one direction will make V_{Isense} stay between the V_{Ihigh} and V_{Ilow} levels. Therefore the current ripple is set by the gain of the current sense amplifier and the difference between the *high* and *low* thresholds.

When either of the $V_{bldc} = V_{gnd}$ states is not able to keep the current

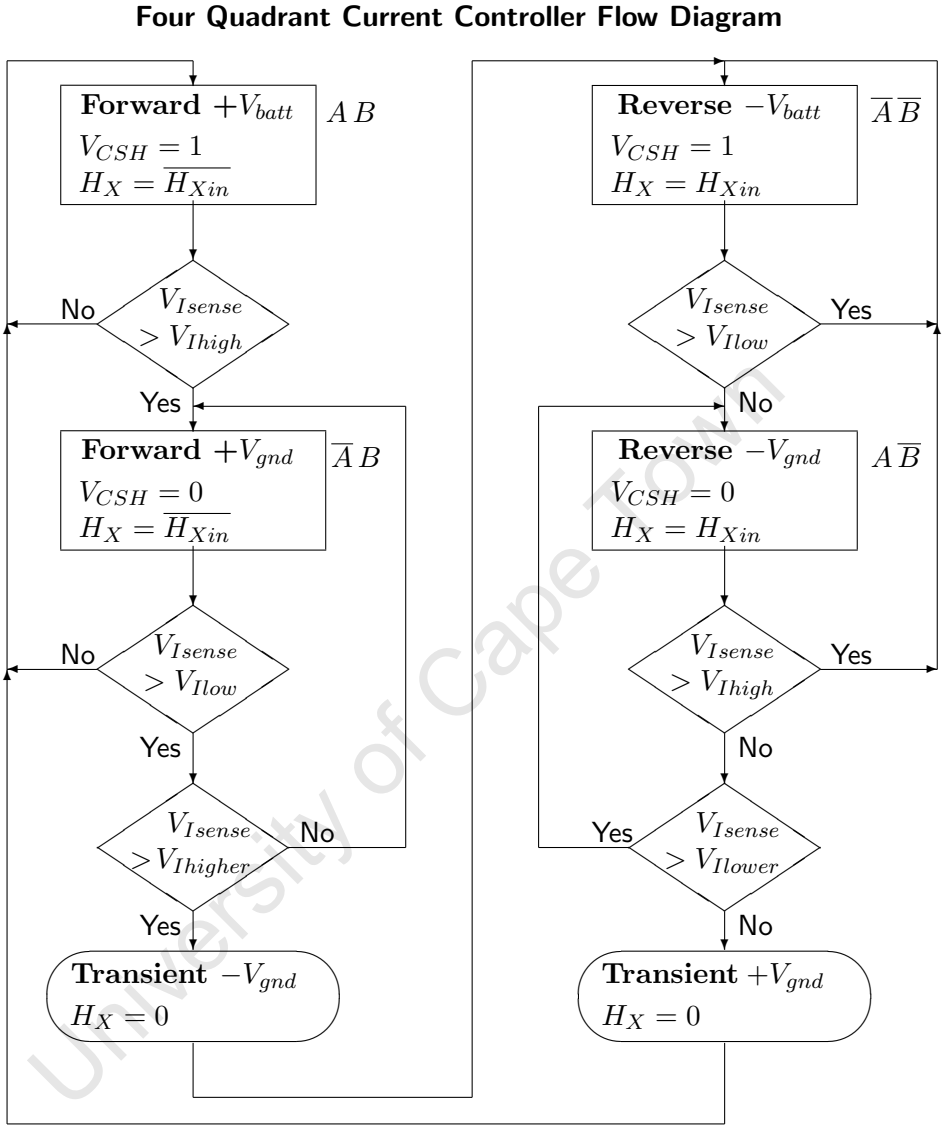

Figure 4.3: The current controller has four states, determined by the outputs of $CMPA$ and $CMPB$. The state numbering shows an 'A' when $CMPA$ is high and '$\overline{A}$' when $CMPA$ is low. The same convention is used for B and $CMPB$. All the Hall sensor signals are forced low briefly in the *Transient* conditional output. This ensures no shoot through currents in the phase switcher. The logical variable H_X shows what happens to each of H_A, H_B and H_C. The signal V_{Isense} is the sum of the throttle input and the polarity corrected current in the sense resistor. V_{CSL} is always the complement of V_{CSH} for the current controller half bridge.

Table 4.1: Determination of State Variables in Four Quadrant Design

V_{Isense} is greater than...				Present State		Next State	
I_{lower}	I_{low}	I_{high}	I_{higher}	A_n	B_n	A_{n+1}	B_{n+1}
No	No	No	No	X	X	1	1
Yes	No	No	No	X	B_n	1	B_n
Yes	Yes	No	No	A_n	B_n	A_n	B_n
Yes	Yes	Yes	No	X	B_n	0	B_n
Yes	Yes	Yes	Yes	X	X	0	0

An "X" in the above table indicates a *don't care* condition.

within the band from V_{Ilow} to V_{Ihigh}, eventually the threshold V_{Ilower} or $V_{Ihigher}$ will be reached. At this point the direction of the applied voltage is changed. Table 4.1 shows how the values of A and B are determined from the current thresholds. The value of A stays the same if A_{n+1} is the same as A_n, and B stays the same if B_{n+1} is the same as B_n.

A comparator produces a digital output when an analog voltage passes a precise reference level. If the output is fed back to adjust the reference level then two possibilities arise: negative feedback, where the output change attempts to reduce the difference between the input signal and the reference signal; or positive feedback, where the output change increases the difference between the reference signal and input. The positive feedback arrangement is called a Schmitt trigger. The comparator configured as a Schmitt trigger can be used as a one bit digital memory and a threshold detection circuit simultaneously.

The strength of positive feedback in a comparator configured as a Schmitt trigger determines the difference between the input thresholds, or tolerance band. The four quadrant controller has two comparators each managing a pair of thresholds. The V_{Ihigh} and V_{Ilow} thresholds are set with R_{CAFB}, a low strength positive feedback path around $CMPA$ in Figure 4.4. The lower resistance of R_{CBFB} increases the difference between the thresholds that $CMPB$ switches at, implementing $V_{Ihigher}$ and V_{Ilower}.

Now V_{Isense} will cause $CMPA$ to output a logic high when it falls below V_{Ilow} and a logic low when V_{Ihigh} is exceeded. The output of $CMPB$ is similarly determined, correlating the outputs of the two comparators exactly to the state variables A and B.

The final task of the current controller is to provide suitable signals to relay the current state to the outside circuits and devices. Table 4.3 is the truth table for how the current sensor, optional digital inverter and half bridge should respond to the values of A and B. In order to keep the parts used to a minimum, the Hall effect position sensors were left inverted in the *Forward* states, allowing $CMPB$ to directly signal both the optionally inverting amplifier and the digital optional inverter. This has no impact on

Table 4.3: Four Quadrant Current Controller Truth Table

State	Inputs			Outputs			
	H_{Xin}	$CMPA$	$CMPB$	H_{Xout}	V_{CSH}	V_{CSL}	V_{Isense}
Fwd $+V_{batt}$	H_X	1	1	$\overline{H_X}$	1	0	buffered
Fwd $+V_{gnd}$	H_X	0	1	$\overline{H_X}$	0	1	buffered
Rev $-V_{gnd}$	H_X	1	0	H_X	0	1	inverted
Rev $-V_{batt}$	H_X	0	0	H_X	1	0	inverted

The subscript $_X$ represents any of the $_A$, $_B$ or $_C$ subscripts.

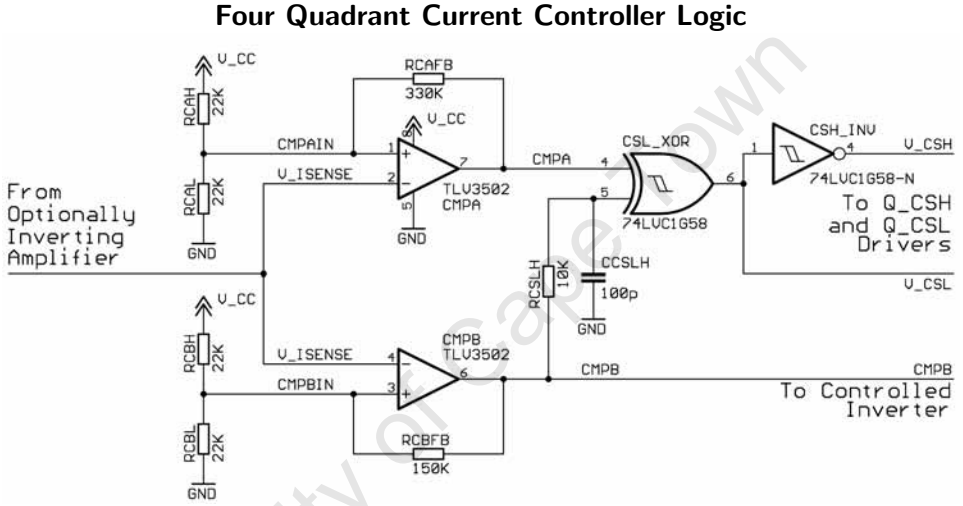

Figure 4.4: The comparators $CMPA$ and $CMPB$ use an external resistor network to achieve Schmitt trigger like operation. They "remember" the state of the digital signals in the current controller and also respond to analog current signal thresholds.

the operation of the VSD since the designation of a direction as forwards is arbitrary.

The timing diagram for this approach is shown in Figure 4.5. The current, I_{bldc}, in the BLDC machine is normally kept between the V_{Ihigh} and V_{Ilow} thresholds by toggling $CMPA$. However, when V_{Isense} escapes the inner tolerance band and $V_{bldc} = 0$, either the $V_{Ihigher}$ or V_{Ilower} threshold will be reached. This causes $CMPB$ to toggle, which applies $+V_{bldc}$ if V_{Ilower} is crossed and $-V_{bldc}$ if $V_{Ihigher}$ is crossed. The current and hence V_{Isense} should respond by gravitating towards being between V_{Ihigh} and V_{Ilow}. If the system is already applying $\pm V_{bldc}$ then nothing more can be done to force I_{bldc} to the desired value. In Figure 4.5 this is marked as *Control Lost*.

The variable B, the output of $CMPB$, is the only one that changes when

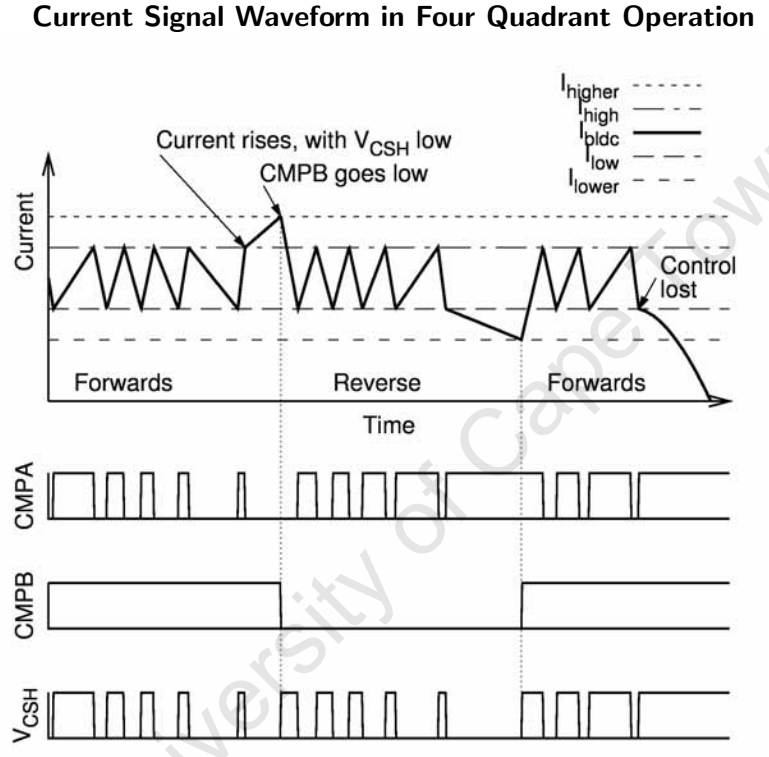

Figure 4.5: Four quadrant operation with unipolar switching is implemented using four thresholds on the current signal. The two inner levels control the current controller half bridge and the outer thresholds control the reversing operation. It is expected that the outer thresholds are reached infrequently because of the large mechanical time constant compared to the electrical one and the input conditioning on the throttle signal.

the direction of the applied voltage changes. Therefore V_{CSH} and V_{CSL} must also change when only $CMPB$ changes. In *Forwards* mode, the value of V_{bldc} increases when V_{CSH} goes high, which corresponds to A going high too. In *Reverse* mode, when A goes high the value of V_{bldc} should still become more positive, but when V_{CSH} goes high here, V_{bldc} goes more negative. So to maintain the relationship between A going high and V_{Isense} increasing, A needs to be optionally inverted based on the direction signal, B.

The resistor-capacitor filter linking B to the **XOR** optional inverter for A provides a delay of approximately $1\mu s$ when changing the state of the V_{CSH} value. This is necessary to allow the protective blanking time in the optional digital inverter to elapse.

The difference between V_{Ihigh} and V_{Ilow} is $160mV$, which should represent approximately $1A$. With the $3m\Omega$ sense resistor, the gain of the current sense amplifier should be around 53.

4.3 Optional Digital Inverter

In order to use the phase switcher without modifying it, the Hall sensors must be manipulated externally to achieve the effect of reversing the machine terminals. The multi-function gate can be configured as an **XOR** gate which will invert or pass through one input based on the level of the other.

Some blanking time is needed in the phase switcher when changing direction, to avoid large current transients caused by both switches in a leg being on simultaneously. The current controller helps in this regard by providing a short time with $V_{bldc} = 0$ for the inversion and blanking processes to complete.

The multi-function gate has three inputs, which can be used to create blanking time and optional inversion. Figure 4.6 shows two resistor capacitor diode arrangements and the Hall sensor signal as inputs to the gate. When the $CMPB$ signal transitions from low to high, the $REVH$ signal is instantly driven high by the diode, forcing the output low. Later on the $REVL$ signal catches up and then signal H_{Ain} is presented inverted at the output. When $CMPB$ goes from high to low, $REVL$ is instantly pulled low, again forcing the output low before the gate functions as a buffer for H_{Ain}. Blanking time is defined as time when all the switches in the phase switcher are off, which occurs when all the inputs are low or all the inputs are high.

The values of $Crevh$, $Crevl$, $Rrevl$ and $Rrevh$ were chosen to accommodate the input thresholds of the 74LVC1G58, which was also a concern in the temperature sensor, described in Section 3.3.2 on page 54. The amount of blanking time, with H_A, H_B and H_C all logic low was approximately $0.5\mu s$.

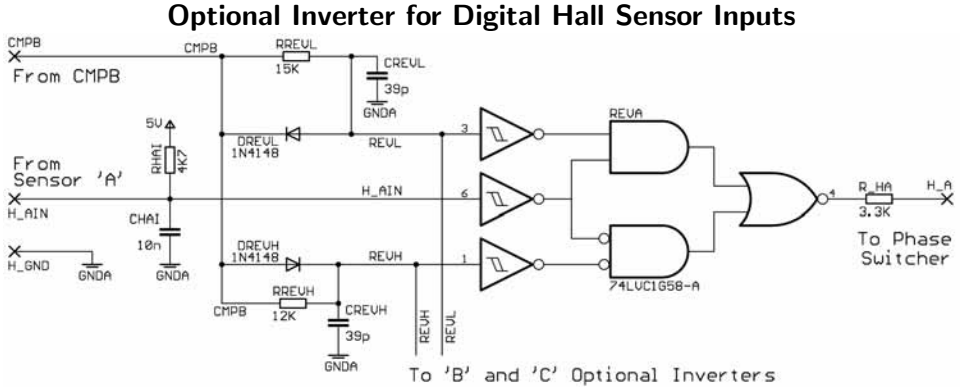

Figure 4.6: The 74LVC1G58 is used here to achieve two purposes at once. Firstly to optionally invert the Hall sensor signal by implementing an **XOR** gate. Secondly to force the output of each sensor to zero briefly during a transition from buffering to inverting and vice versa. This prevents shoot through currents in the phase switcher MOSFETs.

4.4 Optionally Inverting Current Sensor

As with the two quadrant design, a single signal that represents I_{bldc} is needed. The voltage measured across the sense resistor must be combined with an offset, optionally inverted and amplified to satisfy the four quadrant requirements.

The block diagram in Figure 4.7 shows the method used to achieve the optional inversion of the current sensor voltage, V_{Ifilt}. The summing junction adds the throttle input to V_{Ifilt} and $V_{Ifilt} \times -2$, if the switch is closed by $CMPB$. The result is then inverted by OPA to give an output of:

$$V_{Isense} = (CMPB \times -2 \times V_{Ifilt} + V_{Ifilt} + V_{throttle}) \times -G$$

When $CMPB$ is high, the value it has in the equation is $+1$. When $CMPB$ is low its value is 0. V_{Ifilt} is the voltage output of the filter from the two quadrant current sensing arrangement in Section 3.3.3.

The implementation of the optional analog inverter is shown in Figure 4.8. Operational amplifiers (Op-Amps) were used in the inverting amplifier configuration to facilitate the optional inversion process. V_{Iref} is set at $^{V_{CC}}/_{2}$ by the resistor divider. The signal V_{Ifilt} is correctly offset by equal resistances in a divider from V_{CC} to V_{Ifilt}, with the midpoint connected to the input of the amplifier.

In the case of $CMPB$ being high, R_{POLS} and R_{POLH} are a parallel combination with total resistance equal to R_{FILTS}, forming the correct ratio for the resistor divider connected to the input of OPA. OPB multiplies the value of V_{Ifilt} by -2 and adds it to the summing junction of OPA. This results in OPA giving an output of G times V_{Ifilt} with an offset of $^{V_{CC}}/_{2}$.

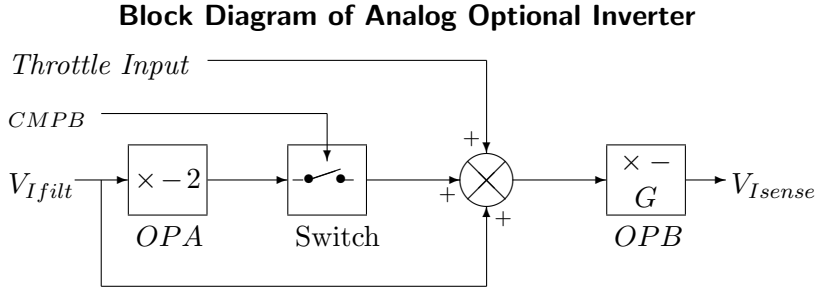

Figure 4.7: The method used to achieve an optional inverter uses an inverting summing amplifier. It adds the original signal, and another input made of twice the original input signal inverted or zero times the original input signal. The final result is plus or minus G times the original input signal. $CMPB$ controls the inclusion of the signal from OPB in the sum calculated by OPA.

When $CMPB$ is low R_{POLS} is at V_{gnd}, causing the R_{POLS} and R_{POLH} resistor divider to have no effect on the output of OPA. OPB is saturated at $+V_{CC}$ so that R_{SUM} now forms the divider with R_{FILTS} to correctly offset V_{Ifilt}. Since OPB is not amplifying, the output, V_{Isense}, is simply $-G$ times V_{Ifilt}, offset by $^{V_{CC}}/_{2}$.

This amplifier arrangement uses the rail to rail output ability of the LM1801 Op-Amp to minimize the offset introduced by changing from buffering to inverting. The resistor capacitor filter at the output of OPA absorbs the transient introduced by OPB slewing from V_{CC} to approximately $^{vcc}/_{2}$. It also limits the maximum switching speed of the VSD, providing protection against a rapidly changing throttle signal.

The gain G of OPA was set at 47, making the tolerance band V_{Ihigh} to V_{Ilow} represent a current of $\approx 1.2A$. The additional current error required to ensure a direction change is then $670mA$. In simulation this turned out to provide enough space to keep the transitions of A and B clean while adequately controlling I_{bldc}.

The throttle signal is added into the sum point of OPA with a resistance of $150k\Omega$. The throttle input signal comes from a $1V$ to $4V$ input device, allowing it to represent currents up to $\pm 33A$.

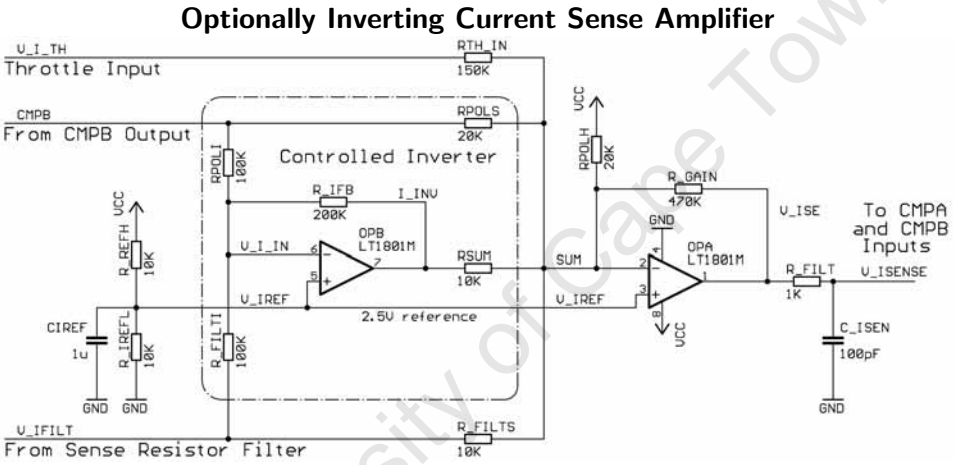

Figure 4.8: The signal $CMPB$ causes OPB to behave as an inverting amplifier or removes its effect on V_{Isense} by causing it to saturate and counteracting the effect of I_{inv} being high by connecting R_{POLS} to V_{gnd}.

Chapter 5

Results

In this section practical measurements of the variable speed drive (VSD) are presented. These include machine parameter, simulation and experimental measurements. The VSD described throughout Chapter 3 was manufactured and used to obtain the experimental results. The simulations were used as a guide to the development of the hardware and verification of the four quadrant design.

The machine used in the VSD for bench testing was a 408 hub motor from Crystalyte [9]. The 409 hub motor was used when testing the controller on an electric bicycle.

5.1 Machine Parameter Measurements

The machine used in the bench testing was attached to an LCR meter to determine the inductance of the windings. This guided the choice of a suitable switching speed and tolerance band. The resistance of the windings was simultaneously measured by the meter. Figure 5.1 shows the inductance measured in a 408 hub motor by the meter at various frequencies of excitation for two phases in series.

At low frequencies the leakage inductance is around $1mH$, but starts dropping off rapidly as the frequency exceeds a kilohertz. The interaction of changing electric current with a magnetic field causes eddy currents and the skin effect, described in Chapter 30 in Mohan [37], pages 744 – 790. These manifest themselves as reduced leakage inductance and increased resistance in magnetic components [14].

The concept of the current controller relies on the machine having a steady inductance. The controller was made to operate below $10kHz$ to ensure smooth operation.

Table 5.1 shows some of the parameters of the 408 and 409 models. The first two digits in the numerical code for the brushless direct current (BLDC) machine represent the width of the magnet material and the rest of the digits

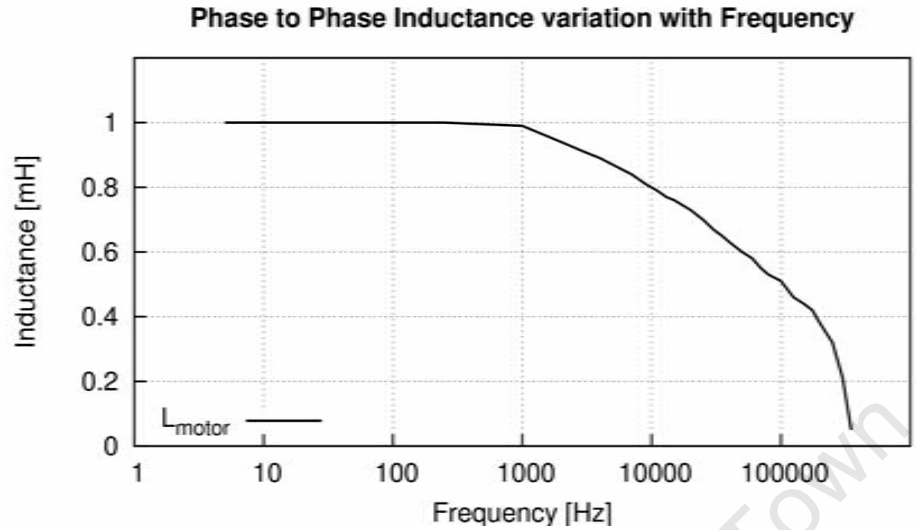

Figure 5.1: The value of L_{phase} varied as the frequency used to measure it was changed. The graph shows a more noticeable decline in apparent inductance as the frequency of the test signal exceeds $1kHz$.

indicate the number of poles. In the 408 motor the phase to phase resistance is less than in the 409 motor because the extra pole requires more wire to implement. The inductance of the 409 motor is higher than the 408 phase to phase inductance for the same reason. The armature constant is once again affected by the number of poles; the more poles there are, the higher the value of k_{arm}. The current limit is affected by the heat dissipation ability of the machine, which for these two models is the same, since they are both the same mechanical size. The 408 has a higher current limit because the internal power dissipation depends on the phase to phase resistance, which is lower than that in the 409.

With the same voltage supply both machines will produce approximately the same rated torque, however the higher electrical resistance of the 409 results in a lower maximum power output than the 408. The power conversion of an electromechanical machine is the product of the mechanical torque and the shaft speed or the generated voltage and armature current.

To quantify the above argument, the direct current (DC) machine equation:

$$V_T = V_{arm} + I_{arm} \cdot R_{arm} \Rightarrow I_{arm} = \frac{V_T - V_{arm}}{R_{arm}} \tag{5.1}$$

is substituted into Equation 3.6, $P = I \cdot V$, to give the electromagnetic power:

$$P_{EM} = \frac{V_T - V_{arm}}{R_{arm}} \cdot V_{arm} \tag{5.2}$$

The electromagnetic conversion rate, P_{EM}, is a maximum when V_{arm} is $\frac{1}{2}V_T$,

Table 5.1: Parameters of the 408 and 409 BLDC Machines

Parameter	408	409	Units
Number of Pole Pairs	8	9	
Phase to Phase Resistance	0.65	0.80	Ω
Phase to Phase Inductance	1.0	1.1	mH
k_{bldc}	1.27	1.47	NmA^{-1}
Current Limit	32	27	A

which is limited by the supply voltage V_{batt}. With a fixed voltage battery, the maximum electromagnetic power transfer is determined by R_{arm}, in the electrical system.

5.2 Simulations

The BLDC motor and controller were simulated using Simulation Program with Integrated Circuit Emphasis (SPICE) version 3f5. The advantage of using a computer to predict the operation of the VSD was that any point in the system could be observed at any time. In the real world, only a few points can be simultaneously observed, because of limited measurement equipment. Provided the simulation uses an accurate model of the physical situation, the results may even be a more useful gauge of the performance, since the parasitic impedances from measurement equipment are absent in the virtual world of simulations.

Appendix A has a listing of the SPICE code used to generate the following simulation results. The generated voltages of the BLDC machine and the Hall effect position sensor signals were simulated using periodic waveforms of the same frequency. The simulated electric machine speed was constant for the duration of two quadrant simulation runs, but was modelled as constantly accelerating for some of the four quadrant tests.

5.2.1 Comparison of Voltage and Current Control

Two simple methods of controlling the power flow between the BLDC machine and the energy storage system are investigated in this section:

Open Loop Voltage Control uses a control signal to set the duty cycle, and hence the average value, of V_{bldc} by pulse width modulation (PWM) of V_{batt}.

Closed Loop Current Control uses a control signal to set a desired current level for I_{bldc}, which is attained using one of the schemes of Section 2.4.2.

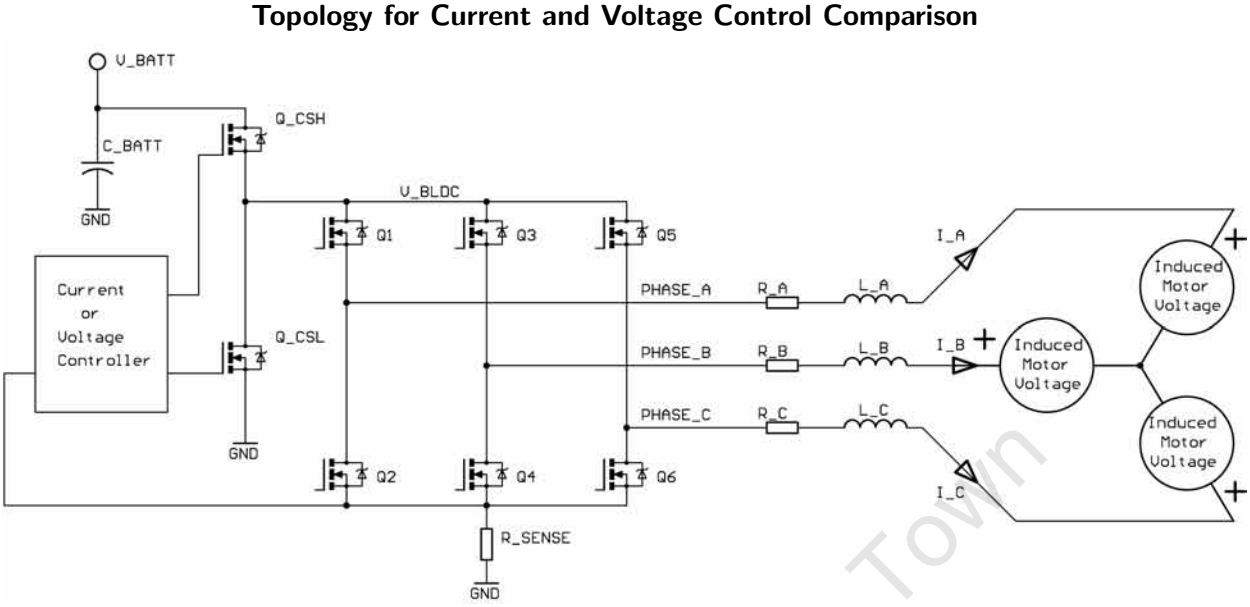

Figure 5.2: The topology used in simulations for comparing the current control method and the voltage control method for BLDC machines.

Figure 5.2 shows the topology of the simulation. The two methods of control are compared based on the currents that flow in the machine phases because the torque output is directly related to them. The control signal in both cases was set to cause approximately the same average current in the machine in both cases.

The speed of the BLDC machine in each case was simulated as constant. The supply voltage, V_{batt}, was set to $30V$ and the metal oxide semiconductor field effect transistor (MOSFET) model used was for an equivalent to the FDP3632.

The results of the simulations illustrate that the tolerance band current control of the motor is better at maintaining a constant phase current. In Figure 5.4, where V_{bus} is modulated with a constant duty ratio, the current flowing in the phase sharply decreases and then slowly rebuilds after each commutation.

Figure 5.3 shows the phase current and V_{bldc} with the tolerance band current control scheme. The phase current is nearly the ideal square shape from Figure 2.5, which would result in an almost constant output torque in the mechanical system. The measured current reduces to zero at every commutation because the newly connected phase has no current flowing in it. The controller compensates for this creating a long positive V_{bldc} pulse at each commutation, which causes the quick build up of current in the newly conducting phase. The shape of the phase current is thus nearly ideal.

Figure 5.4 shows the phase current and V_{bldc} signals when the open loop voltage control scheme is used. In this case the phase current responds as if the voltage applied to it is the product of the duty ratio and V_{batt}. In Khan's work [27], the BLDC mode of his controller obtained similar results to the open loop voltage control simulation.

During normal operation, between commutation events, I_{bldc} and I_{phase}, in active phases, can be predicted with the exponential equation:

$$I_{bldc} = I_{init} + \left(\frac{V_{bldc} - V_{emfBL}}{2R_{phase}} - I_{init} \right) \cdot (1 - e^{-t\frac{R_{phase}}{L_{phase}}}) \tag{5.3}$$

Open loop voltage control forces the duty cycle to be constant, making the average value of V_{bldc} a fraction of V_{batt}. In the tolerance band case, the controller temporarily made V_{bldc} equal to V_{batt} to speed up the commutation, but in the open loop voltage scheme this does not occur. The current in this case will take the same amount of time to reach a steady value after each commutation, regardless of the desired value of I_{bldc}. This means a large variation in output torque, especially noticeable at lower speeds where the ω_m is low and the mechanical system has little stored energy to keep movement smooth.

Inspection of Figure 5.3 and 5.4 indicates that the torque ripple of the tolerance band method is at least half that of open loop voltage control at a current of about $2A$ at half the rated speed.

At higher currents and speeds the two approaches begin to behave more similarly because the difference between the average of V_{bldc} and V_{batt}, which makes the tolerance band method achieve faster commutations, is less.

At the circuit level, both schemes use roughly the same number and type of components. As the simulations have shown, current control has the advantage of being able to produce smoother torque at lower speeds; which is important for VSD to achieve the aim of smooth torque control. Therefore the more desirable type of control for the VSD is current control.

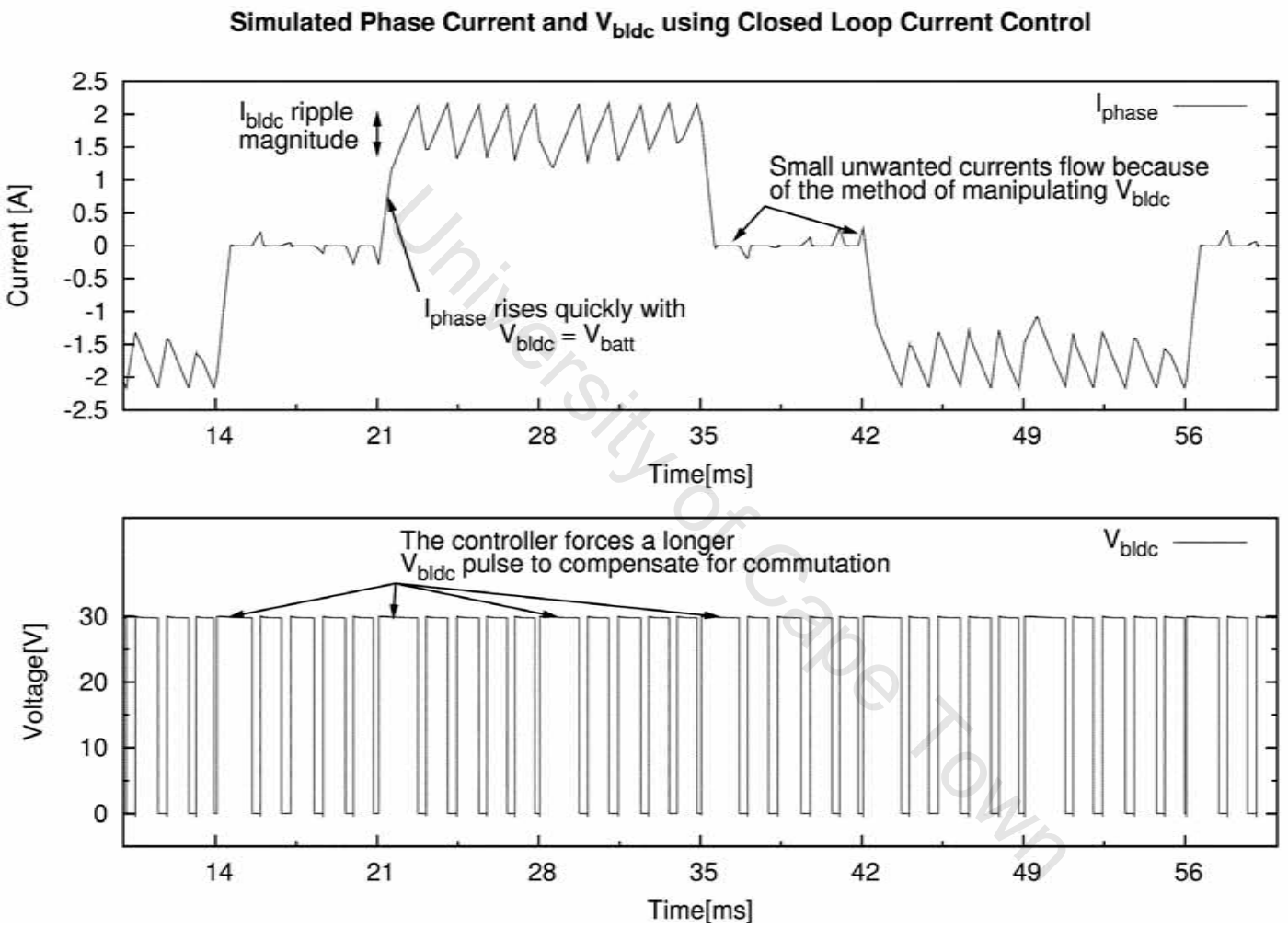

Figure 5.3: I_{phase} and V_{bldc} are simulated for typical motoring operation with a tolerance band current controller. When a commutation event occurs the current controller forces V_{bldc} to V_{batt} so that I_{phase} builds up quickly in the next phase that is active.

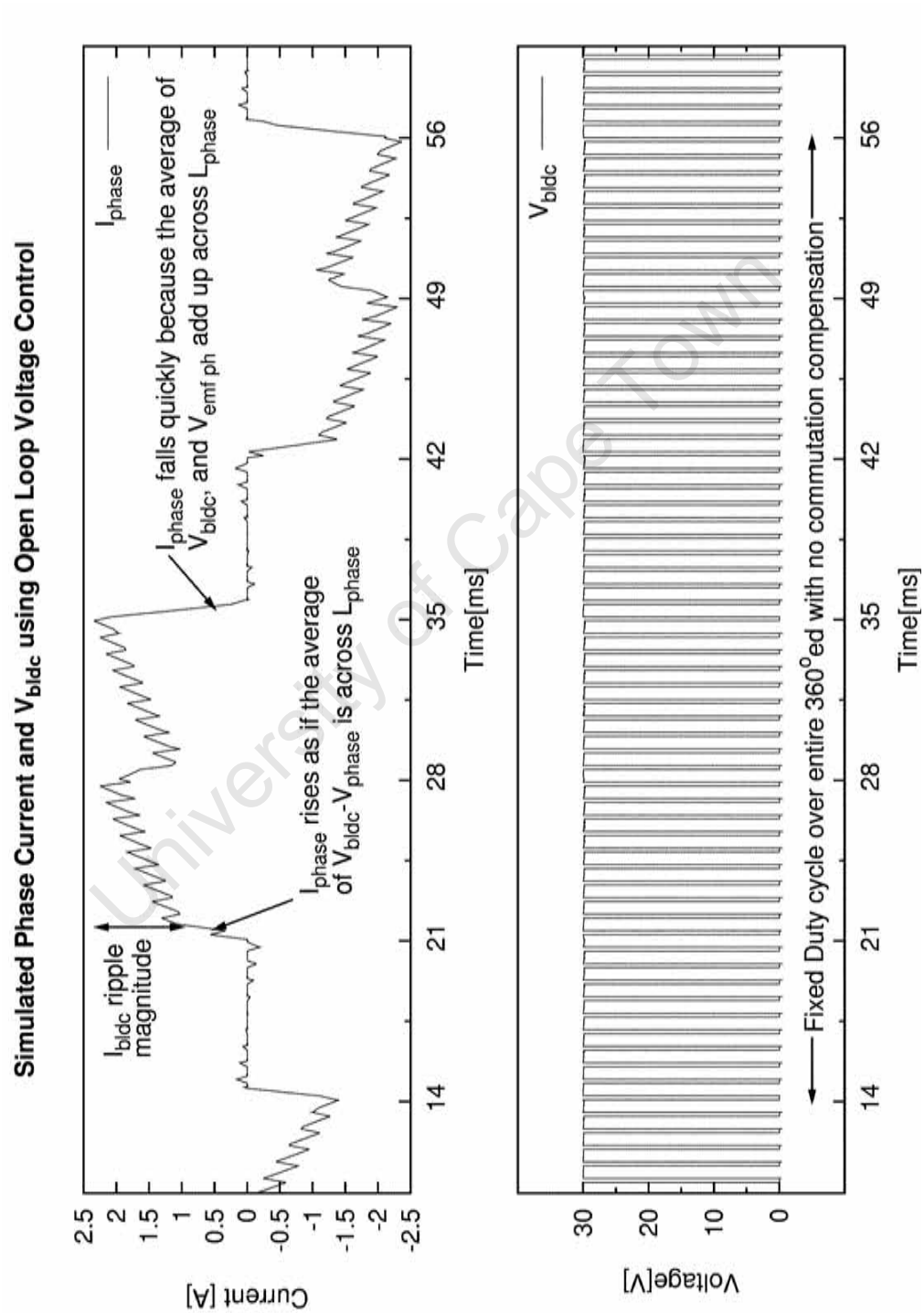

Figure 5.4: I_{phase} and V_{bldc} for a BLDC machine controlled with a fixed average voltage produced by PWM of V_{bldc} with a constant duty ratio. The current takes several time constants, R_{phase}/L_{phase}, to settle after a commutation event. This makes the current ripple magnitude large.

5.2.2 Current Commutation Analysis

The mechanism of current commutation was investigated in two topologies to determine the better approach for measurement of the effective machine current, I_{bldc}.

Simulation Topologies for Assessing Commutation

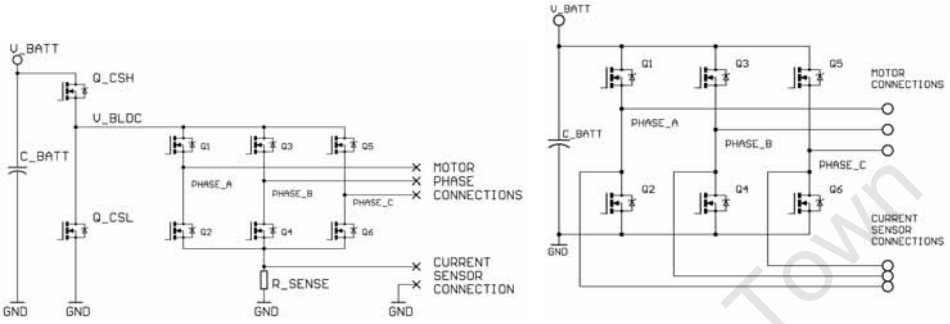

(a) Modular design of this topology is possible. The low number of interconnections between the electronic commutator, current controller and current sensor promotes separate pieces.

(b) Integrated commutation and control logic is necessary to make this arrangement work. The current sensing scheme in simulation uses MOSFET R_{ON}, but the same principles apply if sense resistors are used.

Figure 5.5: Two topologies set up in simulation environment for comparison of how the current measurement scheme affects the system response to commutation.

The modular design of Figure 5.5(a) uses a single current sensor positioned after the electronic commutator, or phase switcher, which experiences a current similar to I_{bldc} or I_{arm}, the effective machine current. The control logic is simple; a separate single channel half bridge current controller and phase switcher logic.

The topology of Figure 5.5(b) uses the signals that drive the MOSFET gates to determine which leg of the inverter bridge to obtain current measurements from. More complex logic functions are needed to implement the unipolar switching scheme because sometimes two switches of Q_2, Q_4 and Q_6 are on at the same time, preventing simple use of the active drive signals as a current branch selection signal.

The current magnitude is controlled using the tolerance band method in both cases.

At each commutation event all three phases become involved, as illustrated in Figure 5.6. The phase that keeps the same connections before, during and after commutation, is referred to as the unswitched phase. The phase that is about to be disconnected is called the previous phase and the phase that is going to change from being unused, to conducting with the unswitched phase, is called the next phase.

The components in Figure 5.6 are labelled with a subscript denoting which phase they belong to. The phases have the following subscripts: **p**, for the previous phase; **n**, for the next phase and **u**, for the unswitched phase.

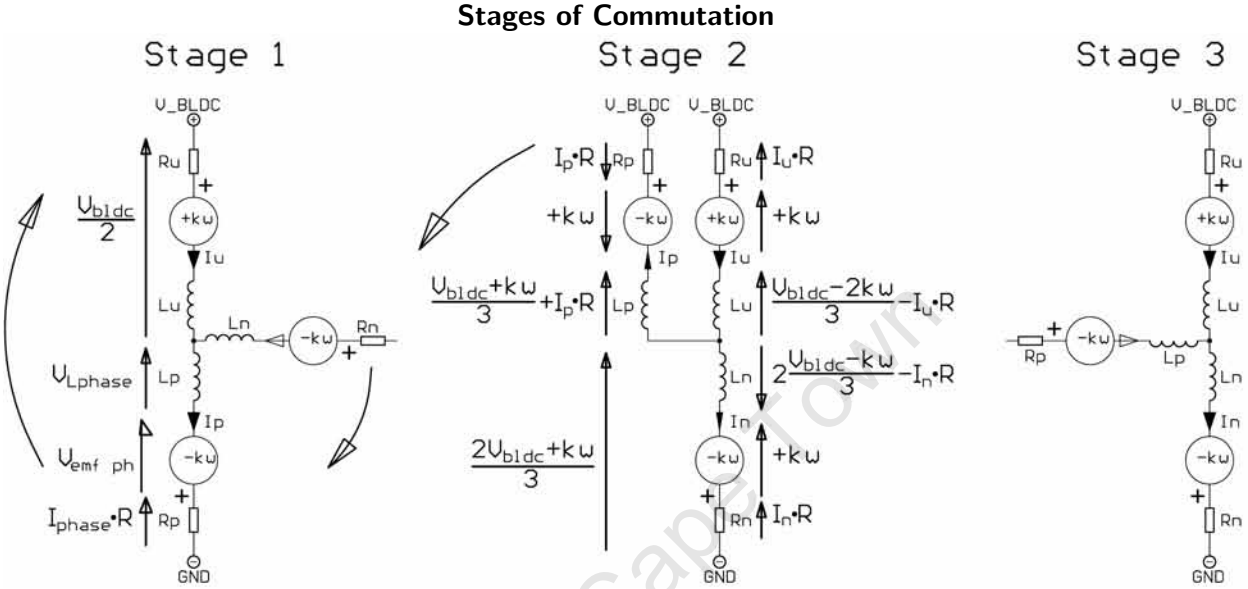

Figure 5.6: Commutation of current from the previous phase to the next phase is broken down into three steps above. In *Stage 1*, the previous and unswitched phases are conducting the current I_{bldc}. Then in *Stage 2* current builds up in next phase while decaying in previous phase. Finally, in *Stage 3* the previous phase current has reached zero and operation continues as normal.

Simulation Result of the Modular Topology

The phase currents and the current in the sense element are plotted in Figures 5.7(a) and 5.7(b), for a positive I_{bldc}, and in Figure 5.7(c) and 5.7(d) for negative I_{bldc}.

During motoring operation with I_{bldc} positive, that is *Stage 1* in Figure 5.6, the normal rate of change of current in the unswitched and previous phases is:

$$\frac{\Delta I_{phase}}{\Delta T} = \frac{\frac{1}{2}V_{bldc} - V_{emf\,ph} - I_{phase} \cdot R_{phase}}{L_{phase}}$$

A commutation event causes the previous phase current to decay through the body diode in one of the two MOSFETs controlling that phase. The next phase current begins to build up when one of the MOSFETs controlling it turns on. The unswitched phase is now in the situation where it is in parallel with the previous phase and in series with the next phase, *Stage 2* in Figure 5.6. Commutation is over when the previous phase current decays to zero. The rate of current change in each phase in the machine, during

the type of commutation shown in Figure 5.6 is:

$\frac{2}{3L_{phase}}\left(\frac{1}{2}V_{bldc} - 2V_{emf\,ph}\right) - I_u R_{phase}$ for the unswitched phase,
$\frac{2}{3L_{phase}}\left(\frac{1}{2}V_{bldc} + V_{emf\,ph}\right) + I_p R_{phase}$ for the previous phase and
$\frac{2}{3L_{phase}}\left(-V_{bldc} + V_{emf\,ph}\right) - I_n R_{phase}$ for the next phase.

When commutation occurs the decay rate of current in the previous phase and the growth rate in the next phase may be unequal. If

$$V_{emf\,ph} < {}^1\!/_4 V_{batt} \text{ and } I_{bldc} > 0$$

then the unswitched phase current increases in magnitude during commutation. This can cause the sensed current to overshoot the tolerance band on completion of commutation. Figure 5.7(a) shows the unswitched phase current increasing, Figure 5.8(a) shows actual tolerance band overshoot. If $V_{emf\,ph} < {}^1\!/_4 V_{bldc}$, the post commutation unswitched phase current will be lower, as it is in Figure 5.7(b). If the situation is severe enough, the sensed current is below the tolerance band when commutation completes. The consistency of the output torque is affected by these mechanisms.

The sensed current is normally the current flowing in the two phases in series, but the instant that commutation occurs, the current in the sensor becomes zero. This is because the previous phase was conducting I_{bldc} through the sensor, but at the commutation instant, the complementary MOSFET body diode allows the previous phase current to circulate within the phase switcher through the unswitched phase. The sense resistor is now just measuring the current in the next phase, which is initially zero. This makes the current controller force V_{bldc} to V_{batt} until the current in the next phase, which is measured by the sensor, reaches I_{high}.

When the motor is in generating mode, in Figures 5.7(c) and (d), the currents in all the phases automatically flow in the path that includes the sense element, therefore commutation causes no glitches in the current signal. The previous phase current slowly decays, making the whole commutation process very smooth, but the electromagnetic power conversion of the machine is compromised by this process. Suppose the total current is kept constant. Then, if one phase is conducting for a long time after it has been switched off; it effectively reduces the torque per amp produced by the machine. This impacts on the efficiency and the capacity for power conversion.

Simulation Result of the Integrated Topology

The phase currents for this design behave exactly the same as the modular topology when in motoring mode. The phase currents in Figures 5.8(a) and (b) match exactly those in Figures 5.7(a) and (b). The sensed current, shown in the bottom plots of Figures 5.8(a) and (b), are derived from the

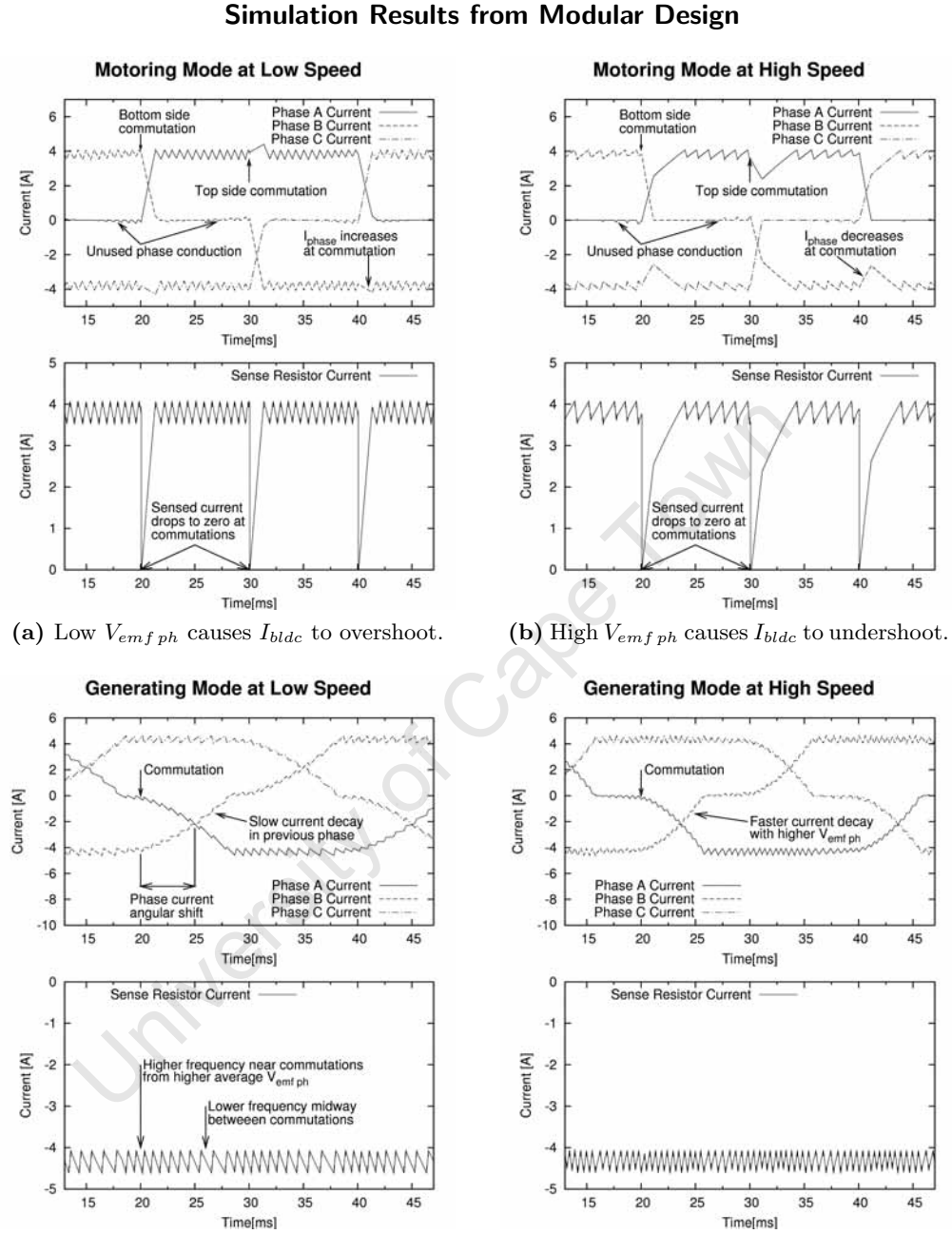

(a) Low $V_{emf\,ph}$ causes I_{bldc} to overshoot.

(b) High $V_{emf\,ph}$ causes I_{bldc} to undershoot.

(c) I_{phase} is phase shifted by commutation.

(d) Higher $V_{emf\,ph}$ reduces I_{phase} shift.

Figure 5.7: Top side and bottom side commutations are handled in the same way, because the current sensor measures the current through the whole phase switcher. In motoring mode, with I_{bldc} positive, the sensed current drops to zero at each commutation because of circulating currents. In generating mode the previous phase current decays through the sense resistor instead of circulating in the phase switcher. This increases commutation time and causes a phase shift between $V_{emf\,ph}$ and I_{phase}.

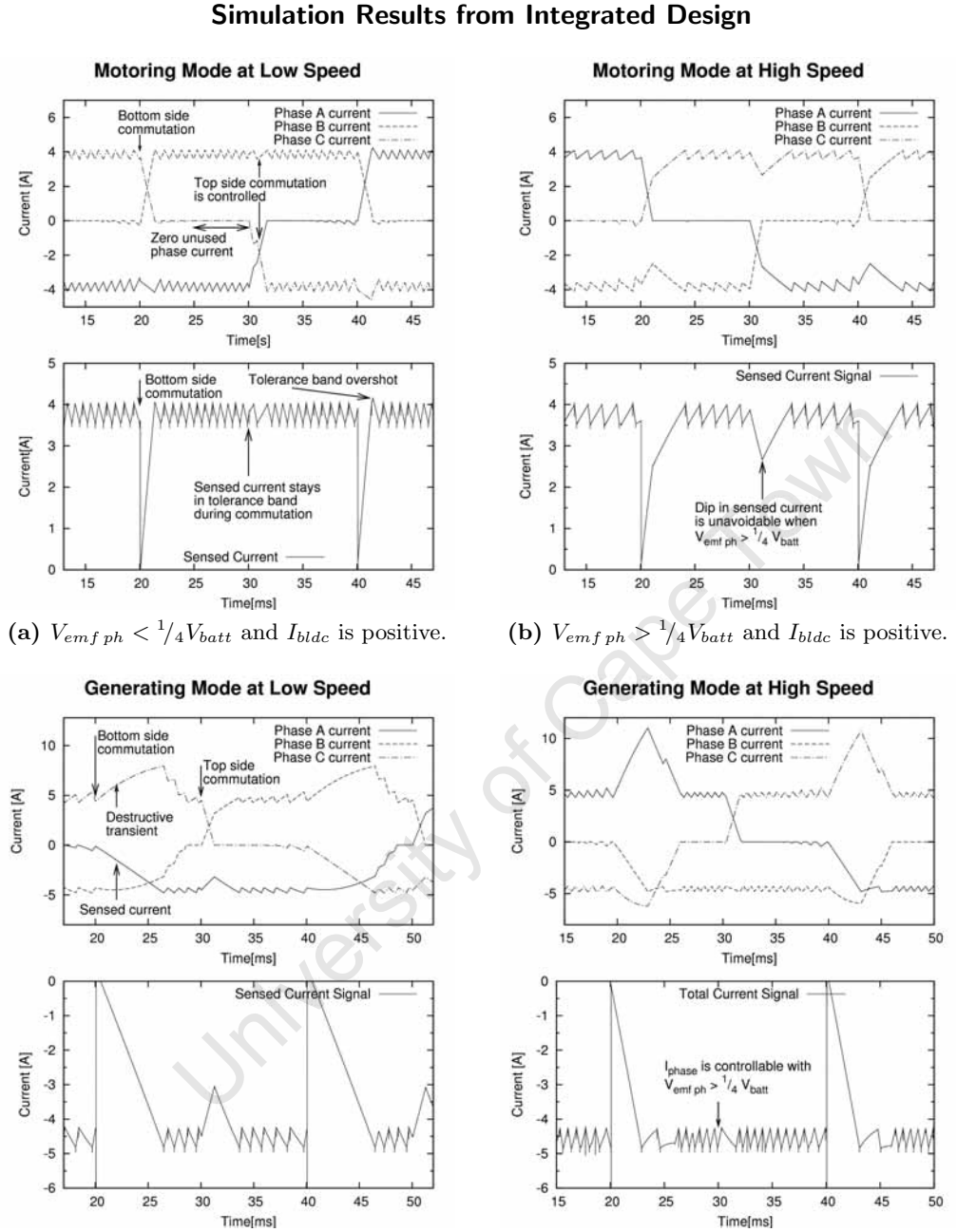

(a) $V_{emf\,ph} < {}^1\!/_4 V_{batt}$ and I_{bldc} is positive.

(b) $V_{emf\,ph} > {}^1\!/_4 V_{batt}$ and I_{bldc} is positive.

(c) $V_{emf\,ph} < {}^1\!/_4 V_{batt}$ and I_{bldc} is negative.

(d) $V_{emf\,ph} > {}^1\!/_4 V_{batt}$ and I_{bldc} is negative.

Figure 5.8: In these tests the current is sensed using R_{ON} of the low side MOSFETs. The commutations are smoother when the unswitched phase is a low side one because I_{bldc} is exactly represented by the current in the unswitched phase. In (a) and (d) the controller keeps the current in the unswitched phase on the V_{gnd} side within the tolerance band for high side commutations. In generating mode, if the unswitched phase is on the high side, it experiences a build up of current until the next phase current reaches the tolerance band. This transient could exceed the ratings of many components in the VSD.

active switch that is connected to V_{gnd}. Only commutations where the previous and next phases are on the V_{gnd} side will cause the sensed current to momentarily fall to zero. There is no difference between the modular and integrated control action taken when a commutation occurs in motoring mode, despite the difference in the sensed current.

One noticeable difference is the shape of the current spike that occurs at every switching event. In the modular design the spikes always develop towards the middle of the tolerance band, in the integrated approach the spikes in the current signal are headed towards a more negative current. Kavanagh *et al.* [26] pointed out that unidirectional disturbances are more difficult to remove than bidirectional ones.

The integrated topology has a distinct problem in the generating mode when commutation occurs. The unswitched phase can temporarily conduct much more current than the controller can handle. In the top plots of Figure 5.8(c) and (d), the unswitched phase has twice the desired current flowing in it. The unwanted large current is only able to build up when the previous and next phases are being switched on the V_{gnd} side, where the current is measured. At the point of commutation, the previous phase stops supplying current sensor information and the task is passed onto the next phase. The controller now sees zero current and tries to compensate by setting the unswitched phase to V_{gnd}, because the generating mode requires the build up of current in the machine before releasing energy to the battery or supply. This step causes the next phase current to rise, but also the previous phase and the unswitched phase currents. When the next phase current reaches the tolerance band, the controller reverts to normal switching and the excess current build up in the previous and unswitched phases are allowed to settle to their steady values.

In the sense resistor current plots of Figures 5.8(c) and (d), the current signal resembles that of the motoring mode, and is unaware of the high circulating current levels during low side commutations.

Another problem with the integrated approach is that the gains of the three current sense branches have to be matched so that steady control can be achieved.

There are problems with both topologies, but the one most suited to the this VSD application is the modular approach. It has simplicity and a safe way of dealing with commutation events in both motoring and generating modes.

Kavanagh *et al.* [26] used a single sensor in the same way as the modular topology. In their solution to a BLDC controller, the bipolar switching scheme was used to ensure the current flowing in the sense element represented I_{bldc} closely. In the modular topology, the sense element still achieves good I_{bldc} representation but has the ability to present the BLDC machine with zero volts as well as $\pm V_{batt}$.

5.2.3 Effect of MOSFET On-Resistance

During the testing of the initial prototype of the VSD, the Q_{CSH} and Q_{CSL} switching became unstable when I_{bldc} was set to a modest current, around $5A$. The initial design used IRF530N MOSFETs as the switching devices, which have an R_{ON} of $90m\Omega$. The problem was investigated in SPICE, which revealed the alternative loop that current flows in when V_{bldc} is V_{gnd}. Figure 5.9 shows the expected current path and the parasitic current path. Zhang *et al.* [60] also reported this potential problem in their work on current sensing using the R_{ON} of a MOSFET.

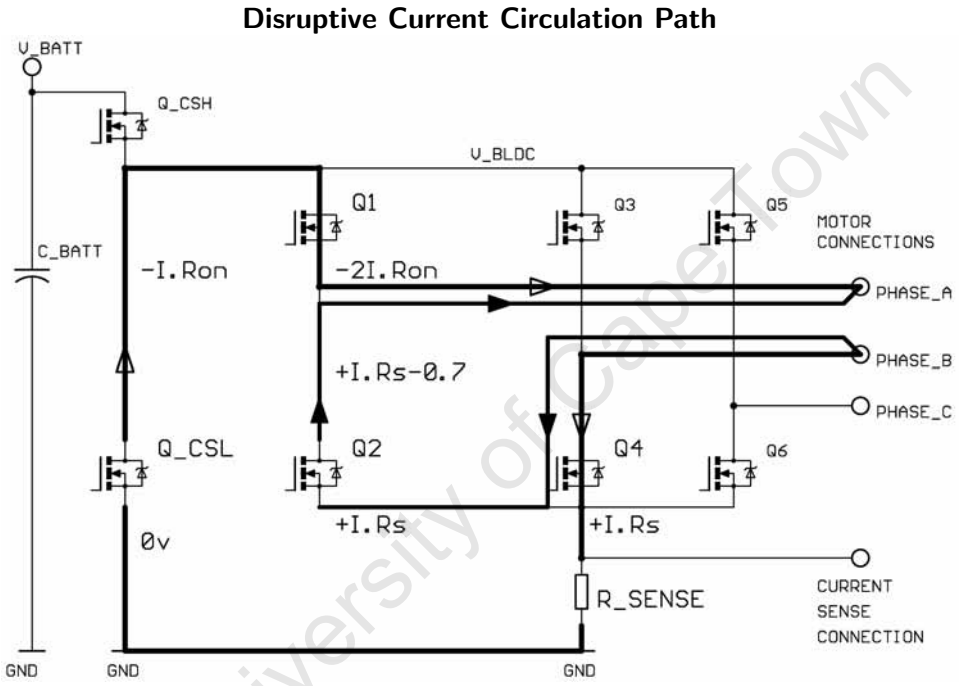

Figure 5.9: The outlined arrow heads point along the expected current path when V_{bldc} is V_{gnd}. The solid arrow heads show the path current takes when $2 \cdot R_{ON} \cdot I_{bldc} + I_{bldc}R_{sense}$ is greater than the diode drop of a MOSFET.

The reason for the switching instability is that the amount of current diverted away from R_{sense} becomes greater than the tolerance band set by OPA in Figure 3.15. This causes an immediate switch back to the previous state, where the current has exceeded the upper threshold on the tolerance band also. The switching frequency becomes very high, limited only by the propagation delay of the current control loop; causing high power dissipation in the switches and possibly their destruction.

Since the controller behaves erratically when high R_{ON} MOSFETs are used, a simulation was devised where the current controller operated normally while the sense resistor current responded to the current stealing effect

of the parasitic conduction path. In the case where R_{ON} of the MOSFETs are low enough to avoid conduction of the body diode of Q_2, in Figure 5.9, the sense resistor current resembles Figure 5.10(a). If the MOSFET R_{ON} is greater than $\approx 0.7 \div (I \times 2)$ then the sense resistor current looks like Figure 5.10(b). The assumption that the other parasitic resistances are small enough to ignore in the circuit is valid since the R_{ON} of the MOSFETs is high.

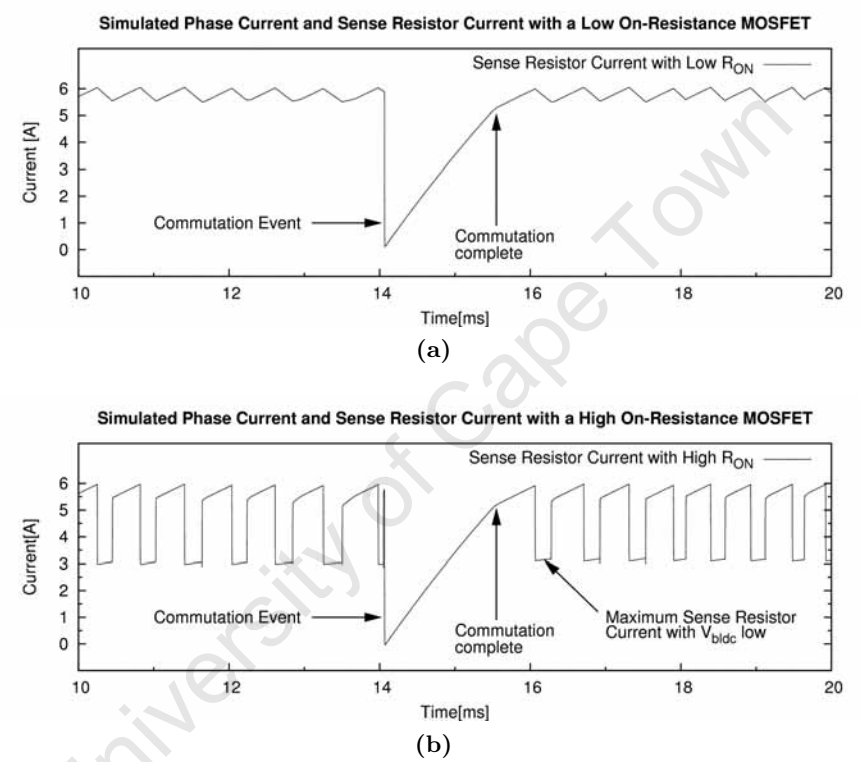

Figure 5.10: The effect of high R_{ON} MOSFETs is to cause current flow in the body diode of an off state switch; redirecting the current that the sense resistor would normally conduct. The sense resistor current in the (a) is the expected result with R_{ON} low. Current increases while V_{bldc} is at V_{batt} and the sense resistor conducts the full current. When V_{bldc} is forced to V_{gnd}, the limit to the amount of current in the sense resistor is $0.7 \div (2 \cdot R_{ON} + R_{sense})$, shown in (b).

To alleviate the problem of the unwanted current flow, a MOSFET with a lower R_{ON} was used in further simulations; resulting in no unwanted diode conduction. The FDP3632 was chosen for the final version of the VSD since it has R_{ON} low enough to avoid the undesirable diode turn on for the whole range of currents that the VSD is designed to handle.

5.3 Four Quadrant Simulation Results

These simulation results verify that the four quadrant design in Chapter 4 is capable of the the following:

- Automatic direction switching to maintain a particular current level.
- Avoiding shoot through currents or cross conduction in the phase switcher.
- Maintaining a constant I_{bldc} or T_m over the range where V_{batt} is large enough to enforce the desired values.
- Producing all possible I_{bldc}, provided V_{batt} is large enough, within $\pm 30A$ at constant speed.

These simulations were also done on SPICE version 3f5 from Berkerly. The speed and position of the BLDC machine was simulated with acceleration in order to perfrom tests that sweep a range of operating points. This also showed that the four quadrant design could handle varying throttle and speed signals and smoothly perform the automatic direction changing. The code used to generate the data in this section is given in Appendix A.

5.3.1 Automatic Direction Switching

To test the automatic direction switching, the throttle input was set so that I_{bldc} was $5A$. The speed of the simulated machine was varied from $-30rad/s$ to $+30rad/s$ to cause the direction to change from *Forwards* to *Reverse*, shown in Figure 5.11(a). In Figure 5.11(b), the direction changed from *Reverse* to *Forwards* when ω_m was simulated from $+30rad/s$ to $-30rad/s$.

When $CMPB$ is high, *cmpbin* is above V_{Iref} which is $\approx 2.5V$, because they are directly linked by the feedback resistors in the current controller design. The "direction" of the VSD can then be interpreted as *Forwards* when $CMPB$ is high or when *cmpbin* is above V_{Iref}.

The two cases when a direction change is required are shown in Figure 5.11. In (a), the current I_{bldc} continues to increase, even with V_{bldc} $=V_{gnd}$. Eventually V_{Ihigh} is exceeded by V_{Isense} and $CMPB$ changes, putting the controller in *Reverse*. The opposite sequence of events causes a direction change in 5.11(a).

The rate of change of current will reverse polarity, as intended, when the following inequality is satisfied:

$$\frac{CMPB \times V_{batt} - I_{bldc}R_{bldc} - V_{emfBL}}{-\overline{CMPB} \times V_{batt} - I_{bldc}R_{bldc} - V_{emfBL}} < 0 \tag{5.4}$$

A change of the controller direction bit, $CMPB$, is needed when the value of $I_{bldc}R_{bldc} + V_{emfBL}$ changes sign. The inequality is false in this situation

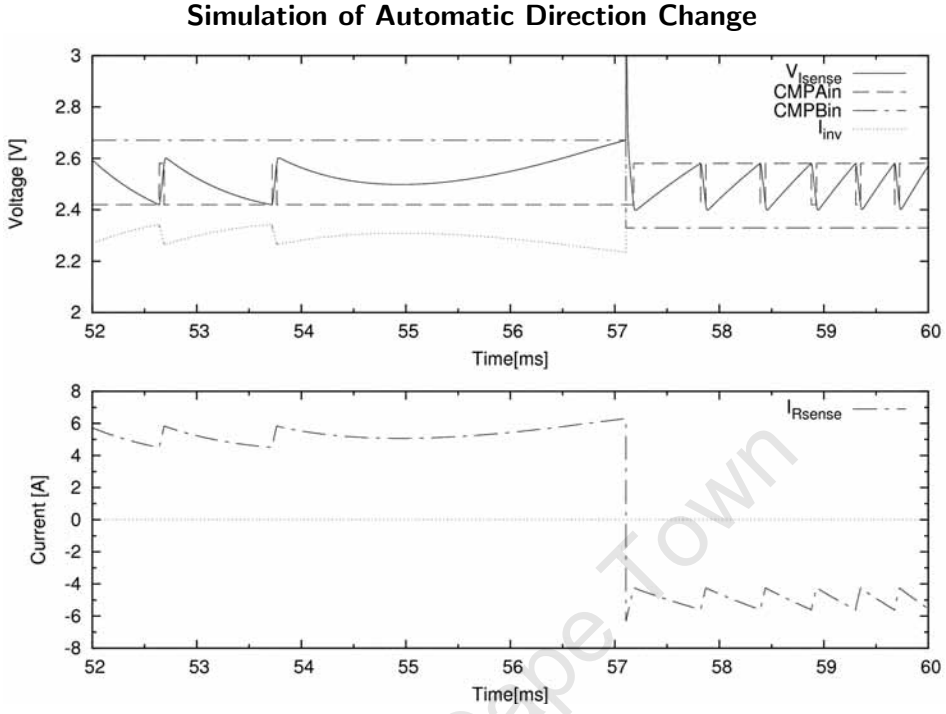

(a) ω_m increasing

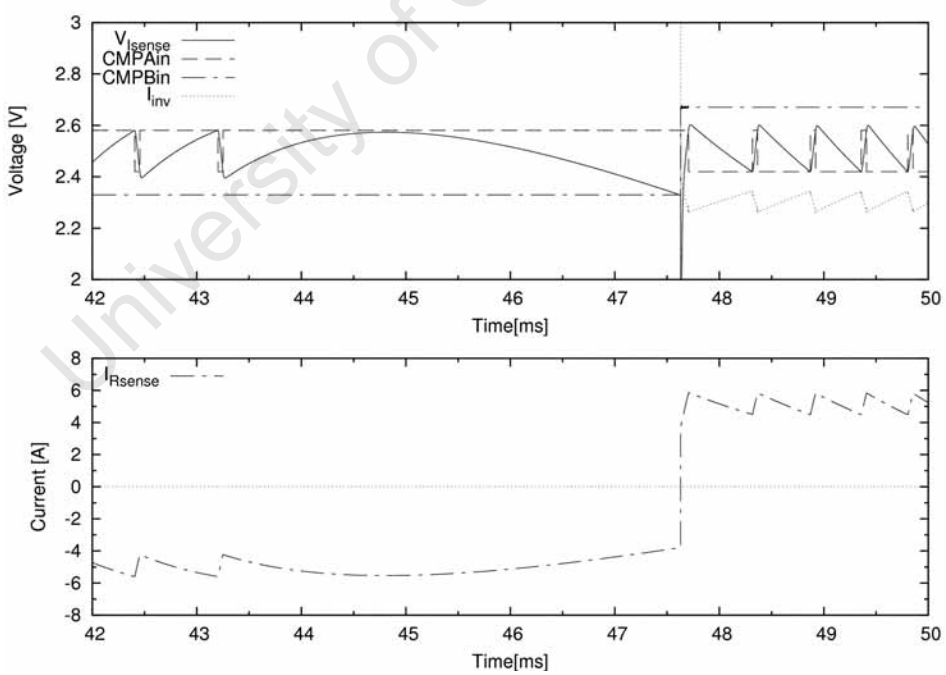

(b) ω_m decreasing

Figure 5.11: The current in the sense resistor becomes exactly the negative of its previous value when $CMPB$ changes value. When $CMPB$ is high, I_{INV} is enabled and adds to V_{Isense} so that I_{Rsense} changes in the same direction. This confirms that the four quadrant controller makes smooth direction transitions, as predicted in Figure 4.5.

because both top and bottom are of the same sign, meaning that L_{bldc} experiences a current build up in the same direction independent of whether V_{batt} or V_{gnd} is applied to V_{bldc}. $CMPB$ represents one unit in Equation 5.4 when it is logic high, and 0 when it is low.

The controller is considered to have lost control of I_{bldc} when both possible applications of V_{batt} fail to steer I_{bldc} back into the tolerance band.

5.3.2 Blanking Time in Digital Optional Inverter

The Hall effect position sensor outputs are forced low for approximately the same time when $CMPB$ has a rising or falling output. H_A, H_B and H_C are the modified position sensor signals generated by the digital optional inverter that are then used as inputs to the phase switcher. The original signals from the sense elements in the BLDC machine are called H_{Ain}, H_{Bin} and H_{Cin}. In Figure 5.12 the signals in the phase switcher that control the upper and lower MOSFETs are combined such that if the low side switch is on, the joint signal measures $-5V$, if the high side switch is on it measures $5V$ and if both switches are off $0V$. This makes it easy to spot the blanking time inserted by the digital optional inverter.

The signals $REVH$ and $REVL$ are shown in the top left of Figure 5.12, clearly showing the deliberately unequal rise and fall times. The built in Schmitt trigger of the 74LVC1G58 turns this into a delay of approximately $0.5\mu s$ during which time H_A, H_B and H_C are forced low. The V_{CSH} and V_{CSL} signals are delayed by about $1\mu s$ so that the phase switcher has time to turn on the MOSFETs that will be conducting next while having no voltage across them.

Each graph in Figure 5.12 is split in the middle so that an illustration of $CMPB$ going high and another of $CMPB$ going low can both be shown. The $0\mu s$ label in each side of each graph mark the time at which $CMPB$ changes.

The code used to generate these results was a trimmed down version of the whole system code. The resolution required to illustrate the actual functionality of the digital optional inverter was unattainable with the full system being simulated.

5.3.3 Simulated Constant Torque Operation

In this simulated test the throttle setting was fixed and ω_m was allowed to vary over the whole range of speeds where the current could still be controlled. Several different levels were simulated to obtain an operating area for the VSD. The family of graphs in Figure 5.13 fit into the shape shown in Figure 3.1, showing successful simulated operation in the whole area of possibilities for the four quadrant controller.

The uneven shape of the curves is a result of sampling the instantaneous current. In the tolerance band scheme, instantaneous current is not always

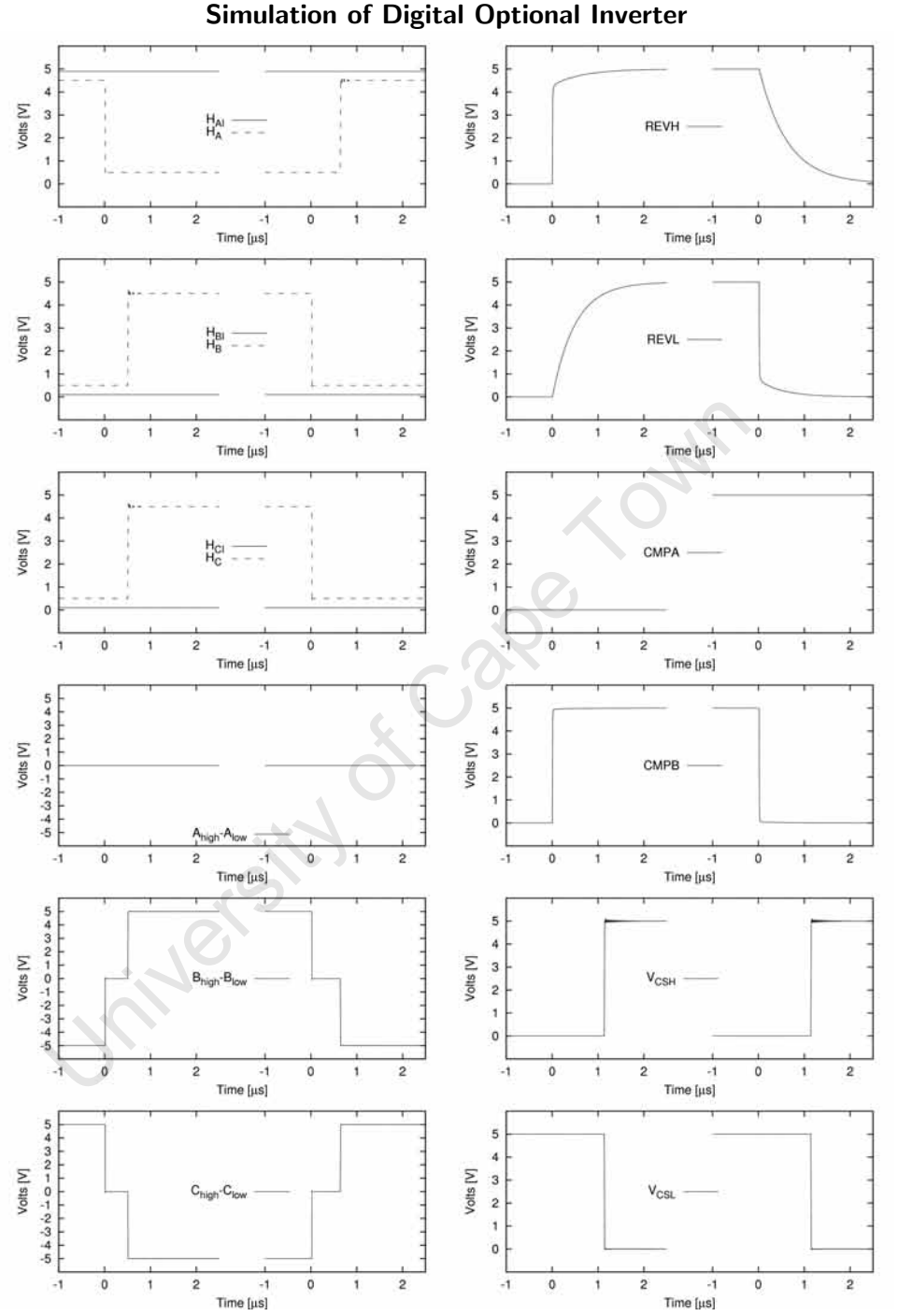

Figure 5.12: The incoming Hall effect position sensor signals are forced to logic low for about $0.5\mu s$ when $CMPB$ changes from high to low or vice versa. V_{CSH} and V_{CSL} are delayed by about $1\mu s$ whenever $CMPB$ causes them to change.

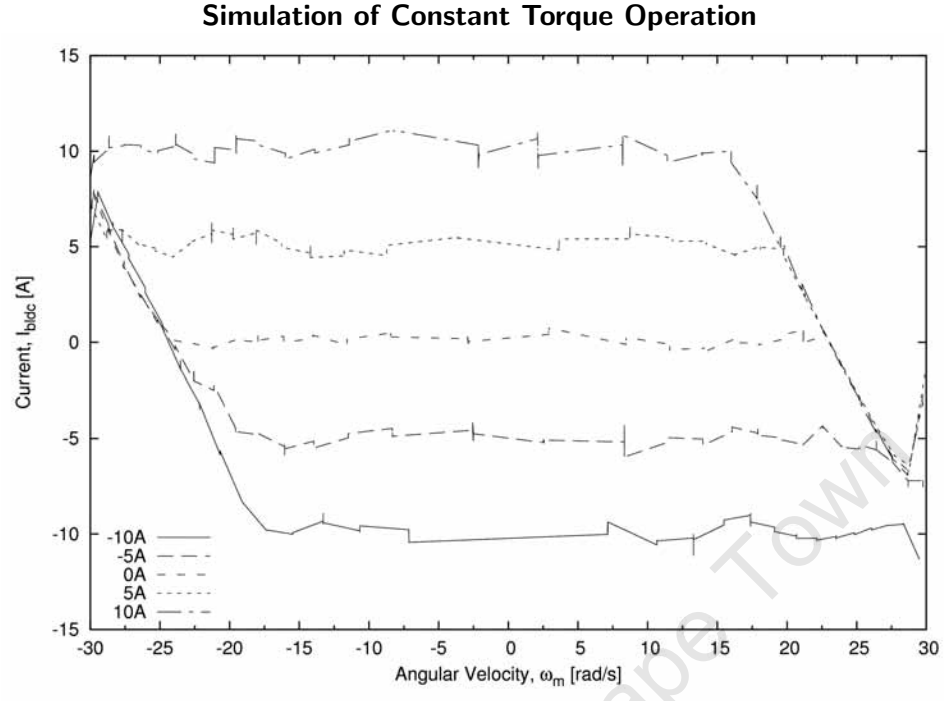

Figure 5.13: The speed of rotation, ω_m, was allowed to vary across the full range while keeping the throttle signal at a constant level. The four quadrant controller automatically switches direction to maintain I_{bldc}.

exactly equal to the average current. The spikes are caused by commutation events and switchings of $CMPA$.

5.3.4 Simulated Constant Speed Operation

The torque was varied between the positive and negative maximums allowable in the BLDC machine, covering active braking zones and crossing from motoring into generating zones. The same can be said for the constant torque simulation since both tests essentially cover exactly the same operating conditions. However in this test the current was simulated up to the maximum value, $\pm 30A$. Figure 5.14 shows each test as a vertical series of points. The outlying points can be easily identified because they don't form a heavy blob on the plot area. The shape in Figure 3.1 is evident in Figure 5.14 as well. As the speed increases the maximum motoring current decreases towards zero. The points are all exactly on constant speed lines since the simulator is capable of creating the impractical situation of a perfectly constant speed.

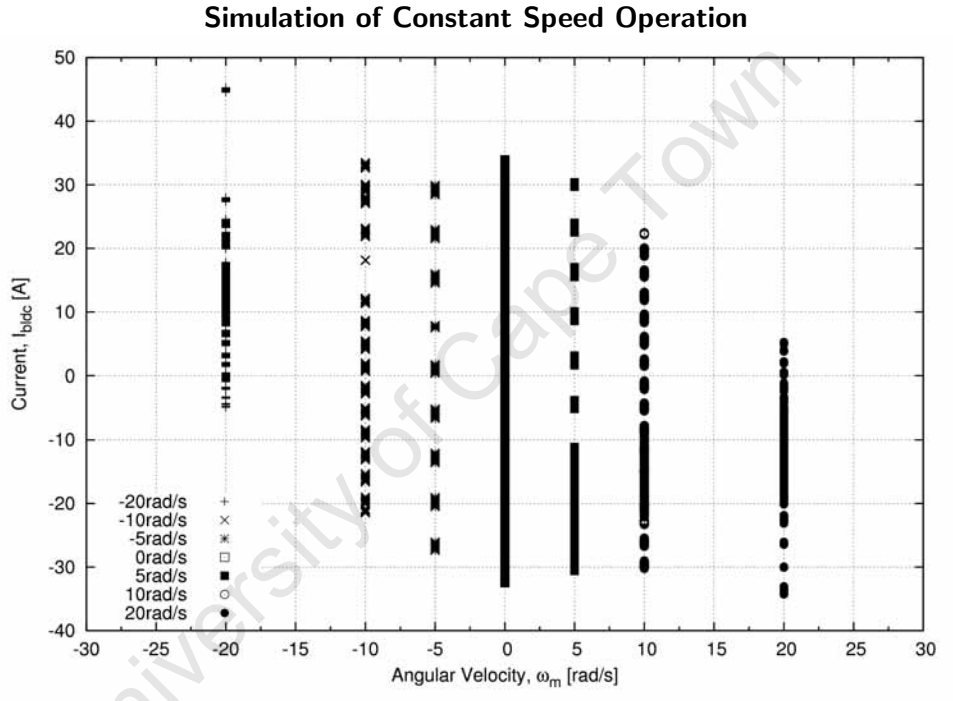

Figure 5.14: In this test the rotation speed, ω_m, was kept constant as the throttle signal was varied from $-30A$ to $+30A$.

5.4 Experimental Results

The controller consists of two main modules:

- The current source
- The motor phase commutator

The controller was tested in motoring and generating modes, at several different current levels.

The test setup, shown in Figure 5.15, was a BLDC machine attached via a belt drive to an induction motor. In this setup the speed and direction could be altered to achieve the desired test conditions.

Figure 5.15 shows the arrangement of equipment in the bench test setup of the VSD. The BLDC machine was mounted on a stand and coupled to an induction motor via a toothed belt. The oscilloscope was used to measure the current flowing in the link between the phase switcher and the current controller and the average voltage across the phase switcher. An in-line power meter between the battery and the controller was used to measure the average battery current and voltage. The scale was used to determine the torque transmitted from the BLDC machine to the induction machine. The speed of the BLDC machine was determined using the frequency that the Hall effect sensors were changing at.

The tests were designed to determine the range of speeds possible for a particular torque. Unfortunately the testing process had limited accuracy and range of results because of the following factors:

Induction Motor Speed The induction machine was controlled by an industrial electronic drive. It was capable of four quadrant operation and used a dump load to remove excess energy. The induction machine had two poles and three phases, with a rated power of $3kW$ at $380V$. There was a three to one reduction gear between the BLDC machine and the induction machine, but the induction motor still struggled to counteract the torque produced by the BLDC machine. This limited the maximum torque that could be transferred between the machines, and thus the maximum current level that could be tested in the controller. As a further consequence of the low torque transfer ability of the system, the low speed operation was poorly handled by the induction machine, reducing the accuracy of low speed measurements.

Torque Measurement The method used to calculate the torque transferred between the two machines involved a standard kitchen scale and a lever attached to the induction machine. This system had the advantage of the low pass filter built into the scale, but was unable to make high speed measurements of torque, and had a relatively low resolution.

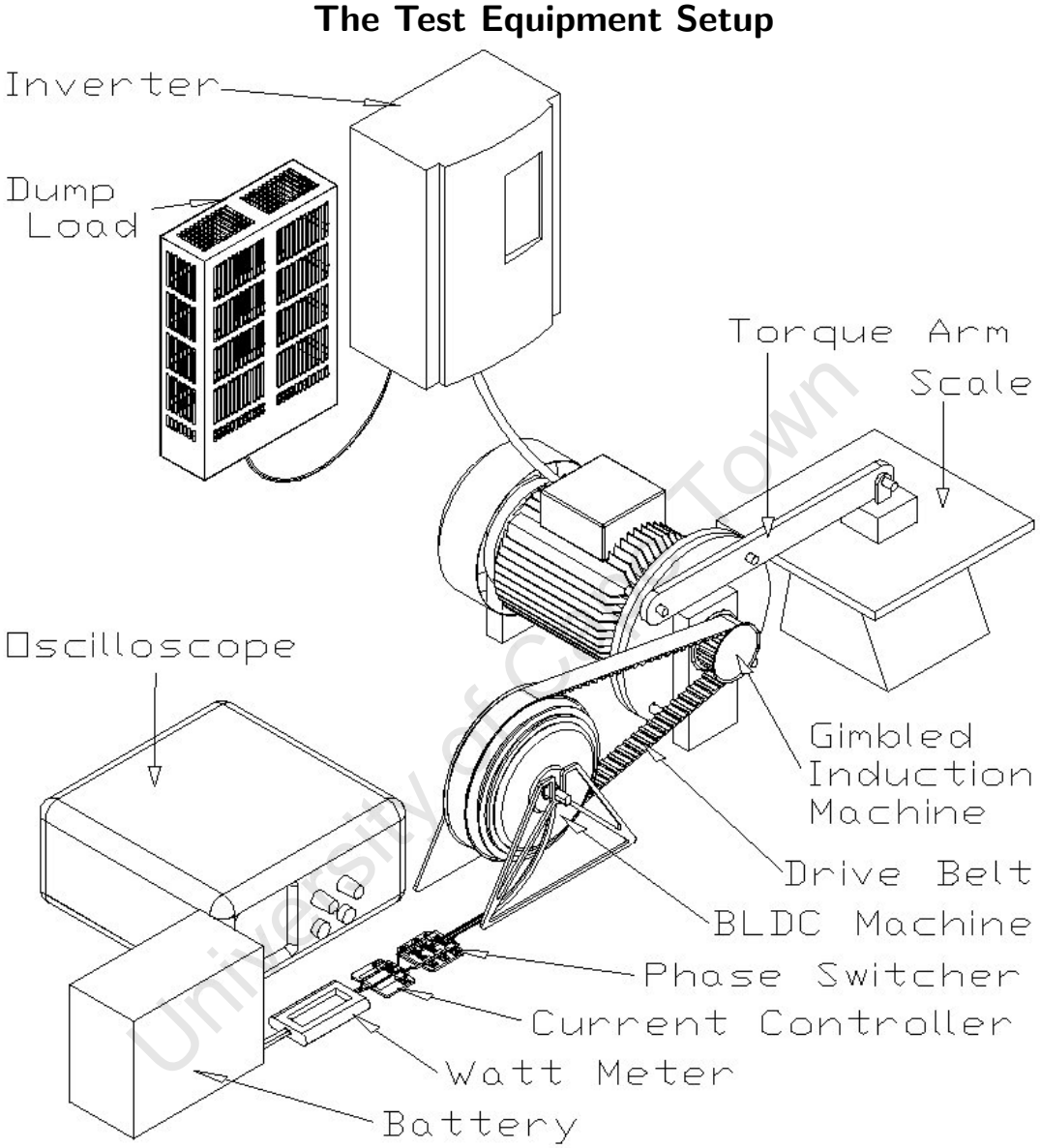

Figure 5.15: The above diagram shows the experimental setup in the laboratory. An induction motor was coupled to the BLDC motor with a toothed drive belt. The inverter drive allowed the induction motor to provide positive or negative torque using a power resistor dump load to remove the excess energy. The BLDC motor controller, that is the phase switcher and current controller, was monitored using an oscilloscope and a watt meter. A $0 - 5V$ signal was used to control the motor. The battery provided energy storage and supply for the system.

Battery Limitations A Sealed Lead Acid battery pack was used in testing because power could be extracted and replaced from the battery pack without causing damage. Most laboratory power supplies exclusively support power transfer to the external circuit and cannot tolerate the opposite direction of transfer. The generating tests caused the battery terminal voltage to rise to damaging levels; later testing incorporated a dump load set up to limit the terminal voltage. In all the tests the terminal voltage of the battery varies with the amount of power drawn from it and its state of charge. To help even out the battery performance, the tests for motoring and generating were done alternately.

5.4.1 Motoring

The inverter and dump load controlled the induction motor. A small control circuit made induction motor behave as a mechanical load, or brake, for the motoring tests of BLDC machine. As mentioned in the previous section, the induction motor drive system was not capable of accurate speed control at low speeds; however with some adjustment, a static test could be done in motoring mode.

The VSD is capable of two quadrant operation, as discussed in the Hardware chapter. The internal resistance of the BLDC machine confined the motoring capabilities to the area where $V_{emfBL} < V_{batt}$. The induction motor speed range further confined testing to points where $\omega_m > 0$, resulting in one of the "Motoring" zones in Figure 3.1 being investigated.

Figure 5.16 shows the current and speed of the BLDC machine with the control input to the VSD fixed at several different levels. The highest test current was $9.5A$ because the design maximum could not be reached with the torque ability of the induction motor. A BLDC motor current of $30A$ was instantaneously achieved during a test where the system was accelerated from rest to the maximum no load speed. The maximum continuous output power from the tests was $236W$.

The active braking zone in the region where $\omega_m < 0$ was achieved with the VSD but no measurements were taken because of the limited induction machine performance.

Each constant current, or constant torque, test eventually reaches the point where V_{batt} is no longer able to overcome the R_{phase} resistances and the V_{emfBL} generated by the BLDC machine as ω_m is increased. This represents the limit that the battery voltage puts on the possible output of the VSD. At this point, in every test, the duty cycle of the controller is 100%, that is the switch Q_{CSH} is permanently on. The bootstrap MOSFET driver supply in Section 3.2.1 makes this possible. All of the curves begin to follow the same trend once 100% duty cycle is reached because the battery is given the same load regardless of the throttle setting.

Figure 5.17 shows the current through the sense resistor and V_{bldc} for

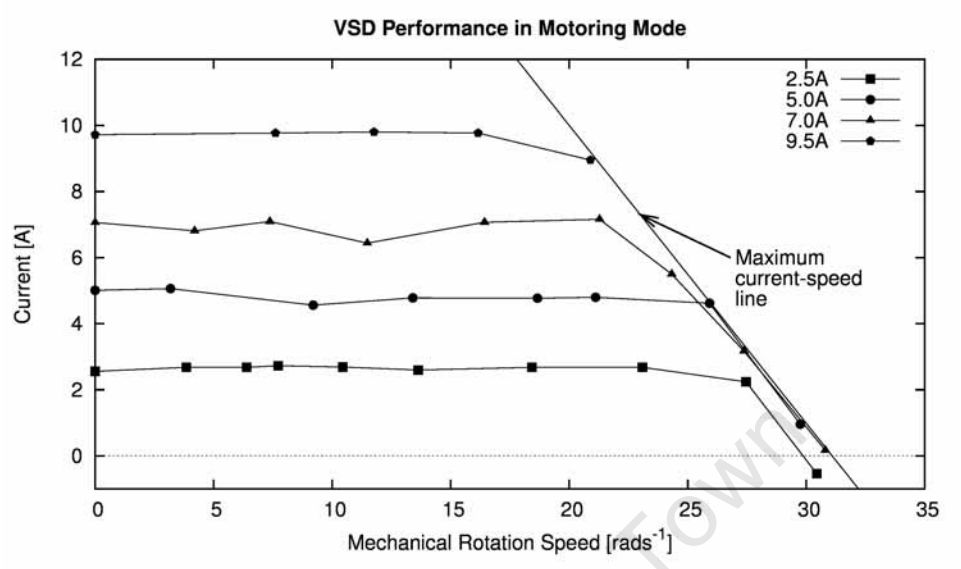

Figure 5.16: Sense resistor current vs speed in motoring mode. The desired current flows in the motor until the speed reaches the point where V_{batt} cannot overcome the I_{bldc} R_{bldc} and V_{emfBL}.

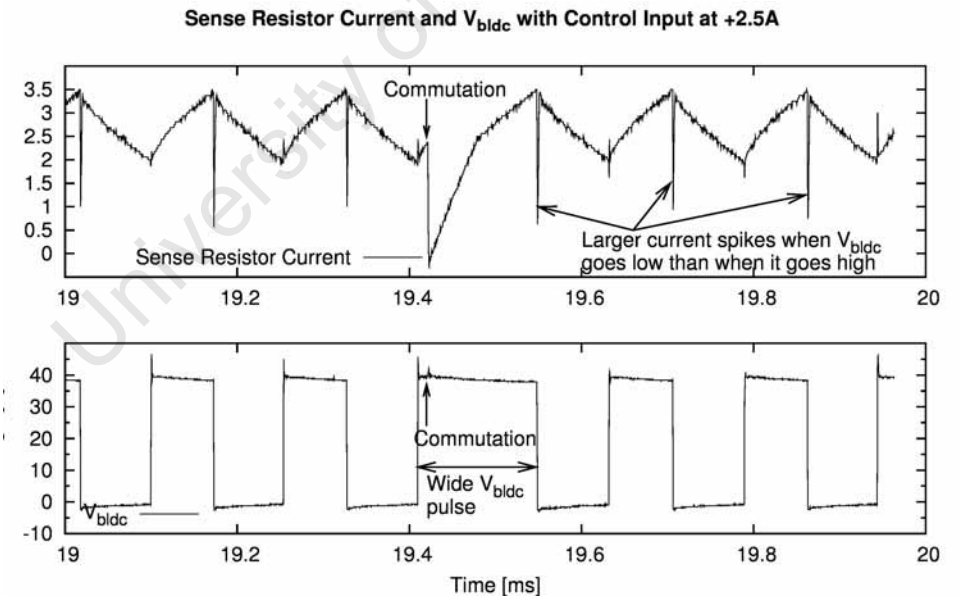

Figure 5.17: The sense resistor current and V_{bldc} as a phase commutation occurs are shown above. The average motor current is around $2.5A$. The controller increases the duty cycle of V_{bldc} to compensate for a commutation. The sense resistor current restarts from zero at each commutation

during a commutation event. The current signal temporarily becomes zero because the current from the previously conducting phase circulates within the phase switcher through unswitched phase when the open circuit phase is switched on.

To compensate for this loss of current signal, the current controller forces V_{bldc} to V_{batt}. The benefit of this action is that the desired phase current is quickly restored in the new phase. The previous phase current always breaks down at a higher rate than the new phase current builds up. This is more obvious at higher currents where the commutation of currents from one phase to the next takes longer.

5.4.2 Generating

The VSD puts the BLDC machine into generating mode when the throttle, or control input, demands a negative I_{bldc}. Once again several constant currents were set up by holding the throttle in various fixed postions while the induction machine was used to vary the speed of the system. In this case the induction machine supplies the mechanical power to the BLDC machine which converts it into stored energy in the battery or heat in the dump load on the BLDC side. Figure 5.18 shows the BLDC machine current measured at different speeds.

The BLDC machine has to be moving to convert mechanical energy to electrical energy. The VSD is designed for two quadrants, one motoring and one generating, both in the same mechanical direction. This means that the active braking zone in the generating quadrant is unreachable by the controller; the best it can do is to effectively short the BLDC machine terminals, causing a maximum negative current that is proportional to ω_m. Points on this line could not be accurately captured with the lack of control of the induction motor at low speed, but the lack of points within the active braking zone is evidence of the unreachable area of operation.

The maximum speed of each test was limited by the rate that the battery and dump load could absorb energy. The $1.5A$ test was run to the highest speed since the power transferred to the battery and dump load is:

$$P = I_{bldc} \cdot V_{bldc} = I_{bldc} \cdot k_{bldc}\omega_m$$

which reaches the absorption power limit of the system at a higher speed. The higher current curves can be seen to have increasingly lower speeds before they end, at which point they reach the same limit.

The battery affected the limits of both the motoring and generating tests by having a terminal voltage that varied approximately linearly with the current drawn from it. This meant that the high outgoing currents reduce the terminal voltage and simultaneously the maximum attainable speed at that current level while motoring. In the generating situation the battery voltage increased with increasing current influx, raising the terminal voltage

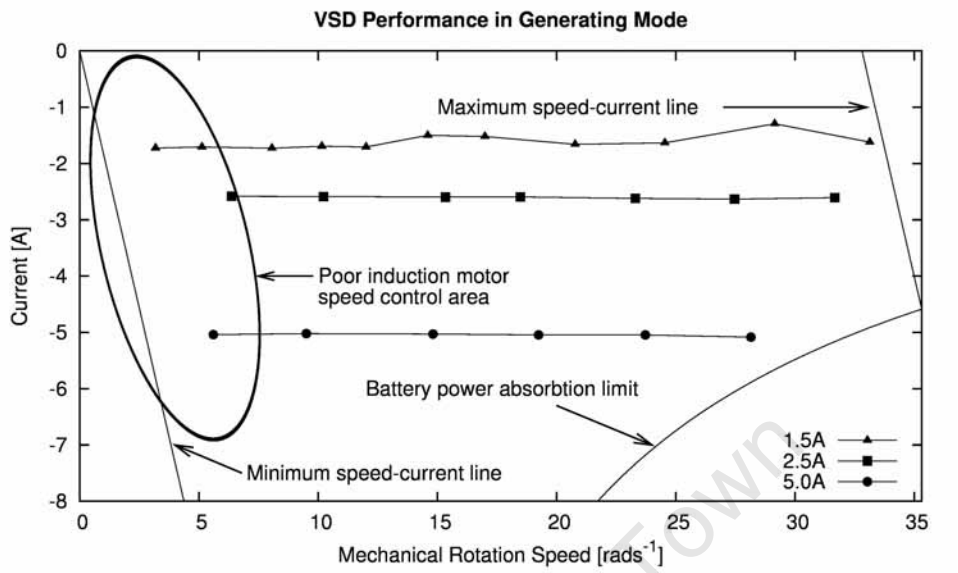

Figure 5.18: I_{bldc} vs ω_m resembles a torque controlled machine characteristic. The minimum speed-current line is on the boundary of the active braking zone that is unreachable with the two quadrant controller. Poor induction motor control prevented measurements on this line. The maximum speed-current line is unreachable at larger current magnitudes because the power absorbed by the battery pack limits the safe I_{bldc} current level.

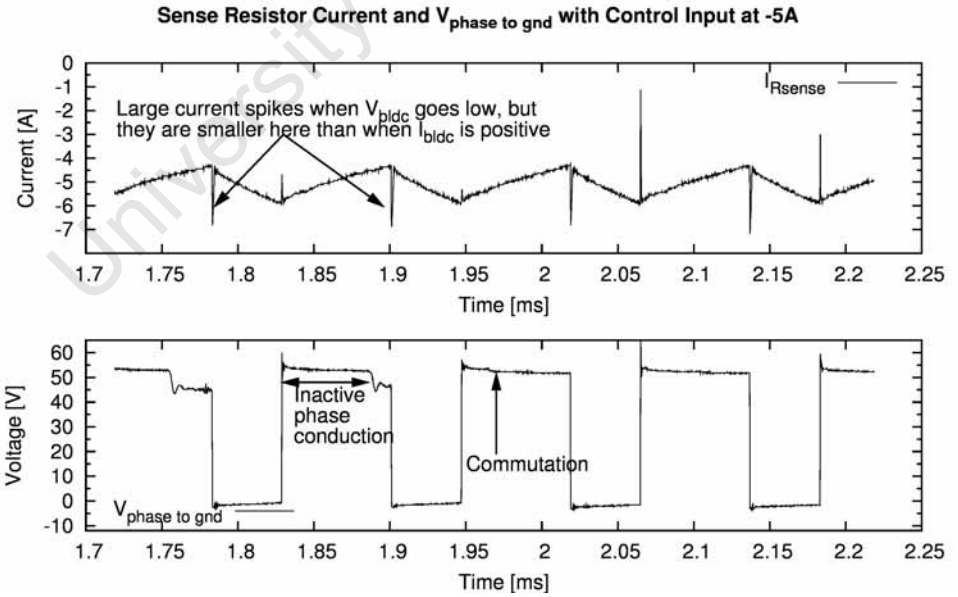

Figure 5.19: The sense resistor current and a phase to phase voltage of the BLDC machine during a commutation in generating mode.

to destructive levels and preventing the test from reaching 100% duty cycle. The maximum power delivered to the battery during testing was $158W$.

The sense resistor current and one phase to phase voltage are shown in Figure 5.19 during a commutation event while regenerating electrical energy. Commutation does not affect the negative current regulation since the body diodes of the MOSFETs always provide a path through the sense resistor, unlike the case in motoring mode where the diodes provide a path that circulates current away from R_{sense}. The mechanical torque on the BLDC machine is smoother when generating electricity, provided the commutation induced phase shift of the phase currents is small.

The current spikes from the MOSFET output capacitance are bigger when V_{bldc} is changing from V_{batt} to V_{gnd}. The direction of I_{bldc} causes V_{batt} to be present across the phase switcher during the period when Q_{CSH} and Q_{CSL} are both off. Thus the change of V_{bldc} from V_{batt} to V_{gnd} causes the voltage across a MOSFET output capacitance to change by V_{batt}, but if V_{bldc} changes in the other direction, the MOSFET output capacitor voltage will only have to change by one diode conduction voltage, $\approx 0.7V$.

Current builds up in the unused phase while V_{bldc} is V_{gnd}. The stepped shape of the phase voltage occurs because the MOSFETs body diodes are forward biased by the built up current, forcing the voltage across the unused phase to be V_{bldc} or V_{gnd}. When the current decays to zero in the unused phase, the phase to phase voltage returns to its open circuit value.

5.4.3 Electric Bicycle Test

Another reason for testing the VSD with a battery was to gain insight into its operation in the real world system. The VSD was installed on a $26''$ mountain bicycle, with a 409 hub motor installed on the rear wheel. Thus it became an electric bicycle, or E-bike.

The electric bike used for testing the controller with a 409 hub motor was set up with an available throttle, designed for single quadrant controllers. This was not ideal because the user had to hold the throttle in approximately the zero position in order to achieve motion with no VSD intervention. The motoring mode worked similarly to the Crystalyte electric bicycle system; an increase in throttle position pushed the rider and bike harder.

The generating mode was entered as soon as the throttle position was reduced below half way. The slowing down effect of the negative torque made the bicycle easier to stop but was not very strong. The inability of the simple controller to enter the active braking zones, from Figure 3.1, meant that the retarding force was reduced at lower speeds, but the accelerating force was strongest at lower speeds. The 409 hub motor used on the bicycle test had higher internal resistance than the 408 hub motor used on bench tests, which resulted in a more limited performance in general when the VSD was installed on the bicycle.

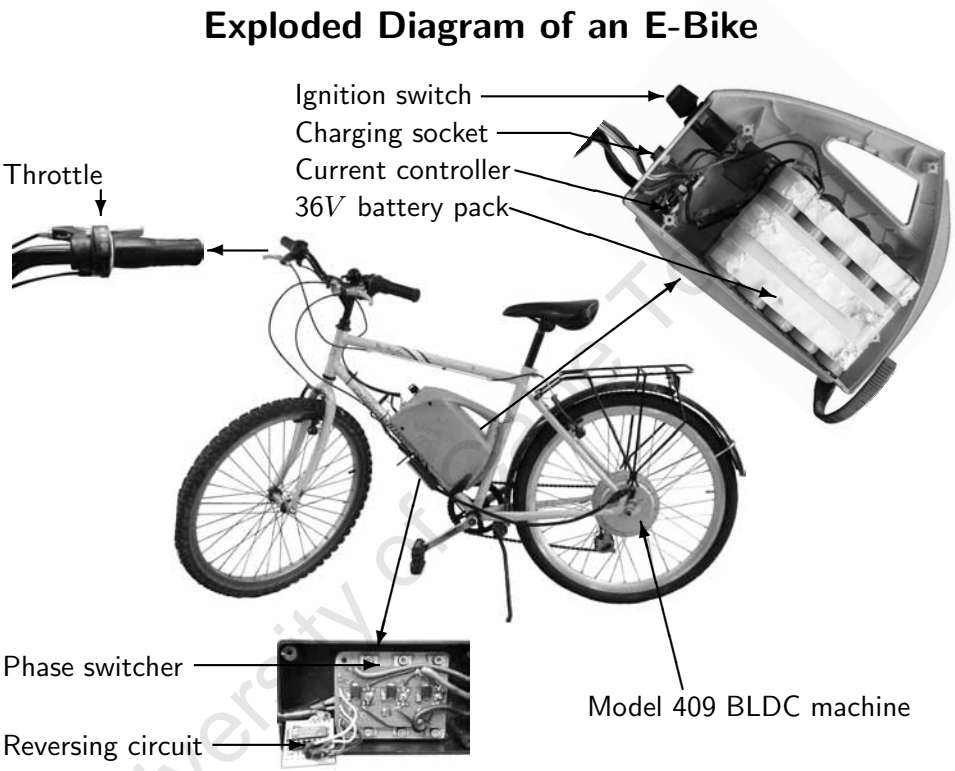

Figure 5.20: The standard mountain bicycle has been fitted with an EV system to transform it into an E-Bike. There is a throttle on the left handle bar grip that generated the current setpoint for the current controller. The battery case contains a $36V$ battery pack and the current controller module. The black box, attached underneath the downbar, is the phase switcher and the 409 BLDC hub motor is fitted to the rear wheel. The ignition switch mounted on the battery case is used to connect the VSD to the battery; when the E-bike is not operational or charging, the switch is put off to prevent the standby current of the VSD from draining the battery.

5.4.4 Operation Frequency

The frequency of operation was deduced using captured data from V_{bldc} measurements. Curves are plotted for a range of current levels in Figure 5.21. From Equation 3.13, it appears that the minimum switching period is independent of $V_{emf\,ph}$ and I_{phase}. However, to arrive at that equation, the condition that $V_{out} = \frac{1}{2}V_{in}$ was true. At the maximum switching frequency, $V_{emf\,ph} + I_{phase}R_{phase} = \frac{1}{2}V_{batt}$. In the top graph of Figure 5.21 are calculated operation frequencies, based on Equation 3.13. The bottom plot is of real data from VSD bench testing.

In Chapter 3, the maximum switching frequency was predicted to be $5kHz$. In the data plotted in Figure 5.21, the real system operates with a maximum frequency around $7kHz$, because V_{batt}, and therefore f_{max}, is higher when the battery pack is accepting a charge. For positive I_{bldc}, f_{max} is closer to the $5kHz$ design prediction.

The curves of frequency against ω_m also show an increase in the maximum switching frequency as the current, I_{bldc}, decreases. This is because V_{batt}, supplied by a series combination of three Sealed Lead Acid batteries, is not perfectly steady for all current flow rates in and out of the battery pack. Instead the battery voltage varies as if it has a significant amount of internal resistance. When a higher current is taken from the battery, the value of V_{batt} is reduced and Equation 3.13 correctly predicts a lower maximum frequency of operation.

In the case where I_{bldc} is less than zero; as the machine speed increases, so does the proportion of current flowing into the battery, causing further battery voltage increase. This can cause the terminal voltage of the battery pack and the operation frequency to continue to increase until the maximum ω_m is reached.

Figure 5.22 reveals another type of frequency variation, from one commutation event to the next. In this plot the frequency of operation is affected by the electro-motive force (EMF) of the unused phase. Every time V_{bldc} is forced to V_{gnd}, the L_{phase} of the unused phase experiences V_L approximately equal to its instantaneous $V_{emf\,ph}$. This causes a current to build up in this phase until V_{bldc} is forced to V_{batt} again. With the topology of this VSD, current in the unused phase circulates in the phase switcher. The current controller observes a smaller L_{bldc} because the circulation of current causes L_{phase} of the unused phase to be in parallel with an active L_{phase}. This is similar to the commutation process. The change in operation frequency from this mechanism is greatest when $V_{emf\,ph}$ of the unused phase is highest, because the circulating current grows fastest. At these points a commutation has recently occurred or is about to occur. As the rotor of the machine moves on, V_{phase} of the unused phase passes through zero and the effect is absent, causing the switching frequency exactly midway between commutation to be lowest.

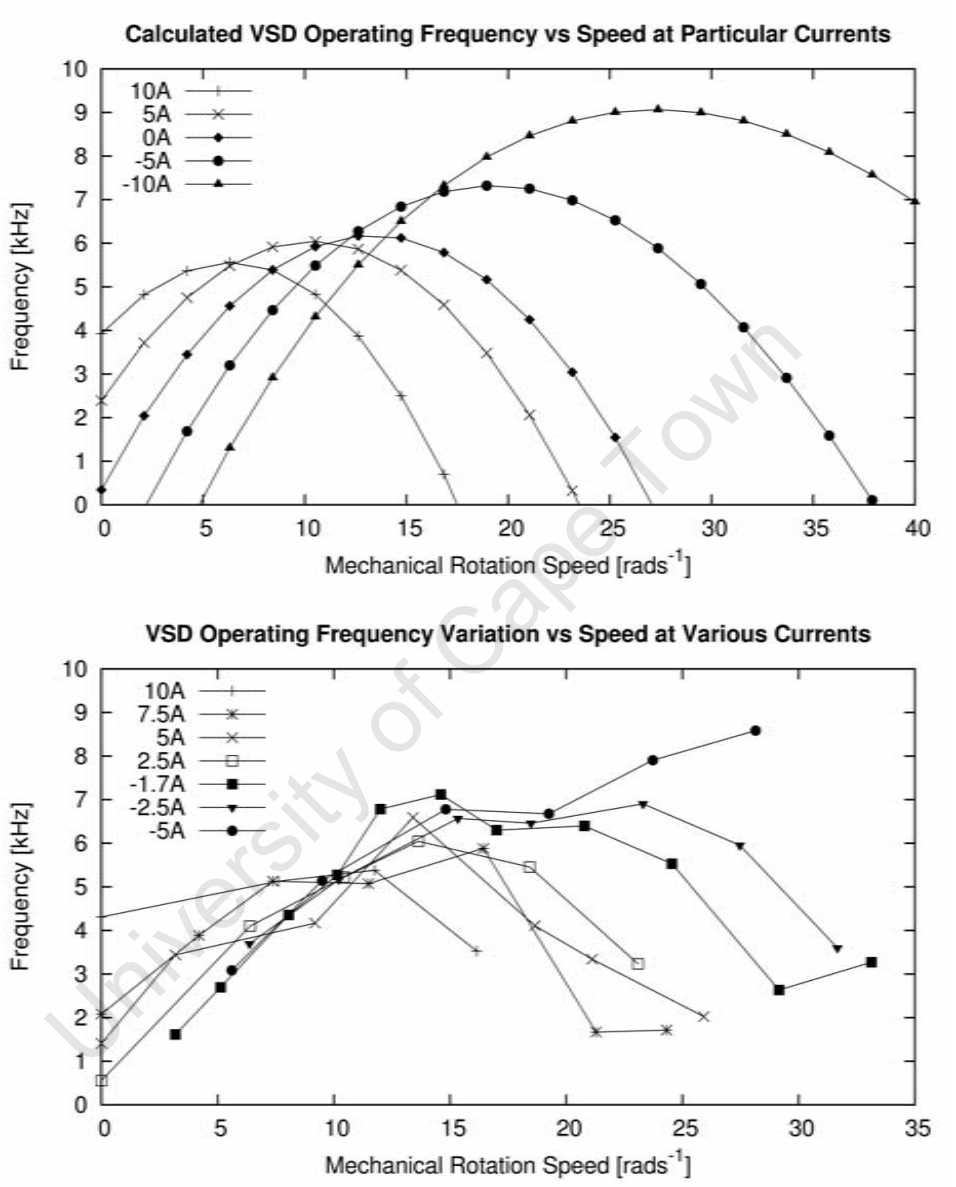

Figure 5.21: The frequency observed at V_{bldc} is plotted against the VSD speed and current level. The shape of each curve is roughly quadratic, as derived in Equation 3.12; however the changing V_{batt} in both motoring and generating operation cause shifting and scaling of the curves. The more positive the value of I_{bldc}, the lower the maximum frequency is.

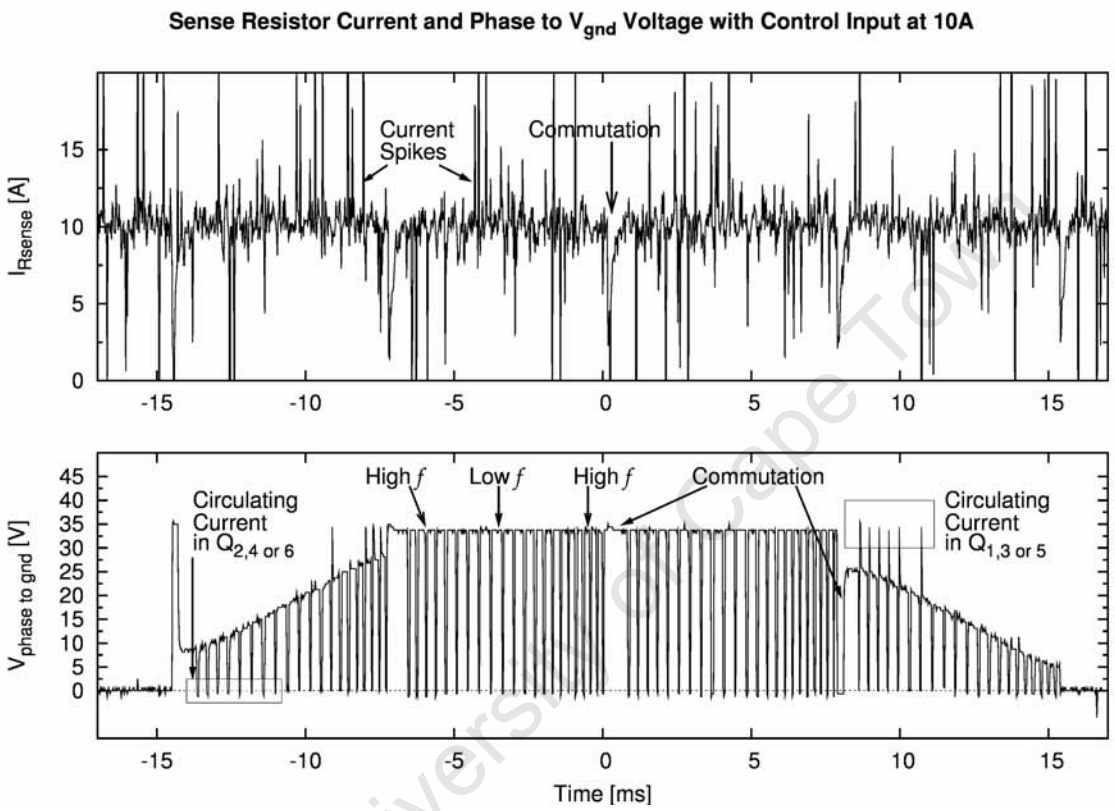

Figure 5.22: The above experimental data shows a phase to phase voltage during operation at $10A$ in motoring mode. A longer pulse occurs at the beginning and the middle of the conduction period in response to commutation. The frequency of operation increases gradually after each commutation event, shown by the narrowing of the pulses. The current sense resistor signal shows the current being limited to the tolerance band except at commutation events. Phase switcher MOSFET capacitances rapidly charge and discharge through the current sense resistor as V_{bldc} changes between V_{batt} and V_{gnd}. This produces spikes in the current signal at each transition of V_{bldc}.

Chapter 6

Conclusions

The overall result of this study is a simple variable speed drive (VSD) based on the discrete multi-function logic gate. It proved to be effective and reliable, capable of surviving insertion into the casing of a hub motor. The tests achieved a power when motoring of $236W$ and a regenerating power of $158W$, limited by the battery and test rig.

Based on the design presented in Chapters 3 and 4, and the results presented in Chapter 5, the following conclusions can be made about a torque controlled VSD for a brushless direct current (BLDC) machine. The conclusions are organised in a similar order to that of the document.

Objectives Reached

Torque controlled operation was achieved by controlling the path and magnitude of current in the BLDC machine. The throttle could set the current, and therefore the torque, to an arbitrary level within the limits of the VSD. This successfully produced positive and negative torques in the *Forwards* direction. The simulations of the four quadrant controller illustrated the possibility to extend operation into the *Reverse* direction too. The VSD provided a similar user experience to an accelerator in an internal combustion engine system.

The VSD was successfully operated in motoring and generating modes, which were determined only by the position of the throttle. This illustrates two quadrant operation, where energy transfer took place from electrical to mechanical and vice versa. The seamless transition from motoring to generating makes the controller suitable for electric vehicles, as no user intervention or extra switches are needed to take full advantage of the system. However, the range of applications for the practical two quadrant drive is limited to vehicles that only require unidirectional movement, such as scooters and electric bicycles.

The use of simple low power logic devices eliminated the need for computer programming and embedded device development software, making the entire design comprehendable to a wider audience. Few analog control ele-

ments were needed for current control because the phase switcher translated the I_{phase}s into a unified signal, which could be dealt with by a single control loop. This was still possible with the four quadrant controller.

The low R_{ON} metal oxide semiconductor field effect transistors (MOSFETs) and small package size of the other integrated circuits (ICs) made it possible to produce the VSD small enough for practical installation on a bicycle. The controller weight was unnoticeable compared to the bicycle it was installed on. The four quadrant controller would similarly have a low impact on the weight of the total system where it would be installed.

Design Investigation

The multi-function gates are very useful for implementing arbitrary two bit logic functions. In the VSD design, the phase switcher used a logic function that is difficult or impossible to find in ICs with four or six gates on a chip. In other places in the circuit the versatility of multi-function gates enabled the implementation of standard logic functions. The digital optional inverter made very good use of all the functionality that multi-function gates have to offer. The multi-function gate can also implement simple memory elements; future designs could be composed using this type of gate as the only logic device.

Analog comparators are useful building blocks in current control systems because they can provide accurate thresholds, digital output and memory all in one device.

The simulation results revealed that the arrangement of power switches affects the commutation process. The relationship between the measured current in the BLDC machine and the equivalent direct current (DC) machine current, or torque, is dependant on the speed of commutation. A faster transfer of current between the commutating phases keeps the relationship between I_{bldc} and T_m more stable. This is evident in the generating or regenerating mode of operation where circulating currents cause a phase shift that reduces the electromagnetic conversion rate of the machine.

The separation of phase switcher and current controller functionality resulted in a simple current measurement system. The different modules were designed in isolation and preliminary tests were done on each module before assembling the whole system. This approach enabled fast isolation of faults and quick replacement of faulty sections of circuitry.

However, the interconnections between the phase switcher and current controller introduced parasitic impedances. This necessitated the insertion of transient voltage suppressors on the phase switcher legs. The parasitic impedances also introduced enlarged transients across the sense resistor, which had to be filtered out. The physical size of the controller was increased by separating the functionality and would not fit within the hub of the 408 or 409 motors. The effect of routing the Hall sensor wires away from the

phase wires, within the hub, could not be determined because all the wires shared the same insulation once exiting the hub.

In the analog optional inverter of the conceptual four quadrant design an operational amplifier (Op-Amp) was used in a non linear mode to achieve the effect of an analog switch. This is a solution that requires very little hardware but suffers large output errors because of offsets in the Op-Amp, which may cause the idea to be abandoned.

Results analysed

The battery voltage determined the maximum possible test speed of the machine in motoring mode. However, the maximum test torque in this mode was limited by the rated torque of the induction machine.

The battery pack exhibited a limited rate of charge acceptance, reducing the ability of the system to succeed at recovering energy. Since the battery was used in the speed against current tests, the possibilities for testing the VSD in generating mode were also limited.

The lowest BLDC machine test speeds achieved in both modes indicates that in motoring mode it would be possible to enter an active braking zone, but not in generating mode. This is also the case for a DC machine with a two quadrant drive, further correlating the similarities between the two machine types.

The measurements of torque were not very accurate and prevented meaningful analysis of efficiency. The scale did give a rough indication that a similar torque was transferred on each test run. The phase switcher effectively aligned the current carrying conductors with the magnetic field in the electric machine.

The electric bicycle test confirmed that the regeneration mode of the VSD produced a negative torque and simultaneously recharged the battery.

The frequency of operation of the VSD varied as the rotor position and load changed. This range of operation frequencies lowers the radio interference produced by switching the high power components. The inactive phase conducts for an interval proportional to the magnitude of $V_{emf\,ph}$. This has the effect of paralleling the inductance of the inactive phase with an active phase, which reduces the inductance seen by the current controller. The tolerance band limits in the current controller are reached faster when the inactive phase conducts for longer, causing the highest operating frequency to occur around commutation events. The simulation of the integrated topology showed no conduction of the inactive phase under certain conditions, which led to a more consistent operation frequency.

In the energy storage system of this VSD, the lead acid battery quickly became overwhelmed with charge in generating mode. The literature review compared some other storage methods, each with their own strengths and

weaknesses. It would appear that the best solution to the energy storage system would be a combination of technologies, such as an ultra capacitor for high intermittent power, and a separate battery for low power high energy density storage. This is what Yan and Patterson [59] proposed in their novel power management scheme. These types of solutions have the potential to perform dramatically better than either original solution in many areas simultaneously.

The modularity in design enables the reuse of the phase switcher in concept when extending the two quadrant design to a four quadrant design.

Chapter 7

Recommendations

Based on the conclusions in the previous section, the following recommendations for future work and improvement on the design are made:

- Improve the performance of the VSD by changing the design. Specifically:
  - Modify the topology so that the unused or inactive phase of the three phase brushless (BL) machine stops conducting as quickly as possible after each commutation event. This would involve increasing the resolution of the position sensor to $720°ed/n$ and changing the switching pattern that forces $V_{bldc} = 0V$. A six switch, three leg, inverter bridge circuit, as in the integrated topology of Section 5.2.2, would do the job. The switching pattern would ensure that the inactive phase does not conduct by turning on an appropriate pair of top or bottom side switches to force $V_{bldc} = 0V$. For the three phase machine, the side used for $V_{bldc} = 0V$ would change at $60°ed$ intervals, but at a point exactly $30°ed$ after each commutation. This resembles one of the bus clamped space vector pulse width modulation (SVPWM) switching schemes detailed by Narayanan *et al.* [40]. Both two and four quadrant designs would benefit from this improvement.
  - Implement the four quadrant design for operation in all possible zones. Small three and four wheeled electric vehicles (EVs) could then be controlled with this system.
  - Exploit the multi-function gate versatility more. In the VSD in this project there are places where a multi-function gate could have been used in place of a more specific component. The Schmitt trigger input on these multi-function gates could even be used to replace analog components in the tolerance band control method.
- Improve the input and output systems, as follows:

  - Use a lossless current sensing scheme. The sense resistor complicates layout and dissipates power, reducing efficiency. A lossless scheme could reduce the parasitic inductance introduced into the high power loop, reducing the transient voltages and filtering requirements.
  - Reduce coupling between the position sensor signals and the high power signals. Position sensor wires should be routed along a separate path, away from the phase wires. One way to achieve this would be to have the controller mounted inside the case of the machine.
  - Reduce the power required to determine position. The Hall sensors used a significant amount of power to bias the electronics, comparable to the amount that a sensorless scheme might consume. Future systems may include both types of sensor. The Hall sensors could be used from rest up to the speed where a sensorless scheme gives reliable position information and then be switched off.
  - Use a center zero throttle. The throttle used in this project output the lowest voltage possible when left idle, in future testing on this type of VSD a throttle that settles in the middle of the output range should be used. The effect of an offset on the efficiency and usability of the system could then be investigated.

- Improve the energy storage scheme. The new range of ultra capacitors hold the potential to radically improve the performance of an energy storage system when combined with a battery. The ability of ultra capacitors to accept and deliver energy quickly and efficiently is a huge advantage when trying to manage acceleration and deceleration.

- Improve on the test equipment. Several parts of the test system did not have the accuracy or ability to measure the performance of the system. The following improvements are proposed:

  - Utilize a higher torque lower speed machine in place of the induction motor in the test rig.
  - Install a load cell to measure torque output of the BLDC machine. This would enable the observation of torque ripple from the BLDC machine and controller and the parasitic torque from the friction in the system.
  - Install a position sensor on the induction machine. The induction machine inverter drive had difficulty in maintaining a consistent speed at low rpm, which prevented accurate measurements. With a position sensor, the inverter drive could compensate for friction and achieve smoother low speed operation.

Appendix A

Simulation Code

The Simulation Program with Integrated Circuit Emphasis (SPICE) code used to generate the results in Section 5.2.1 is spread across multiple files. The tolerance band simulation code differs from the constant voltage pulse width modulation (PWM) code in only one place: the definition of the throttle signal. In the listings below, the include files are concatenated and presented continuously across pages 125 to 127.

The following listing was used to perform the tolerance band simulation.

```
*spice circuit :PMDC motor: controller with Separate Hbridge +2A
*2.5v is 0A after that it should be +1A per +3m*30 volts
*set up the throttle position
Vinput  V_Ihigh          0       DC 2.7

.include IbridgeK.cir
.include Rbridge.cir
```

This listing was used to do the constant voltage PWM simulation.

```
*spice circuit to simulate current in PMDC motor with 25% of excess voltage applied**
*the back emf of the motor is 20V so 20/30 * period is the 0%duty cycle
*so to get a  +25% value we take 2/3 + 1/3 * 1/4

*the Throttle input        v_off      v_pulsed   delay   rise    fall    high    T
Vpwr V_Ihigh 0 DC 1.0 pulse(0.1v         4.9v    2m      0.5u    0.5u    549.5u  720u)

.include IbridgeK.cir
.include Rbridge.cir
```

```
*General include file for different current tests.

*included models of components used in VSD design
.include ../SPICE_models/Logic/74HC2G74_Mark.mdl
.include ../SPICE_models/Comparators/LM393_Texas.mdl
.include ../SPICE_models/Opamps/LF412_National.mdl
.include ../SPICE_models/Diodes/Junction/UF4007_Thomatronic.mdl
.include ../SPICE_models/Mosfets/IRF3205s_IR.mdl

*low voltage inputs*************************************************************
*hall sensor signals simulated with pulse waveforms
VHA    HA    gnda    DC  4     pulse(4.9   0.1     14m     100u    100u    20.9m   42m)
VHB    HB    gnda    DC  0.5   pulse(0.1   4.9     7m      100u    100u    20.9m   42m)
VHC    HC    gnda    DC  0.1   pulse(4.9   0.1     0m      100u    100u    20.9m   42m)

*control signal*****************************************************************
*I_TH_HIGH is provided by parent file

*power supplies*****************************************************************
Vgnd     gnd      0        DC 0V

*current controller linear regulator
Vcur     1        gnd      DC 5.0
rv_cc    V_CC     1        1.0ohms
cv_cc    V_CC     gnd      3.3u

*phase switcher linear regulator
Vphsw    2        gnda     DC 5.0
rvcc     VCC      2        1.0ohms
cvcc     VCC      0        3.3u

*the logic per gate section*****************************************************
*pinouts         in       inv_in   Qbot    Qtop     pwr      gnd
.subckt PMDCSW   A        B        LG      HG       vdd      vss

*input 2 is inverted in the gate model before being ANDed with input 1
*this is the function provided by the multifunction gate 74LVC1G58
Xandinv          B        A        LG      vdd      vss      invand
Xinvand          A        B        HG      vdd      vss      invand
.ends    PMDCSW

*gate signals for Q 1&2, Q 3&4 and Q 5&6
XHA_BphaseA      HB       HC       A_low   A_high   VCC      gnda     PMDCSW
XHB_CphaseB      HC       HA       B_low   B_high   VCC      gnda     PMDCSW
XHC_AphaseC      HA       HB       C_low   C_high   VCC      gnda     PMDCSW

*The RS_LATCH*******************************************************************
*Pinouts:        CLK      D        Q_not   GND      Q        !R       !S       VCC
XRS_LATCH        gnd      gnd      Q_not   gnd      Q        I_DEC    I_INC    V_CC 74HC2G74

*Comparator section*************************************************************
*LM393 model used here since TLV3502 model was unavailable
* CONNECTIONS:   NON-INVERTING INPUT
*                |              INVERTING INPUT
*                |              |              POSITIVE POWER SUPPLY
*                |              |              |        NEGATIVE POWER SUPPLY
*                |              |              |        |       OPEN COLLECTOR OUTPUT
*SUBCKT LM393    1              2              3        4       5
XCMPA            V_Isense       V_Ilow         V_CC     gnd     I_INC    LM393
XCMPB            V_Ihigh        V_Isense       V_CC     gnd     I_DEC    LM393

*stability improvement interlinking resistor
R_CPL            V_Isen         V_Isense       100ohm
*comparator output pullup resistors
R_INC            V_CC     I_INC    10000
R_DEC            V_CC     I_DEC    10000
```

```
*Amplifier Section*****************************************************************
* connections:    non-inverting input
*                 |             inverting input
*                 |             |       positive power supply
*                 |             |       |       negative power supply
*                 |             |       |       |       output
*                 |             |       |       |       |
*SUBCKT LF412/NS  1             2       99      50      28
*Tolerance band generating amplifier*
XOPA            Tin             TOL     412pwr  412gnd  V_Ilow  LF412NS
R_ToutFB        V_Ilow          TOL     8.2K
R_TOLFB         V_Ilow          TOL     410K

*throttle attaches to V_Ihigh
R_TinH          V_Ihigh         Tin     82K
R_TinL          Tin             gnd     82K
R_TOLH          V_CC            TOL     820K
R_TOLL          TOL             gnd     820K
R_Tout          TOL             gnd     8.2K

*Filtered current signal amplifier*
XOPB            V_Ioffset       V_Iref  412pwr  412gnd  V_Isen  LF412NS
R_IFB           V_Isen          V_Iref  180K
C_Gain_fin      V_Isen          V_Iref  50p

*the current amplifier input resistors
R_IrefH         V_CC            V_Iref          10k
R_IrefL         V_Iref          gnd             10k
R_FiltH         V_CC            V_Ioffset       10k
R_FiltL         V_Ioffset       V_Ifilt         10k

V412    412pwr  V_CC    DC 1.4v
V412gnd 412gnd  gnd     DC -1.375v

*motor model section***************************************************************
*motor has three star connected inductors in its model
*resistance in series and parallel
*trapezoidal voltage as the back emf
Lan     phaseA  neutal  5000uH IC=0
Lbn     phaseB  neutbl  5000uH IC=0
Lcn     phaseC  neutcl  5000uH IC=0
Rla     phaseA  neutal  5K
Rlb     phaseB  neutbl  5K
Rlc     phaseC  neutcl  5K
Ran     neutal  neutral 0.35ohms
Rbn     neutbl  neutrbl 0.35ohms
Rcn     neutcl  neutrcl 0.35ohms
Vemfa   neutral ntrl    pulse(-10   10   0m  7m  7m  14m  42m) DC 0
Vemfb   neutrbl ntrl    pulse(-10   10  14m  7m  7m  14m  42m) DC -10
Vemfc   neutrcl ntrl    pulse( 10  -10   7m  7m  7m  14m  42m) DC 10

*Battery voltage*******************************************************************
Vbatt   batt    gnd     30volts
Rbus    batt    vbatt   0.1
Cbus    vbatt   gnd     1000u


*sense Resistor and filter*********************************************************
Rsense  gnda    gnd     3m
Lfilt   gnda    filr    10u
Rfilt   V_Ifilt filr    10
Cfilt   V_Ifilt gnd     470n
Vgnda   gnda    sense   DC 0.0V
```

```
*Power MOSFET switches*****************************************************
*Phase Switcher MOSFETs
*               Drain   Gate    Source
XQ1             V_bldc  DR_AH   phaseA          irf3205s
XQ3             V_bldc  DR_BH   phaseB          irf3205s
XQ5             V_bldc  DR_CH   phaseC          irf3205s

XQ2             phaseA  DR_AL   gndaA           irf3205s
XQ4             phaseB  DR_BL   gndaB           irf3205s
XQ6             phaseC  DR_CL   gndaC           irf3205s

*Current Controller MOSFETs
XQ_CSH          vbatt   DRV_CSH V_bldc          irf3205s
XQ_CSL          V_bldc  DRV_CSL gnd             irf3205s

*the mosfet drivers*********************************************************
EQ1     DRV_AH  phaseA  A_high  gnda    1.8
EQ3     DRV_BH  phaseB  B_high  gnda    1.8
EQ5     DRV_CH  phaseC  C_high  gnda    1.8

EQ2     DRV_AL  gndaA   A_low   gnda    1.8
EQ4     DRV_BL  gndaB   B_low   gnda    1.8
EQ6     DRV_CL  gndaC   C_low   gnda    1.8

ECSH    DRV_CSH V_bldc  V_CSH   0       1.8
ECSL    DRV_CSL gnd     V_CSL   0       1.8

*simulation of driver internal resistance
RQ1G    DRV_AH  DR_AH   10
RQ2G    DRV_BH  DR_BH   10
RQ3G    DRV_CH  DR_CH   10
RQ4G    DRV_AL  DR_AL   10
RQ5G    DRV_BL  DR_BL   10
RQ6G    DRV_CL  DR_CL   10

*deadtime generation section
CCSH    V_CSH   gnd     100p    IC=0
R_CSH   V_CSH   Q       820
D_CSH   V_CSH   Q       UF4007
CCSL    V_CSL   gnd     100p    IC=5
R_CSL   V_CSL   Q_not   820
D_CSL   V_CSL   Q_not   UF4007

*Record Current in phase switcher low side mosfets*************************
VQ2     gndaA   sense   DC 0
VQ4     gndaB   sense   DC 0
VQ6     gndaC   sense   DC 0

*scaling of the sense resistor voltage to get sensible plots****************
Ecurrent        Isense gnd      sense   gnd     333.33
Ccurrent        senseN gnd      1u
Rfilter         Isense  senseN  1




*the administrative bit, auto run and save simulation *********************
*       step    stop    start   minstep UseInitialConditions
.tran   0.05m   60m     10m     50u     UIC

*columns 1, 7, 3, 13 and 2 get read by gnuplot,*****************************
*they should contain the phase and bus currents
.save vemfb#branch senseN phasea phaseb phasec
+vemfa#branch vemfc#branch neutal neutbl neutcl V_Isense V_bldc
```

Simulation Code for Four Quadrant VSD

ω_m of the BLDC machine was imitated with a non linear source which depended on the voltage across a capacitor charged at constant current, representing time. An arbitrary speed time profile was then possible. θ_e was obtained by integrating ω_m. Minor adjustments were made to conduct constant the separate constant speed and constant torque tests.

```
*Four Quadrant Controller tested at constant current of 0A, all speeds
*the throttle should demand 1 amp for every 45mV away from 2.5V
*for 10 amps that means 45*0=   0mV away from 2.5V =>2.5V

V_th    V_throttle      gnd     DC 2.5

.include ./IbridgeFQ.cir
.include ./RbridgeQ.cir
```

This is the RbridgeQ.cir file:

```
*putting the time variable into th circuit*****************************************
Itime   t       gnd     DC -1u
Ctime   t       gnd     50n IC=0
*t should reach 2 units by the time the test is over
bomega  omega   gnd     v=30-30*v(t,gnd)
btheta  theta   gnd     v=30*v(t,gnd)-15*V(t,gnd)*v(t,gnd)

*columns get read by gnuplot,*****************************************************
*they contain all the useful variables
*there are 36 of them, plus one for time
.save V_Isense I_inv gnda V_Ifilt V_throttle cmpain cmpbin V_CSH V_CSL
+HAI HBI HCI HA HB HC DRV_AH DRV_AL DRV_BH DRV_BL DRV_CH DRV_CL
+bemfa#branch bemfb#branch bemfc#branch neutral neutrbl neutrcl ntrl
+phaseA phaseB phaseC V_bldc vbatt V_iref omega theta

*this allows the simulation to actually run without timestep problems
.OPTION ITL4=50

.tran 0.05m 100m 0.01m 1.5u UIC
```

This is the IbridgeHQ.cir file:

```
*calculation of hall signals


*theta is in radians
bhallB  HBI     gnda    v=5*u(sin(V(theta,gnd) + pi*7/6))
bhallA  HAI     gnda    v=5*u(sin(V(theta,gnd) + pi/2))
bhallC  HCI     gnda    v=5*u(sin(V(theta,gnd) - pi/6))
*************************************************************************
bemfa   neutral ntrl    v=v(omega,gnd)*1.212*(asin(sin(v(theta,gnd)))
+-uramp(asin(sin(v(theta,gnd)))-pi/6)
++uramp(-asin(sin(v(theta,gnd)))-pi/6))

bemfb   neutrbl ntrl    v=v(omega,gnd)*1.212*(asin(sin(v(theta,gnd)+pi*2/3))
+-uramp(asin(sin(v(theta,gnd)+pi*2/3))-pi/6)
++uramp(-asin(sin(v(theta,gnd)+pi*2/3))-pi/6))

bemfc   neutrcl ntrl    v=v(omega,gnd)*1.212*(asin(sin(v(theta,gnd)-pi*2/3))
+-uramp(asin(sin(v(theta,gnd)-pi*2/3))-pi/6)
++uramp(-asin(sin(v(theta,gnd)-pi*2/3))-pi/6))

*Rgnd   ntrl    0       15Meg
*Rgnda  gnda    gnd     3m
*.tran 100u 100m 0 10u UIC
```

This is the IbridgeFQ.cir file:

```
*Four Quadrant Drive include file
.control
set filetype=binary
.endc

.include ../SPICE_models/Mosfets/IRF3205s_IR.mdl
.include ../SPICE_models/Logic/xor.mdl
.include ../SPICE_models/Logic/74LVC1G58.mdl
.include ../SPICE_models/Comparators/LM393_Texas.mdl
.include ../SPICE_models/Opamps/LF412_National.mdl
.include ../SPICE_models/Diodes/Junction/1N4148_Diodes_Inc.mdl

*low voltage inputs*************************************************************
.include ./IbridgeHQ.cir
*hall sensor signals simulated with pulse waveforms
*VHA   HAI   gnda   DC  4     pulse(4.9 0.1     14m     100u    100u    20.9m   42m)
*VHB   HBI   gnda   DC  0.5   pulse(0.1 4.9     7m      100u    100u    20.9m   42m)
*VHC   HCI   gnda   DC  0.1   pulse(4.9 0.1     0m      100u    100u    20.9m   42m)
********************************************************************************

*power supplies*****************************************************************
vpsw    1       gnda    DC 5.0
rfivev  fiveV   1       0.02
cfivev  fiveV   gnda    33u

vcur    2       gnd     DC 5.0
rv_cc   V_CC    2       0.02
cv_cc   V_CC    gnd     33u

vgnd    gnd     0       DC      0

*the logic per gate section*****************************************************

.subckt PMDCSW  A       B       LG      HG      vdd     vss
*input 2 is inverted in the gate model before being ANDed with input 1
*this is the function provided by the multifunction gate 74LVC1G58
Xinvand         A       B       HG      vdd     vss     invand
Xandinv         B       A       LG      vdd     vss     invand
.ends   PMDCSW

*gate signals for Q 1&2, Q 3&4 and Q 5&6
XICA    HB      HC      A_low   A_high  fiveV   gnda    PMDCSW
XICB    HC      HA      B_low   B_high  fiveV   gnda    PMDCSW
XICC    HA      HB      C_low   C_high  fiveV   gnda    PMDCSW

*Reversing Circuit with blanking time******************************************

RREVH           CMPB    revh    1.5K
CREVH           revh    gnda    390p
DREVH           CMPB    revh    1N4148

RREVL           CMPB    revl    1.2K
CREVL           revl    gnda    390p
DREVL           revl    CMPB    1N4148
*.SUBCKT 74HC58 pin1    pin6    pin3    out     pwr     gnd
XrevA           revh    HAI     revl    HA      fiveV   gnda    74HC58
XrevB           revh    HBI     revl    HB      fiveV   gnda    74HC58
XrevC           revh    HCI     revl    HC      fiveV   gnda    74HC58

*Half bridge reversing circuit*************************************************
Xcsl_xor        cshl    CMPA    cshl    V_CSL   V_CC    gnd     74HC58
*vcs            V_CSL   gnd     DC 0
Xcsh_inv        V_CSL   V_CC    V_CC    V_CSH   V_CC    gnd     74HC58
RCSLH           CMPB    cshl    10K
CCSLH           cshl    gnd     100p
```

```
*Comparators of tolerance band*****************************************************
* CONNECTIONS:   NON-INVERTING INPUT
*                | INVERTING INPUT
*                | | POSITIVE POWER SUPPLY
*                | | | NEGATIVE POWER SUPPLY
*                | | | | OPEN COLLECTOR OUTPUT
*                | | | | |
*SUBCKT LM393    1 2 3 4 5
XCMPB           cmpbin  cmpbv   412pwr  gnd     rev     LM393
Rcmpbu          rev     V_CC    2K
XCBB            rev     CMPB    V_CC    gnd     buffer
*this marks the end of the approximation to a better comparator*

RCBFB           cmpbin  CMPB    150k
RCBL            cmpbin  gnd     22k
RCBH            cmpbin  V_CC    22K

*components to stabilise the simulation
Ccmpbf          cmpbr           gnd             0.5n
Rcmbpin         V_Isense        cmpbr           10000
Rcmpbi          cmpbv           cmpbr           1
Ccmpaf          cmpar           gnd             0.1n
Rcmbain         V_Isense        cmpar           100
Rcmpai          cmpav           cmpar           1

*CMPA for determining the magnitude of v_bldc
XCMPA           cmpain  cmpav   412pwr  gnd     par     LM393
Rcmpau          par     V_CC    2K
XCBA            par     CMPA    V_CC    gnd     buffer
*this marks the end of the approximation to a better comparator*

RCAFB           cmpain  CMPA    330k
RCAL            cmpain  gnd     22k
RCAH            cmpain  V_CC    22K

*Opamps for current signal*********************************************************

*reference voltage resistor divider
R_irefl         VCC     V_IREF  10K
R_irefh         V_IREF  gnd     10K
Ciref           V_IREF  gnd     1u ic=2.5v

* connections:    non-inverting input
*                 |   inverting input
*                 |   |   positive power supply
*                 |   |   |   negative power supply
*                 |   |   |   |   output
*                 |   |   |   |   |
*                 |   |   |   |   |
*SUBCKT LF412NS  1   2   99  50  28
XOPA            V_IREF          sum             412pwr  412gnd  V_ISE   LF412NS
R_gain          V_ISE           sum             470K
R_filt          V_ISE           V_Isense        1K
C_isen          V_Isense        gnd             100p

*Cungain                CMPB            gnd             1u
RPOLI           CMPB            V_I_IN          100.055K
R_FILTI         V_Ifilt         V_I_IN          100K
XOPB            V_IREF          V_I_IN          412pwr  412gnd  I_INV   LF412NS
R_IFB           V_I_IN          I_INV           200K
Rsum            I_INV           sum             10K

RPOLS           CMPB    sum     20K

RPOLH           VCC             sum     20.114K
```

```
R_FILTS          V_Ifilt          sum      10K
Rth_in           V_throttle       sum      150K

*this is the approximation to the 74LVC1G66 analog switch
*.model  answ SW Ron=10m Roff=100Meg Vt=2.5 Vh=0.7
*Scmpb           I_ANSW  sum      CMPB gnd         answ

Vccs     VCC     gnd      DC 5v
V412     412pwr  VCC      DC 1.372v
V412gnd  412gnd  gnd      DC -1.371v

*motor model section*************************************************************
*motor has three star connected inductors in its model
*resistance in series and parallel
*trapezoidal voltage as the back emf
Lan      phaseA  neutal   500uH IC=0
Lbn      phaseB  neutbl   500uH IC=0
Lcn      phaseC  neutcl   500uH IC=0
Rla      phaseA  neutal   5K
Rlb      phaseB  neutbl   5K
Rlc      phaseC  neutcl   5K
Ran      neutal  neutral  0.35ohms
Rbn      neutbl  neutrbl  0.35ohms
Rcn      neutcl  neutrcl  0.35ohms
*the motor emfs are generated by the file IbridgeHQ.cir

*Battery voltage*****************************************************************
Vbatt    batt    gnd      30volts
Rbus     batt    vbatt    0.01
Cbus     vbatt   gnd      1000u


*sense Resistor and filter*******************************************************
Rsense   gnda    gnd      3m
*Lfilt   gnda    V_Ifilt  10u
*Rfilt   V_Ifilt filr     10
Rfilt    V_Ifilt gnda     0.01
Vgnda    gnda    sense    DC 0.0V
*Cfilt   V_Ifilt gnd      70n


*Power MOSFET switches***********************************************************

*Phase Switcher MOSFETs
*                Drain    Gate     Source
XQ1              V_bldc   DR_AH    phaseA          irf3205s
XQ3              V_bldc   DR_BH    phaseB          irf3205s
XQ5              V_bldc   DR_CH    phaseC          irf3205s

XQ2              phaseA   DR_AL    gndaA           irf3205s
XQ4              phaseB   DR_BL    gndaB           irf3205s
XQ6              phaseC   DR_CL    gndaC           irf3205s

*Current Controller MOSFETs
XQ_CSH           vbatt    DRV_CSH  V_bldc          irf3205s
XQ_CSL           V_bldc   DRV_CSL  gnd             irf3205s

*the mosfet drivers**************************************************************
EQ1      DRV_AH  phaseA   A_high   gnda     1.8
EQ3      DRV_BH  phaseB   B_high   gnda     1.8
EQ5      DRV_CH  phaseC   C_high   gnda     1.8

EQ2      DRV_AL  gndaA    A_low    gnda     1.8
EQ4      DRV_BL  gndaB    B_low    gnda     1.8
EQ6      DRV_CL  gndaC    C_low    gnda     1.8
```

```
ECSH    DRV_CSH V_bldc  VCSH    gnd     1.8
ECSL    DRV_CSL gnd     VCSL    gnd     1.8

*simulation of driver internal resistance
RQ1G    DRV_AH  DR_AH   10
RQ2G    DRV_BH  DR_BH   10
RQ3G    DRV_CH  DR_CH   10
RQ4G    DRV_AL  DR_AL   10
RQ5G    DRV_BL  DR_BL   10
RQ6G    DRV_CL  DR_CL   10

*deadtime generation section
CCSH    VCSH    gnd     100p    IC=0
R_CSH   VCSH    V_CSH   820
D_CSH   VCSH    V_CSH   1N4148
CCSL    VCSL    gnd     100p    IC=5
R_CSL   VCSL    V_CSL   820
D_CSL   VCSL    V_CSL   1N4148

*Record Current in phase switcher low side mosfets**********************************
VQ2     gndaA   sense   DC 0
VQ4     gndaB   sense   DC 0
VQ6     gndaC   sense   DC 0

*scaling of the sense resistor voltage to get sensible plots************************
Ecurrent        Isense gnd      sense   gnd     333.33
Ccurrent        senseN gnd      1u
Rfilter         Isense  senseN  1
```

References

References are arranged in alphabetical order according to the first author's surname.

[1] Acarnley, P.P., Watson, J.F., April 2006. **Review of Position-Sensorless Operation of Brushless Permanent-Magnet Machines.** *In: IEEE Transactions on Industrial Electronics*, Vol. 53, No. 2, pp. 352 – 362.

[2] Agilent Technologies, March 2008. **Application Note 290: Practical Temperature Measurements.** Online, available May 2009: www.agilent.com

[3] Analog Devices, 1999. **AD594/AD595 – Monolithic Thermocouple Amplifiers with Cold Junction Compensation, Datasheet.** Online, available February 2006: www.analog.com

[4] Aydin, M., Huang, S., Lipo, T.A., June 2006. **Torque Quality and Comparison of Internal and External Rotor Axial Flux Surface-Magnet Disc Machines.** *In: IEEE Transactions on Industrial Electronics*, Vol. 53, No. 3, pp. 822 – 829.

[5] Bai, G., Gao, R.W., Sun, Y., Han, G.B., Wang, B., 2007. **Study of high-coercivity sintered NdFeB magnets.** *In: Journal of Magnetism and Magnetic Materials*, Vol. 308, pp. 20 – 23.

[6] Britten, M.D., de Vries, I.D., Tapson, J., January 2007. **Discrete Logic Permanent Magnet Brushless DC Motor Controller.** *In: Proceedings of the* 16_{th} *Southern African Universities' Power Engineering Conference*, pp. 132 –134.

[7] Cappelletti, P., 1998. **Flash Memory Reliability.** *In: Microelectronics Reliability*, Vol. 38, No. 2, pp. 185 – 188.

[8] Carrichi, F., Crescembini, F., Noia, G., Pirolo, D., 1994. **A bidirectional DC-DC converter for DC link voltage control and regenerative braking in PM motor drives for EVs.** *In: IEEE Applied Power Electronics Conference 1994, Ninth,* pp. 381 – 386.

[9] **Crystalyte Controller for E-Bike.** Online, available June 2007: http://www.crystalyte.com/Control.htm

[10] Dake, T., Özalevli, E., June 2008. **A Precision High-Voltage Current Sensing Circuit.** *In: IEEE Transaction on Circuits and Systerms – I: Regular Papers*, Vol. 55, No. 5, pp. 1197 – 1202.

[11] Dallago, E., Passoni, M., Sassone, G., December 2000. **Lossless Current Sensing in Low-Voltage High-Current DC/DC Modular Supplies.** *In: IEEE Transactions on Industrial Electronics*, Vol. 47, No. 6, pp. 1249 – 1252.

[12] Dallago, E., Passoni, M., Sassone, G., Venchi, G., May 2000. **Novel current transducer in a single-phase active power factor correction system.** *In: IEEE Transactions on Power Electronics*, Vol. 15, No. 3, pp. 529 – 535.

[13] Dixon, J.W., Leal, I.A., March 2002. **Current Control Strategy for Brushless DC Motors Based on a Common DC Signal.** *In: IEEE Transactions on Power Electronics*, Vol. 17, No. 2, pp. 232 – 240.

[14] Dixon, L.H., 2003. **Eddy Current Losses in Transformer Windings and Circuit Wiring.** USA: Texas Instruments. Online, available August 2009: www.ti.com

[15] Dixon, L., 1999. **Application Note U-140: Average Current Mode Control of Switching Power Supplies.** USA: Texas Instruments (Originally Unitrode Corporation, New Hampshire, USA).

[16] Ertugrul, N., Acarnley, P. January 1994. **A New Algorithm for Sensorless Operation of Permanent Magnet Motors.** *In: IEEE Transactions on Industry Applications*, Vol. 30, No. 1, pp. 126 – 133.

[17] Gifford, P., Adams, H., Corrigan, D., Vendatesan, S., 1999. **Development of advanced nickel/metal hydride batteries for electric and hybrid vehicles.** *In: Journal of Power Sources*, Vol. 80, pp. 157 – 163.

[18] Green, T.C., Williams, B.W., July 1989. **Derivation of motor line-current waveforms from the DC-link current of an inverter.** *In: IEE Proceedings B*, Vol. 136, No. 4, pp. 196 – 204.

[19] Hartas, P., Shahin, A., Nuttall, K.I., Shimmin, D.W., March 2001. **A Novel Permanent Magnet DC Motor and Sensorless Electrical Drive System.** *In: Electric Power Components and Systems*, Vol. 29, No. 1, pp. 15 – 28.

[20] Horowitz, P., Hill, W., 2003. **The art of electronics, Second Edition.** India: Cambridge University Press.

[21] Hwang, C.C., Chang, J.J., 2000. **Design and analysis of a high power density and high efficiency permanent magnet DC motor.** *In: Journal of Magnetism and Magnetic Materials*, Vol. 209, pp. 234 – 236.

[22] Ishikawa, T., Slemon, G. R., March 1993. **A Method of Reducing Ripple Torque in Permanent Magnet Motors without Skewing.** *In: IEEE Transactions on Magnetics*, Vol. 29, No. 2, pp. 2028 – 2031.

[23] Jang, J., Sul, S., Ha, J., Ide, K., Sawamura, M., July 2003. **Sensorless Drive of Surface-Mounted Permanent-Magnet Motor by High-Frequency Signal Injection Based on Magnetic Saliency.** *In: IEEE Transactions on Industry Applications*, Vol. 39, No. 4, pp. 1031 – 1039.

[24] JUMO PROCESS CONTROL INC., **Platinum-chip temperature sensors in SMD style to EM 60 751.** Online, available December 2008: www.JumoUSA.com.

[25] Kang, S., Sul, S., November 1995. **Direct Torque Control of Brushless DC Motor with Nonideal Trapezoidal Back EMF.** *In: IEEE Transactions on Power Electronics*, Vol. 10, No. 6, pp. 796 – 802.

[26] Kavanagh, R.C., Murphy, J.M.D., Egan, M.G., July 1988. **Innovative Current Sensing for Brushless DC Drives.** *In: Third International Conference on Power Electronics and Variable Speed Drives*, No. 291, pp. 354 – 357.

[27] Khan, M.A., 2001. **Design of a Universal PM motor drive.** *MSc. Thesis.* Cape Town, South Africa: University of Cape Town.

[28] Kim, S.H., Doose, C., May 1997. **Temperature Compensation of NdFeB Permanent Magnets.** *In:Proceedings of the Particle Accelerator Conference*, Vol. 3, pp. 3227 – 3229.

[29] Lee, M.L., Park, J.S., Lee, W.J., Yun, S.H., Lee, Y.H., Kim, B.Y., February 1998. **A Polarimetric Current Sensor Using an Orthogonally Polarized Dual-Frequency Fibre Laser.** *In: Measurement Science and Technology*, Vol. 9, pp. 952 – 959.

[30] Lee, Y.W., Yoon, I., Lee, B., January 2004. **A simple fiber-optic current sensor using a long-period fiber grating inscribed on a polarization-maintaining fiber as a sensor demodulator.** *In: Sensors and Actuators*, Part A, Vol. 112, pp. 308 – 312.

[31] Lepkowski, J., 2003. **AN894: Motor Control Sensor Feedback Circuits.** USA: Microchip Technology Incorporated.

[32] Lin, B., 2000. **Conceptual design and modeling of a fuel cell scooter for urban Asia.** *In: Journal of Power Sources*, Vol. 86, pp 202 – 203.

[33] Linear Technology, 2001. **LTK001 – Thermocouple Cold Junction Compensator and Matched Amplifier, Datasheet.** Online, available February 2006: www.linear-tech.com

[34] Maxwell Technology, 2009. **BC Power Series BOOSTCAP Ultracapacitors Datasheet.** Online, available January 2009: www.maxwell.com

[35] Maxim Dallas Semiconductors, May 2005. **MAX5023/MAX5024 – 65V, Low-Quiescent-Current, High-Voltage Linear Regulators with μP Reset and Watchdog Timer.** Online, available June 2008: www.maxim-ic.com

[36] Maxim Dallas Semiconductors, January 2007. **MAX5033 – 500mA, 76V, High-Efficiency, MAXPower Step-Down DC-DC Converter.** Online, available June 2008: www.maxim-ic.com

[37] Mohan, N., Undeland, T.M., Robbins, W.P., 2003. **Power Electronics, Converters, Applications and Design. 3rd Ed.** USA: John Wiley & Sons, Inc.

[38] Moreira, J.C., December 1996. **Indirect Sensing for Rotor Flux Position of Permanent Magnet AC Motors Operating Over a Wide Speed Range.** *In: IEEE Transactions on Industry Applications*, Vol. 32, No. 6, pp. 1394 – 1401.

[39] Nakashima, S., Inagaki, Y., Miki, I., December 2000. **Sensorless Initial Rotor Position Estimation of Surface Permanent-Magnet Synchronous Motor.** *In: IEEE Transactions on Industry Applications*, Vol. 36, No. 6, pp. 1598 – 1603.

[40] Narayanan, G.,Krishnamurthy, H.K., Zhao, D., Ayyanar, R., July 2006. **Advanced Bus-Clamping PWM Techniques Based on Space Vector Approach.** *In: IEEE Transactions on Power Electronics* Vol. 21, No. 4, pp. 974 – 984.

[41] National Semiconductor, November 2000. **LM35 – Precision Centigrade Temperature Sensors.** Online, available June 2007: www.national.com

[42] National Semiconductor, March 2005. **LM5100A/LM5101A – 3.0 Amp High Voltage High Side and Low Side Driver.** Online, available June 2007: www.national.com

[43] Obridko, I., Ginosar, R., September 2006. **Minimal Energy Asynchronous Dynamic Adders.** *In: IEEE Transactions on Very Large Scale Integration Systems*, Vol. 14, No. 9, pp. 1043 – 1047.

[44] Patterson, D. and Spée, R., September 1995. **The Design and Development of an Axial Flux Permanent Magnet Brushless DC Motor for Wheel Drive in a Solar Powered Vehicle.** *In: IEEE Transactions on Industry Applications*, Vol. 31, No. 5, pp. 1054 – 1061.

[45] Panasonic, August 2003. **Valve Regulated Lead Acid Batteries: Individual Data Sheet - LC-RA1212P.** Online, available 2005: www.panasonic.com

[46] Rose, B., January 2006. **Are Hydrogen and Fuel Cells a Practical Solution to Our Energy Needs?** *Presentation slides: Washington Seminar Series – The Dimensions of Energy Policy in the 21st Century: Technology, Economics, and Politics.* Online, available 2009: www.fuelcells.org

[47] RS Components, March 1999. **Thermistors, Data Sheet.** Online, available December 2008: www.RS-Components.co.za

[48] Sen, P.C., 1997. **Principles of Electric Machines and Power Electronics. 2nd Ed.** USA: John Wiley & Sons, Inc.

[49] Sen, P.C., December 1990. **Electric Motor Drives and Control – Past, Present, and Future.** *In: IEEE Transactions on Industrial Electronics*, Vol. 37, No. 6, pp. 562 – 575.

[50] Shao, J., Nolan, D., Teissier, M., Swanson, D., December 2OO3. **A Novel Microcontroller-Based Sensorless Brushless DC (BLDC) Motor Drive for Automotive Fuel Pumps.** *In: IEEE Transactions on Industry Applications*, Vol. 39, No. 6, pp. 1734 – 1740.

[51] Shen, J.X., Zhu, Z.Q., Howe, D., December 2004. **Sensorless Flux-Weakening Control of Permanent-Magnet Brushless Machines Using Third Harmonic Back EMF.** *In: IEEE Transactions on Industry Applications*, Vol. 40, No. 6, pp. 1629 – 1636.

[52] STATEK Corporation, December 2008. **TS Series Miniature Quartz Temperature Sensor.** Online, available December 2008: www.statek.com

[53] Szepesi, T., October 1987. **Stabilizing the Frequency of Hysteretic Current-Mode DC/DC Converters.** *In: IEEE Transactions on Power Electronics*, Vol. PE-2, No. 4, pp. 302 – 312.

[54] Takahashi, I., Koganezawa, T., Su, G., Ohyama, K., May 1994. **A Super High Speed PM Motor Drive System by a Quasi-Current Source Inverter.** *In: IEEE Transactions on Industry Applications*, Vol. 30, No. 3, pp. 683 – 690.

[55] Tesla Motors, January 2009. **Tesla Motors Website.** Online, available 2009: www.teslamotors.com

[56] Trzynadlowski and A.M., Legowski, S., January 1994. **Minimum-Loss Vector PWM Strategy for Three-Phase Inverters.** *In: IEEE Transactions on Power Electronics*, Vol. 9, No. 1, pp. 26 – 34.

[57] Van der Broeck,H.W., Skudelny, H.C., Stanke G.V., January/February 1988. **Analysis and Realization of a Pulsewidth Modulator Based on Voltage Space Vectors.** *In: IEEE Transactions on Industrial Applications*, Vol. 24, No. 1, pp. 142 – 150.

[58] Vektrex, February 2009. **Vectrex Current Sensors.** Online, available 2009: www.vektrex.com

[59] Yan, X., Patterson, D., 2001. **Novel power management for high performance and cost reduction in an electric vehicle.** *Renewable Energy*, Vol. 22, pp. 177 – 183.

[60] Zhang, Y., Zane, R., Prodic, A., Erickson, R., Maksimovic, D., September 2004. **Online Calibration of MOSFET On-State Resistance for Precise Current Sensing.** *In: IEEE Power Electronics Letters*, Vol. 2, No. 3, pp. 100 – 103.

[61] Zheng, J.P., Jow, T.R., 1996. **High energy and high power density electrochemical capacitors.** *In: Journal of Power Sources*, Vol. 62, pp. 155 – 159.

[62] Zhou, K., Wang, D., February 2002. **Relationship between Space-Vector Modulation and Three-Phase Carrier-Based PWM: A Comprehensive Analysis.** *In: IEEE Transactions on Industrial Electronics*, Vol. 49, No. 1, pp. 186 – 196.